Synthesis and pharmacological characterization of 3-isothiazolols and 3-isoxazolols as competitive antagonists of insect GABA receptors

（昆虫 GABA 受容体の競合的アンタゴニストとしての 3-イソチアゾロール類および 3-イソキサゾロール類の合成と薬理学的特性）

Genyan Liu

2016

Synthesis and pharmacological characterization of 3-isothiazolols and 3-isoxazolols as competitive antagonists of insect GABA receptors

by

Genyan Liu

A dissertation submitted in partial fulfillment of the requirements for the degree of Doctor of Philosophy

The United Graduate School of Agricultural Sciences

Tottori University

2016

Contents

List of figures and tables

Abbreviations

CA	competitive antagonist
CC	common cutworm
CNS	central nervous system
DMF	*N, N*-dimethylformamide
DMSO	dimethyl sulfoxide
EC_{50}	half maximal effective concentration
ECD	extracellular domain
ESI+	positive electrospray ionization
FLIPR	fluorometric imaging plate reader
FMP	FLIPR membrane potential
GABA	γ-aminobutyric acid
GABAR	GABA receptor
GluCl	glutamate-gated chloride channel
GlyR	glycine receptor
GPCR	G protein-coupled receptor
HF	housefly
HRMS	high-resolution mass spectrometry
5-HT_3R	5-hydroxytryptamine (serotonin) type 3 receptor
IC_{50}	half maximal inhibitory concentration
LD_{50}	median lethal dose
LGIC	ligand-gated ion channel
MS	mass spectrometry
nAChR	nicotinic acetylcholine receptor

NCA	noncompetitive antagonist
4-PHP	4-(4-piperidyl)-1-hydroxypyrazole
4-PIOL	5-(4-piperidyl)-3-isoxazolol
RDL	an insect GABAR subunit named after “Resistance to DieLdrin”
Rdl	RDL-encoding gene
RDLR	RDL GABA receptor
SBP	small brown planthopper
SOS	standard oocyte solution
TEVC	two-electrode voltage clamp
Thio-4-PIOL	5-(4-piperidyl)-3-isothiazolol
TM	transmembrane domain

Chapter 1

Introduction

1.1. γ-Aminobutyric acid (GABA)

γ-Aminobutyric acid (GABA, Fig. 1.1), a major inhibitory neurotransmitter in the nervous systems, was identified as a free amino acid in the brain in the 1950s (Awapara et al., 1950; Roberts and Frankel, 1950). Since GABA was recognized as a neurotransmitter in 1957 (Bazemore et al., 1957), the complicated mechanisms that contribute to GABA-mediated neurotransmission have been extensively studied using pharmacological, eletrophysiological, and biochemical techniques.

In GABAergic neurons, GABA is primarily synthesized by decarboxylation of the neurotransmitter glutamate in a reaction that is mediated by the cytosolic enzyme L-glutamic acid decarboxylase and the cofactor pyridoxal phosphate. GABA is packaged into synaptic vesicles by means of the vesicular GABA transporter, and is then released from the presynaptic nerve terminals by calcium-dependent exocytosis of these vesicles. When released into the synaptic cleft, GABA exterts its inhibitory effects by interacting with ionotropic GABA receptors (GABARs) in perisynaptic and extrasynaptic locations to induce a chemical to electrical transduction (Enna and Möhler, 2007; Olsen and Sieghart, 2008). GABA also activates metabotropic GABARs to mediate prolonged postsynaptic inhibition and presynaptic neurotransmitter release (Bowery et al., 2002). The inhibitory effect of GABA plays an important role in the central nervous system (CNS) because of the

widespread distribution of GABAergic neurons in the brain. It has been suggested that 30–40% of central neurons might use GABA as a primary neurotransmitter (Enna and Möhler, 2007). In addition, GABA also plays an important role in the development and function of the peripheral nervous system. GABA is considered to be involved in the control of many physiological mechanisms, such as the secretion of hormones, the regulation of cardiovascular functions, and the sensation of pain and anxiety (Enna and Möhler, 2007).

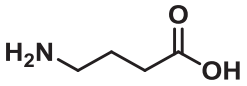

Figure 1.1 Chemical structure of GABA.

1.2. GABARs

GABARs mediate inhibitory synaptic neurotransmission in the nervous systems of animals, and are extensively studied as potential targets of drugs and insecticides. GABARs have been classified into metabotropic and ionotropic types on the basis of their structure and pharmacology. The metabotropic GABAR, which belongs to G protein-coupled receptors (GPCRs), activates the inwardly rectifying potassium ion channels to induce slow postsynaptic inhibition of neurons (Bowery et al., 2002). Activation of presynaptic metabotropic GABAR also inhibits neurotransmitter release by suppressing neuronal calcium conductance (Bettler et al., 2004; Bowery et al., 2002). This dissertation primarily focuses on ionotropic GABARs, and especially on insect ionotropic GABARs. The ionotropic GABAR, which falls into the Cys-loop family of ligand-gated ion channels (LGICs), mediates fast inhibitory synaptic transmission by binding to GABA. Other well-known members of the

Cys-loop family include nicotinic acetylcholine receptors (nAChRs), 5-hydroxytryptamine type 3 receptors (5-HT_3R), and glycine receptors (GlyRs) (daCosta and Baenziger, 2013; Lester et al., 2004; Sine and Engel, 2006). The name "Cys-loop" comes from a conserved disulfide-bond between two cysteine residues at the N-terminal extracellular domain (ECD) of the subunits in these receptors (Nys et al., 2013; Sine and Engel, 2006).

The ionotropic GABAR is composed of five homologous subunits arranged symmetrically around a chloride-permeable channel (Fig. 1.2A). Each subunit of the GABAR possesses a long N-terminal ECD, a transmembrane domain (TM) with four α-helical segments (TM1–TM4), and an intracellular loop connecting TM3 and TM4 segments (Fig. 1.2B). The TM2 α-helix from each subunit forms the lining of the ion channel pore, in which the components of the channel's gate are included. Upon the binding of GABA or other agonists, the ionotropic GABAR allows chloride ions to flux into the cell interior, resulting in hyperpolarizing potentials. The membrane hyperpolarization suppresses the excitability of nerve or muscle. The ionotropic GABARs are well-established targets for insecticides. Structural and pharmacological differences between insect and mammalian ionotropic GABARs might provide opportunities to develop selective and safe pest control agents.

1.2.1. Mammalian GABARs

Mammalian GABARs are classified into two major types A and B ($GABA_A$Rs and $GABA_B$Rs). The ionotropic $GABA_A$Rs belong to the Cys-loop family of LGICs, whereas the metabotropic $GABA_B$Rs are heterodimeric GPCRs (Bowery et al., 2002; Olsen and Sieghart, 2008). The $GABA_A$Rs consist of five subunits arranged symmetrically around an integral

chloride ion pore. Beginning with the α_1 and β_1 subunit genes cloned from bovine brain in 1987 (Schofield et al., 1987), a total of nineteen subunit genes (α_{1-6}, β_{1-3}, γ_{1-3}, ε, δ, π, θ, and ρ_{1-3}) have been identified in mammals (Olsen and Sieghart, 2009). The most abundant subtype of $GABA_ARs$ in the brain consists of two α_1, two β_2, and one γ_2 subunits (Sieghart and Sperk, 2002). GABARs composed of ρ_{1-3} subunits are homomeric or pseudo-heteromeric receptors and classified as type-C GABARs ($GABA_CRs$), which are predominantly found in the vertebrate retina (Zhang et al., 2001).

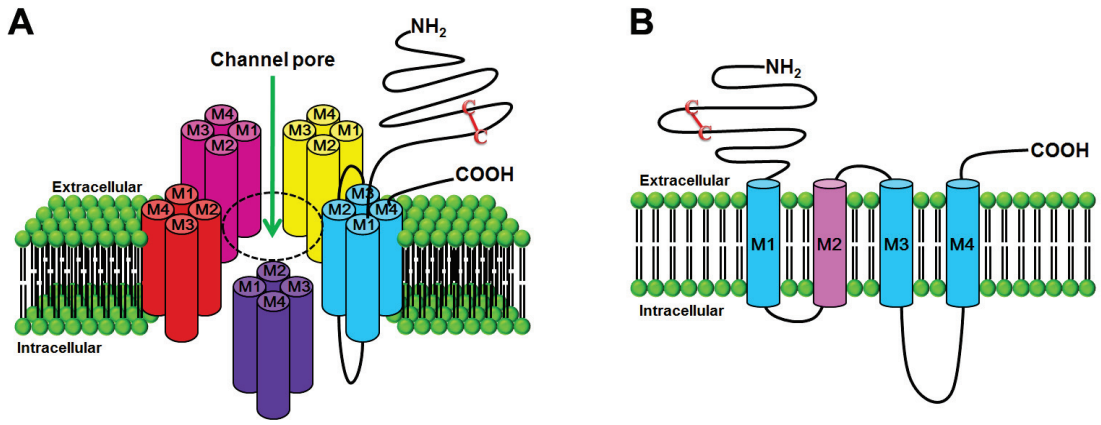

Figure 1.2 Schematic presentation of the ionotropic GABAR. (A) Assembly of five subunits forming a chloride channel. (B) Side view of a single subunit. Four TMs are labeled with M1, M2, M3, and M4.

An X-ray structure of the human $GABA_AR$ β3 homopentamer cocrystallized with benzamidine has been recently solved at 2.97 Å (Miller and Aricescu, 2014; PDB ID: 4COF, Fig. 1.3). This is the first and only three-dimensional structure of the $GABA_AR$ reported to date, although it is unclear whether the β3 homopentamers constitute a defined physiological population of $GABA_ARs$. Before the determination of this crystal structure, the insights concerning structure, gating mechanism, and ligand recognition of ionotropic GABARs were

derived from the related structures as follows: the *Torpedo marmorata* and mouse nAChRs (Dellisanti et al., 2007; Unwin, 2005), the snail acetylcholine binding proteins (AChBPs) (Brejc et al., 2001; Celie et al., 2005; Hansen et al., 2005), the integral prokaryotic LGICs from *Erwinia chrysanthemi* (Hilf and Dutzler, 2008) and *Gloeobacter violaceus* (Bocquet et al., 2009; Hilf and Dutzler, 2009), and the *Caenorhabditis elegans* glutamate-gated chloride channel (GluCl) (Hibbs and Gouaux, 2011). These structures revealed that the overall architecture of the Cys-loop receptors appears to be conserved and consists of five homologous membrane-spanning subunits.

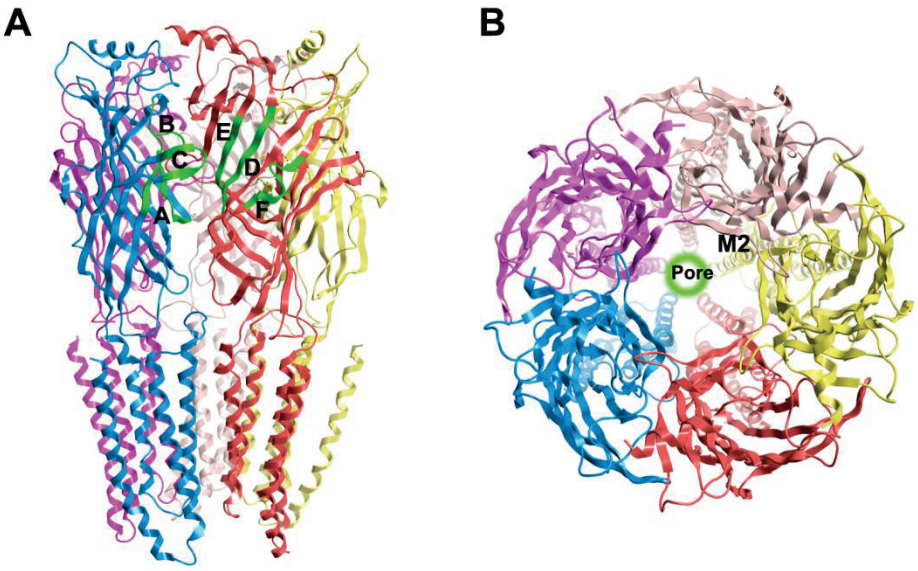

Figure 1.3 Architecture of the human $GABA_AR$ β3 homopentamer (PDB: 4COF). The structural figures were prepared with MOE software (Version 2014.09, Chemical Computing Group, Montreal, Canada). The subunits are colored differently. (A) Side view. Putative loops A–F of the orthosteric binding site are indicated in green. (B) Top view. Five TM2s form the chloride channel pore.

1.2.2. Insect GABARs

Several decades of research revealed that both ionotropic and metabotropic GABARs are present in the CNS and the neuromuscular junction of insects (Buckingham and Sattelle, 2010; Ozoe, 2013). A gene encoding an insect GABAR subunit was first cloned from fruit flies (*Drosophila melanogaster*) via the mapping of the locus conferring *r*esistance to the *d*ie*l*drin, hence being named '*rdl*' (ffrench-Constant et al., 1991). The orthologous genes have also been cloned from various insect species (Buckingham et al., 2005; Buckingham and Sattelle, 2010; Ozoe, 2013). Heterologous expression of RDL subunits in *Xenopus laevis* oocytes demonstrated a relationship to the mammalian ionotropic GABARs on the basis of their ability to open chloride channels upon GABA activation (ffrench-Constant et al., 1993). Alternative splicing of *rdl* at exons 3 and 6 produces four subunit variants (RDL_{ac}, RDL_{ad}, RDL_{bc}, and RDL_{bd}; Fig. 1.4) in housefly (HF, *Musca domestica*), and other insect species (ffrench-Constant and Rocheleau, 1993; Ozoe et al., 2009). These splicing variants may increase the diversity of the physiology and pharmacology of insect RDL GABARs (RDLRs). RDLRs expressed in *Xenopus* oocytes or *Drosophila* S2 cells serve as a platform for the discovery of novel insecticides or an appropriate model to study insect ionotropic GABARs (Buckingham et al., 1994; Millar et al., 1994).

Two other GABAR-like subunits named GRD and LCCH3 have been cloned first from *Drosophila* (Harvey et al., 1994; Henderson et al., 1993, 1994) and subsequently from other insect species (Ozoe, 2013). The *Drosophila* GRD and LCCH3 subunits are coassembled to form a GABA-gated cation channel when expressed in *Xenopus* oocytes (Gisselmann et al., 2004). As cation channels are considered to be excitatory receptors, the RDL is the only

subunit that constitutes inhibitory GABARs in insects at the moment. RDLRs are generally deemed to be structurally and pharmacologically representative for insect ionotropic GABARs. However, insect RDLRs and mammalian GABARs have different pharmacological sensitivities to a range of ligands. One major difference is that most RDLRs are insensitive to bicuculline, which is a representative competitive antagonist (CA) of $GABA_A$Rs.

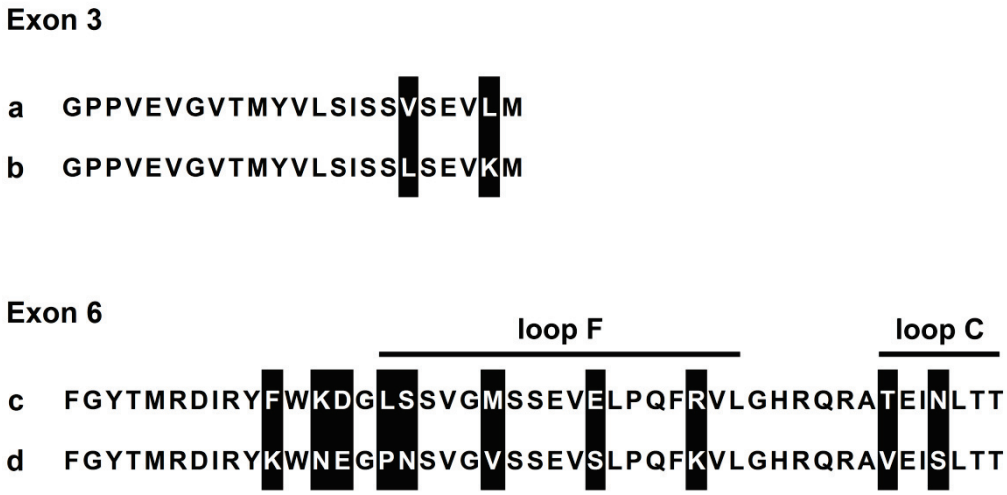

Figure 1.4 Alignments of amino acid sequences encoded by exons 3a, 3b, 6c, and 6d of HF *Rdl*. Putative loops F and C of the orthosteric binding site are indicated by overbars. Exons 3a and 3b differ by two amino acid residues, and exons 6c and 6d differ by ten residues, seven of which are located within putative loops F and C. Different amino acids are indicated by white text in a black background.

1.3. Ionotropic GABAR ligands

Ionotropic GABARs are regulated by multiple types of ligands acting at distinct sites (hereafter ionotropic GABARs are referred to as GABARs, unless otherwise noted). The GABA binding site also known as the orthosteric binding site, which is directly responsible

for the chloride channel opening, is located at the extracellular N-terminal interface between two adjacent subunits that are termed as the principal and complementary subunits (Fig. 1.5). Like other Cys-loop receptors, the orthosteric site of GABARs is composed of six discontinuous loops A–F, where loops A–C are from the principal subunit and loops D–F are from the complementary subunit (Fig. 1.5). Agonists and CAs share this common orthosteric site.

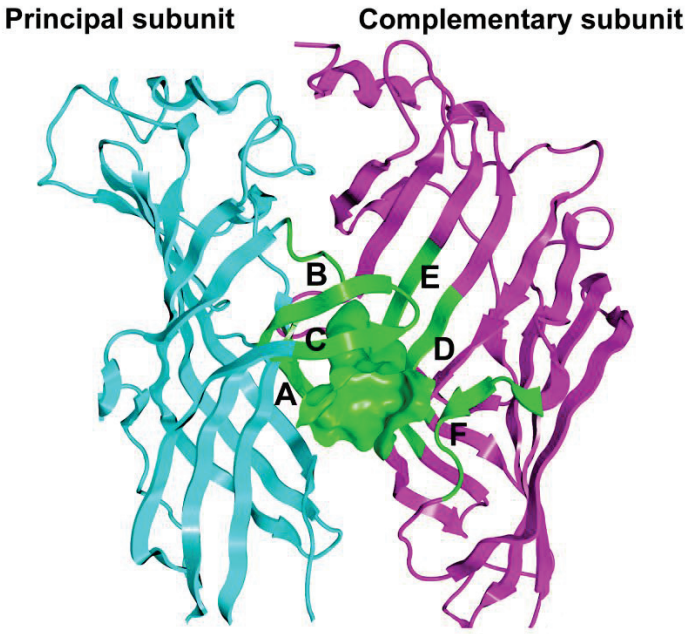

Figure 1.5 The orthosteric binding site formed by two adjacent subunits in a HF RDLR homology model. The crystal structure of the homopentameric human β3 $GABA_AR$ (PDB: 4COF) was used as a template to construct the model. The molecular surface of the orthosteric binding pocket was created using MOE 2014.09 software (Chemical Computing Group, Montreal, Canada). The principal and complementary subunits are colored in cyan and magenta, respectively. The loops A–F are colored in green.

Noncompetitive antagonists (NCAs) bind to allosteric binding sites different from the GABA recognition site, and are also termed as channel blockers as they directly block

chloride channels. In addition, GABARs contain several allosteric sites for a variety of positive modulators, such as benzodiazepines, barbiturates, avermectins, and neurosteroids (Olsen and Sieghart, 2009; Rudolph and Möhler, 2006).

1.3.1. Agonists

Systematic modification of the natural neurotransmitter GABA indicated that GABARs can be activated by a number of compounds. Representative agonists are shown in Figure 1.6. Mammalian $GABA_ARs$ and $GABA_CRs$ have different pharmacological responses to agonists. For instance, muscimol and isoguvacine are potent full agonists at $GABA_ARs$ but weak partial agonists at $GABA_CRs$ (Krall et al., 2015; Zhang et al., 2001). 5-Methyl-1*H*-imidazole-4-acetic acid (5-Me-IAA) is a selective $GABA_CR$ agonist with little activity at $\alpha1\beta2\gamma2$ $GABA_ARs$ (Johnston et al., 2010). Some agonists also display differential effects on various $GABA_ARs$ subtypes. 4,5,6,7-Tetrahydroisoxazolo-[5,4-c]pyridin-3-ol (THIP) is a partial agonist at $\alpha4\beta3\gamma2$ $GABA_ARs$, whereas it is a super agonist for $\alpha4\beta\delta/\alpha6\beta\delta$ $GABA_ARs$ (Krall et al., 2015). 5-(4-Piperidyl)-3-isothiazolol (thio-4-PIOL) is a parital agonist at extrasynapitc $GABA_ARs$ with sigificantly lower efficacy at synapitc $GABA_ARs$ (Hoestgaard-Jensen et al., 2013). Insect GABARs are sensitvie to both $GABA_AR$ and $GABA_CR$ agonsits. Muscimol is one of the most potent agonists at *Drosophila* RDLRs expressed in *Xenopus* oocytes (McGonigle et al., 2010). Several studies indicated that native and cloned GABARs from different insect species and nematodes are sensitive to most of mammalian GABAR agonists (Barbara et al., 2005; Kaji et al., 2015; Narusuye et al., 2007; Ozoe, 2013). However, the activity of thio-4-PIOL at insect GABARs has yet to be determined. I first observed that

thio-4-PIOL was an antagonist of insect GABARs, which will be mentioned in the following Chapter 2.

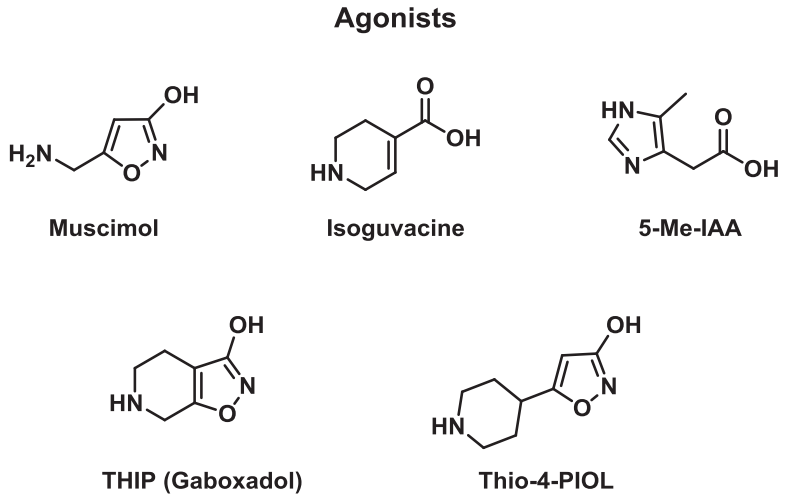

Figure 1.6 Chemical structures of representative agonists at GABARs.

1.3.2. NCAs

A large number of structurally diverse NCAs of GABARs including natural proudcts and synthetic compounds have been indentified (Fig. 1.7). Picrotoxin containing an equimolar mixture of picrotoxinin and picrotin was isolated from the fruit of the climbing plant *Anamirta cocculus*. It has been known as an antagonist to inhibit GABARs for decades (Casida and Durkin, 2015). Picrotoxinin is a more potent NCA than picrotin. Picrotoxin is not specific for GABARs as it also blocks other Cys-loop receptors such as GlyRs and 5-HT_3Rs (Das et al., 2003; Wang et al., 2006).

Bicyclophosphates such as 4-*t*-butylbicyclophosphorothionate (TBPS) as another class of identified NCAs were first found to show high affinity to rat GABARs and low activity to HF GABARs (Ju and Ozoe, 1999; Ozoe, 2013). Introduction of an isopropyl group into the

3-position of TBPS and an alky group with appropriate length into the 4-position resulted in analogues that exhibited excellent selectivity for HF versus rat GABARs (Ju and Ozoe, 2000; Ju et al., 2010; Ozoe, 2013). Further modification of the bicyclophosphates generated another series of bicycloorthocarboxylate NCAs such as 4'-ethynyl-4-*n*-propyl-bicycloorthobenzoate (EBOB), which exhibits high affinity for both mammalian and insect GABARs. Subsequently, [^{3}H]EBOB has been developed to be a useful radioligand for labeling the NCA blocker sites of both vertebrate and invertebrate GABARs (Cole and Casida, 1992).

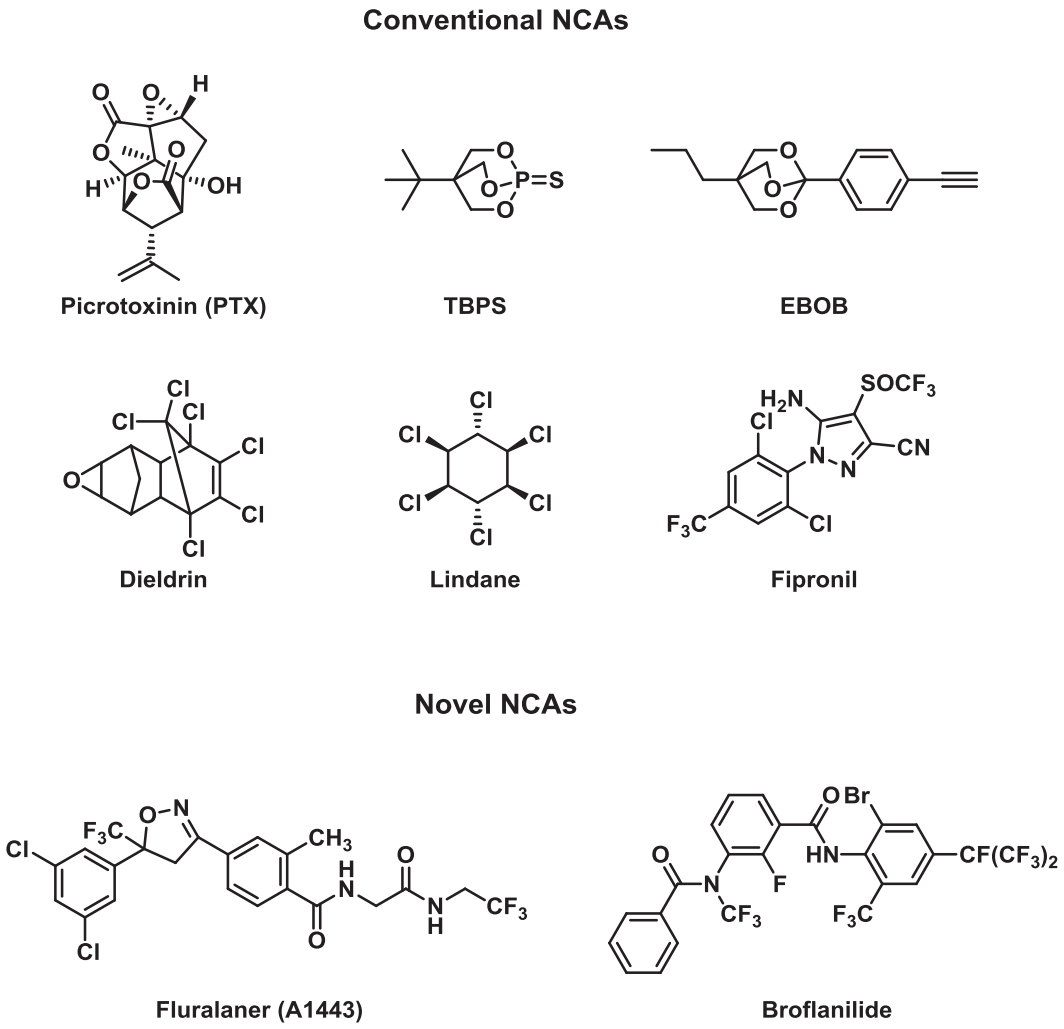

Figure 1.7 Chemical structures of representative NCAs at GABARs.

The polychlorocycloalkanes such as lindane and dieldrin (Fig. 1.7) were developed as NCA insecticides and widely used in the mid-to-late 20th century. Nowadays these insecticides have been banned in most of the world due to their high risks for human health and environment. Fipronil is the first successful phenylpyrazole insecticide that blocks both invertebrate GABARs and GluCls (Kita et al., 2014; Zhao et al., 2004). It has high activity against various insect pests and relative low toxicity against mammals.

The above-mentioned NCAs are classified as a conventional type in this dissertation. These NCAs are considered to act at the channel pore formed by five TM2 segments in GABARs (Fig. 1.8). A number of studies indicated that 2' and 6' amino acids are of most importance for the bindings of these conventional NCAs in GABARs (Ozoe et al., 2009; Ozoe, 2013; Fig. 1.8B). Unfortunately, insect pests have generated resistance to these conventional NCA insecticides. Mutations A2'S, A2'G, and A2'N in RDLRs have been reported to be associated with insecticide resistance in various insect species (Domingues et al., 2013; ffrench-Constant et al., 1991; Nakao et al., 2010, 2011, 2012; Nakao and Hirase, 2013; Taylor-Wells et al., 2015).

Two novel chemotypes of insecticidal NCAs, including isoxazolines and benzamides, were developed in the last five years (Casida and Durkin, 2015; Fig. 1.7). These novel antagonists were reported to act at a distinct allosteric site(s), which differ(s) from those for conventional NCAs, and are effective against insecticide-resistant pests carrying A2' mutations in their RDLRs (Casida, 2015; Gassel et al., 2014; Lahm et al., 2013; Nakao et al., 2013; Nakao and Banba, 2015; Ozoe et al., 2010, 2013). Researchers from Nissan Chemical Industries Ltd. discovered the insecticidal isoxazolines. Fluralaner and afoxolaner are two

new commercially available ectoparasiticides derived from the isoxazolines (Beugnet et al., 2015; Sparks and Nauen, 2014). Scientists from Mitsui Chemicals Argo Inc. found the benzamides also termed as meta-diamides. One of the benzamides, broflanilide, is expected to become a promising insecticide because it overcomes the emerging resistance of insect pests to conventional NCAs (Nakao and Banba, 2015; Sparks and Nauen, 2014).

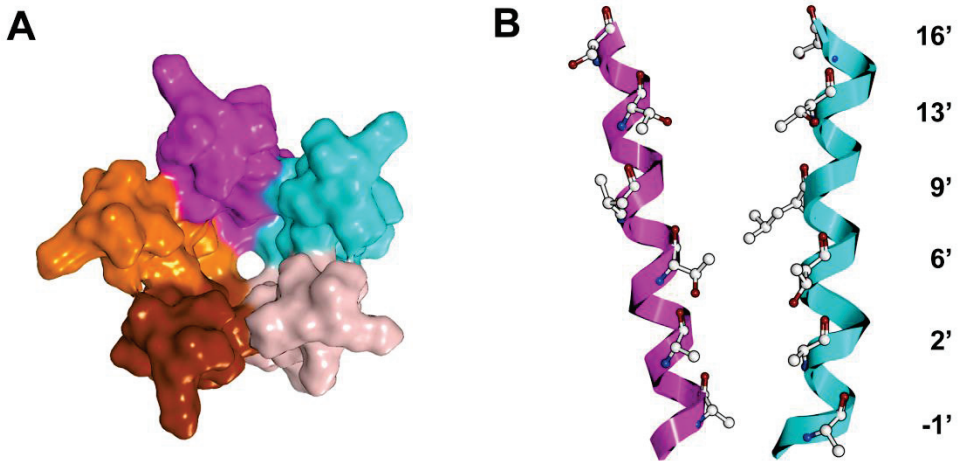

Figure 1.8 Channel pore of the HF RDLR homology model. The model is same as the previously mentioned in Figure 1.5. (A) Channel pore formed by five TM2 segments. Different subunits are colored differently. (B) Two adjacent TM2 segments of the pore with pore-facing residues labeled and side chains in stick representation. These residues are designated with an index numbering system for the TM2 membrane-spanning region (Charnet et al., 1990).

1.3.3. CAs

CAs are useful molecules to characterize the othosteric binding site of GABARs. Bicuculline and gabazine (SR95531) are representative $GABA_AR$ CAs, and (1,2,5,6-tetrahydropyridin-4-yl)methylphosphinic acid (TPMPA) is the most selective $GABA_CR$ CA (Johnston et al., 2010; Johnston, 2013; Fig. 1.9). A convulsant amidine steroid RU5135

(3α-hydroxy-16-imino-5β-17-aza-androstan-11-one) was reported to acted as a CA with low nanomolar potency at mammalian GABARs, and it was also a GlyR antagonist sharing a common site with strychnine (Olsen, 1984; Johnston, 2013).

CAs bind to the orthosteric site but inhibit the activation of the receptors as NCAs do. In addition to the established NCAs of insect GABARs, CAs may also prove useful in developing novel insecticides. However, our knowledge on insect GABAR CAs is scanty compared with those on NCAs and mammalian GABAR CAs. Gabazine exhibits weak or moderate antagonistic activity against insect GABARs, whereas bicuculline is inactive against most insect GABARs (Ozoe, 2013). A 5-phenyl-substituted gabazine analogue was found to be a moderate CA with micromolar affinity at the parasitic nematode *Ascaris suum* GABARs, whereas it has relative low activity at mammalian GABARs (Duittoz and Martin, 1991; Martin et al., 1995). These findings are useful for designing selective insecticides using gabazine analogues. Our recent studies revealed that the antagonism of insect RDLRs by gabazine analogues is enhanced by introducing bulky aromatic groups into the 3-position of the dihydroiminopyridazine ring (Rahman et al., 2012, 2014). In addition, chrodrimanin B, a meroterpenoid, was reported to most likely act at the orthosteric site of the silkworm (*Bombyx mori*) RDLRs to inhibit GABA-induced response (Xu et al., 2015; Fig. 1.9). It shows nanomolar potency at *B. mori* RDLRs but much weaker activity at human α1β2γ2 $GABA_A$Rs (Xu et al., 2015). This selectivity is also informative to design safe insecticides. However, it has yet to be solved whether this compound is a CA. To control insecticide-resistant pests, it is nessesary to develop insecticides that act at novel targets or at novel sites of the target.

Studies on novel high-affinity CAs and their interaction mechanisms will be of great importance for developing novel GABAR-targeting insecticides.

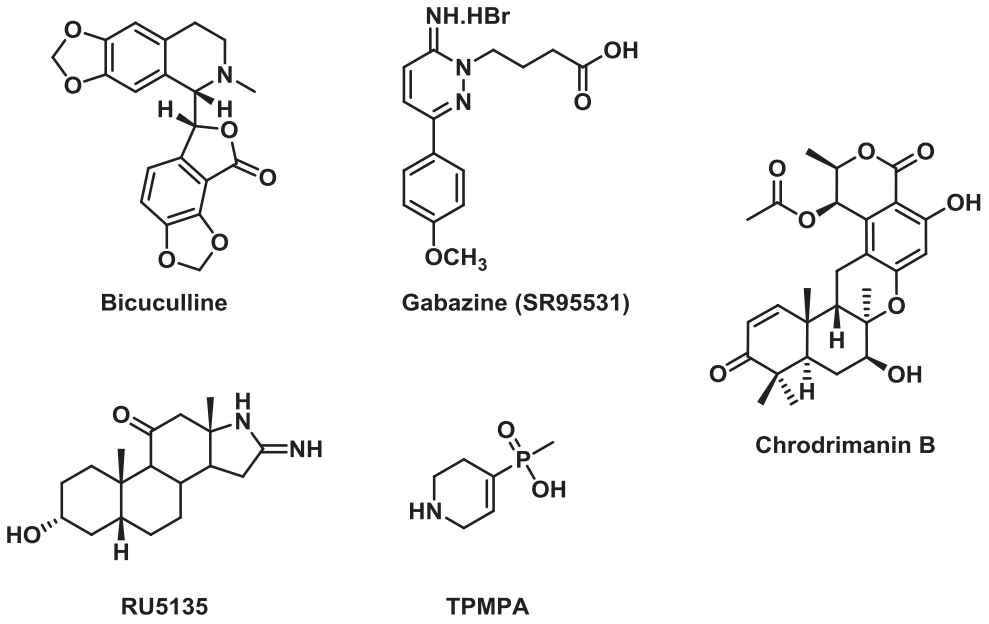

Figure 1.9 Chemical structures of representative CAs at GABARs.

1.4. Objectives

Efforts focused on insect GABARs might further develop novel insecticides because of the presence of multiple binding sites in insect GABARs. CAs have the potential to become novel insecticides as they inhibit GABARs by binding to the orthosteric site, which differs from the allosteric sites of NCA insecticides. However, CAs of insect GABARs have not been well understood and no potent CA is available at present. The objective of this dissertation is to seek effective CAs for insect GABARs. The design and synthesis of probable CAs for insect GABARs in the present study are primarily based on two lead compounds, thio-4-PIOL and muscimol, which are partial and full agonists of $GABA_AR$s, recepectively (Fig. 1.10). This study may provide useful information for characterizing the

orthosteric binding site of insect GABARs through the synthesis of these new CAs, subsequent interpretation of their structure-activity relationships, and further prediction of their interaction mechanisms by molecular simulations.

1.4.1. Thio-4-PIOL analogues

Thio-4-PIOL, 5-(4-piperidyl)-3-isoxazolol (4-PIOL), and 4-(4-piperidyl)-1-hydroxy-pyrazole (4-PHP) (Fig. 1.10) were first reported to be partial agonists of $GABA_A$Rs (Frølund et al., 1995; Hoestgaard-Jensen et al., 2013; Krall et al., 2015; Kristiansen et al., 1991). Several series of 4-substituted 4-PIOL and thio-4-PIOL analogues, and 5-substituted 4-PHP analogues (Fig. 1.10) were then developed as potent CAs of mammalian $GABA_A$Rs (Frølund et al., 2002, 2005, 2007; Krehan et al., 2006; Møller et al., 2010; Mortensen et al., 2002). These antagonists have not been evaluated in insect GABARs. To explore CAs that act at the orthosteric site of insect GABARs, I first synthesized a series of 4-substituted thio-4-PIOL analogues (Fig. 1.10) and examined their antagonism of insect RDLRs cloned from three insect species using a fluorescent imaging plate reader (FLIPR) membrane potential (FMP) or a two-electrode voltage clamp (TEVC) assay. The details are described in Chapter 2.

1.4.2. Muscimol analogues

Another series of CAs was designed on the basis of the muscimol structure and the findings from the previously synthesized thio-4-PIOL analogues. Muscimol is an agonist of insect GABARs, which contains a 3-isoxazolol moiety. In fact, 4-PIOL and thio-4-PIOL were derived from the structural modification of muscimol. The studies in Chapter 2

indicated that introduction of bicyclic aromatic substituents into the 4-position of thio-4-PIOL led to analogues with significantly enhanced antagonism of insect RLDRs. It is plausible that introduction of the same substituents into the 4-position of muscimol possibly assist in increasing the antagonism of insect RDLRs. Thus, I describe the synthesis of a series of 4,5-disubstituted 3-isoxazolols (Fig. 1.10) and their antagonism of four splice variants of HF RDLRs in Chapter 3.

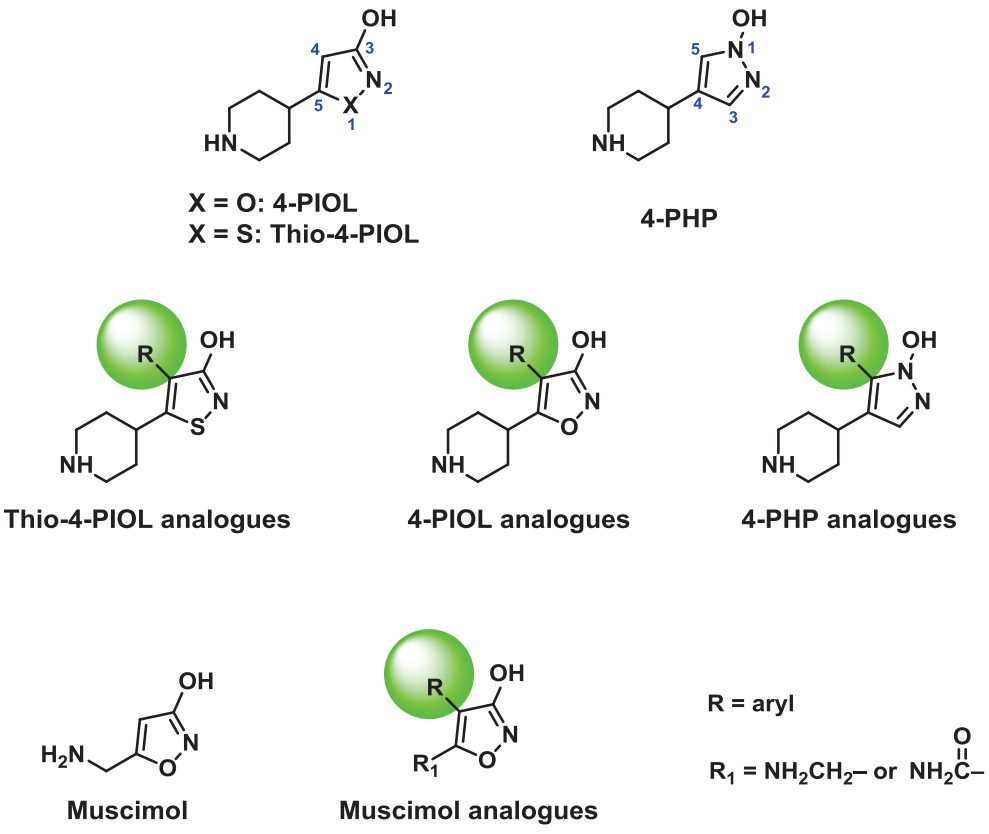

Figure 1.10 Chemical structures of 4-PIOL, thio-4-PIOL, 4-PHP, muscimol, and their analogues as the target compounds for synthesis. The aryl-substituted positions of these analogues are indicated in green.

1.4.3. 4-PIOL and 4-PHP analogues

To verify the bioisosteric potentials of the 3-isoxazolol and the 1-hydroxypyrazole for competitive antagonism of insect GABARs, I further pharmacologically characterized three 4-substituted 4-PIOLs and a 5-substituted 4-PHP (Fig. 1.10) in three insect RDLRs expressed in *Xenopus* oocytes using the TEVC method. Potential interactions between the potent ligands and the orthosteric site of insect RDLRs were discussed through homology modeling and molecular docking studies. The details are described in Chapter 4.

Chapter 2

Competitive antagonism of insect GABA receptors by 4-substituted 5-(4-piperidyl)-3-isothiazolols

2.1. Introduction

Insect RDLRs contain multiple binding sites for a variety of ligands and are one of important targets of insecticides and parasiticides. Practical insecticides, such as dieldrin and fipronil, bind to a common allosteric site within the chloride channel and lead to a channel block (Ozoe, 2013). Two novel classes of ectoparasiticides/insecticides, isoxazolines (Gassel et al., 2014; Ozoe et al., 2010) and benzamides (Nakao et al., 2013; Ozoe et al., 2013), act as antagonists at a distinct allosteric site(s) in RDLRs. In contrast to these NCAs, little is known about CAs of RDLRs. Studies on the interaction of agonists with amino acid residues in the orthosteric site of RDLRs revealed that the agonist profile of RDLRs differ from those of $GABA_A$Rs and $GABA_C$Rs (Buckingham and Sattelle, 2010; Lummis et al., 2011; Ashby et al., 2012), and identification of specific CAs of insect RDLRs might provide useful information that leads to the development of safe insecticides. As CAs inhibit receptor activation by binding to a site that is distinct from the sites of NCAs (Othman et al., 2012), information on CAs might also be utilized for the development of novel insecticides or parasiticides that are effective against emerging insects resistant to conventional GABAR-targeting insecticides, such as fipronil (Nakao et al., 2011, 2012).

Several gabazine analogues synthesized in our previous study showed greater antagonism

of insect GABARs than gabazine (Rahman et al., 2012, 2014). Recently, a series of 4-substituted 4-PIOL and thio-4-PIOL analogues was developed as potent competitive $GABA_AR$ antagonists in mammals (Frølund et al., 2002, 2005, 2007; Krehan et al., 2006; Mortensen et al., 2002; Fig. 1.10). The bioisosteric replacement of the 3-isoxazolol moiety of 4-PIOL with 1-hydroxypyrazole also led to potent CAs in mammalian $GABA_ARs$ (Møller et al., 2010). These antagonists have not been tested for their antagonism of insect GABARs. To explore the orthosteric site of insect RDLRs, I synthesized a novel series of 4-substituted thio-4-PIOL analogues and provide a first account for the relationship between their structure and antagonism of RDLRs cloned from three insect species including small brown planthopper (SBP, *Laodelphax striatellus*), common cutworm (CC, *Spodoptera litura*), and HF.

2.2. Materials and methods

2.2.1. General methods for chemistry

All reagents and solvents were purchased from Wako Pure Chemical Industries, Ltd. (Osaka, Japan) and Tokyo Chemical Industry Co., Ltd. (Tokyo, Japan), unless otherwise noted. Melting points were determined using a YANACO MP-500D micro melting pointing apparatus and are uncorrected. ^1H and ^{13}C NMR spectra were recorded using a JEOL JNM A-400 spectrometer. Chemical shifts are reported in parts per million (ppm) on the δ scale, and coupling constants, *J*s, are reported in hertz (Hz). Multiplicities are reported as ‘s’ (singlet), ‘d’ (doublet), ‘t’ (triplet), ‘q’ (quartet), ‘h’ (heptet), ‘m’ (multiplet), and ‘b’ (broad). Mass spectra (MS) were measured using a JEOL JMS-GC mate II (electron ionization) or a

Waters XEVO (positive electrospray ionization, ESI+) mass spectrometer. High-resolution mass spectral (HRMS) data were obtained using an ESI+ mode on a Waters SYNAPT G2 or a Waters LCT Premier XE spectrometer.

All air- and moisture-sensitive reactions were performed under an argon atmosphere using the syringe-septum technique, and glassware was oven-dried prior to use. Compounds were visualized on thin layer chromatography (silica gel 60 F254 plates, Merck KGaA, Darmstadt, Germany) using UV light or $KMnO_4$ spraying reagent. Column chromatography was performed using silica gel (Wakogel C-200, 75−150 μm, Wako). Compounds containing the 3-isothiazolol moiety were visualized using $FeCl_3$ spraying reagent. The major intermediates were synthesized in six steps as shown in Scheme 2.1 according to a previously reported method (Krehan et al., 2006).

Scheme 2.1 Synthesis of intermediates **4** and **6**[a]

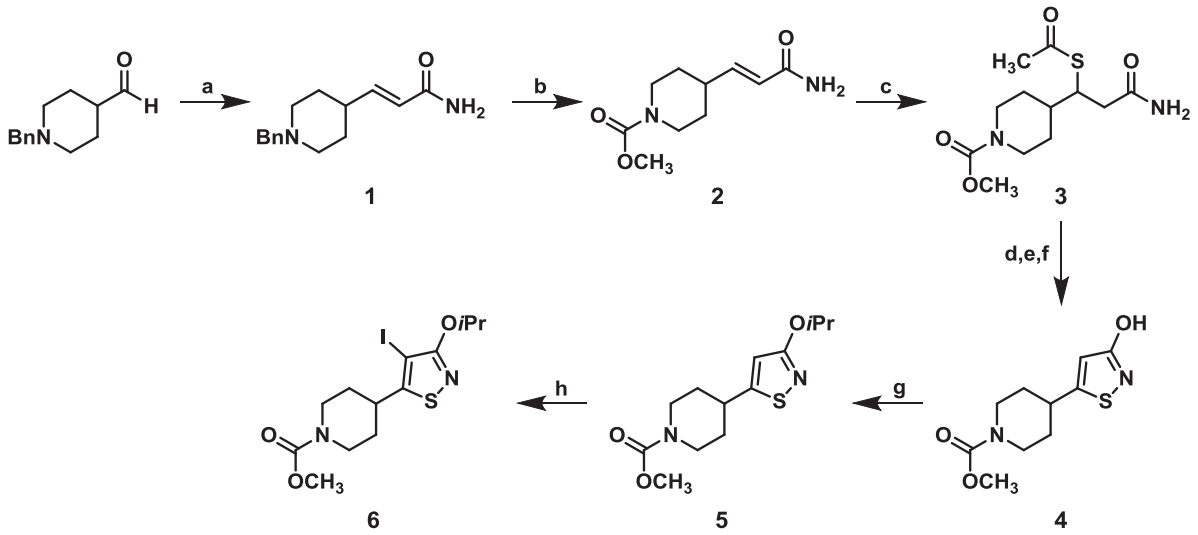

[a]Reagents and conditions: (a) Diethyl 2-amino-2-oxoethylphosphonate, NaH, rt; (b) $ClCOOCH_3$, rt; (c) CH_3COSH, EtOAc, rt; (d) aq. NaOH rt; (e) 30% H_2O_2, 50 °C; (f) SO_2Cl_2, $ClCH_2CH_2Cl$, rt; (g) *i*-PrBr, DMF, K_2CO_3, 70 °C (h) ICl, HOAc, H_2O, 80 °C.

2.2.2. Synthesis of (*E*)-3-(1-benzyl-4-piperidyl)acrylamide (1)

Sodium hydride (60%, 2.56 g, 64 mmol) was added slowly to a suspension of diethyl 2-amino-2-oxoethylphosphonate (Zhang et al., 2009) (12.48 g, 64 mmol) in dimethoxyethane (120 mL) followed by dropwise addition of a solution of *N*-benzyl-protected 4-formylpiperidine aldehyde (6.50 g, 32 mmol) in dimethoxyethane (10 mL). The reaction mixture was stirred for 3 h at room temperature and then quenched with water (50 mL).The pH was adjusted to 2 with 2M HCl, and the acidic phase was washed with Et_2O (3 × 100 mL). Then the pH was adjusted to 10 with 4M NaOH to precipitate the product. The alkaline water phase was filtered and extracted with Et_2O (3 × 100 mL). The combined organic phases were dried, evaporated under reduced pressure, and combined with the filtered product. Recrystallization (EtOAc) gave **1** (6.7g, 85%) as light yellow solid. mp 150–152 °C. ^{1}H NMR ($CDCl_3$): δ 7.35–7.21 (5H, m, Ar–H), 6.83 (1H, dd, *J* = 15.6, 6.8 Hz, C<u>H</u>=CHCO), 5.79 (1H, dd, *J* = 15.6, 1.5 Hz, CH=C<u>H</u>CO), 5.40 (2H, bs, CON<u>H</u>$_2$), 3.50 (2H, s, C<u>H</u>$_2$–Ph), 2.95–2.87 (2H, d, *J* = 11.7 Hz, C<u>H</u>$_2$NC<u>H</u>$_2$), 2.20–1.92 (3H, m, C<u>H</u>$_2$NC<u>H</u>$_2$, $CH_2CH_2C\underline{H}CH_2CH_2$), 1.71 (2H, m, $CH_2C\underline{H}_2CHC\underline{H}_2CH_2$), 1.56–1.43 (2H, dq, *J* = 12.7, 3.4 Hz, $CH_2C\underline{H}_2CHC\underline{H}_2CH_2$). MS: *m/z* 244.2 $[M]^+$.

2.2.3. Synthesis of (*E*)-3-(1-methoxycarbonyl-4-piperidyl)acrylamide (2)

Methyl chloroformate (5 mL, 65.2 mmol) was added quickly to a suspension of compound **2** (7.95 g, 32.6 mmol) in CH_2Cl_2 (30 mL). The reaction mixture was stirred for 4 h, evaporated under reduced pressure, and added to water (60 mL). The aqueous phase was extracted with EtOAc (5 × 60 mL). The combined organic phases were dried and evaporated

giving a white solid. Recrystallization (EtOAc) afforded **2** (5.42 g, 78%) as colorless crystals. mp 152–153 °C. ^{1}H NMR ($CDCl_3$): δ 6.82 (1H, dd, *J* = 15.6, 6.8 Hz, C<u>H</u>=CHCO), 5.81 (1H, dd, *J* = 15.6, 1.5 Hz, CH=C<u>H</u>CO), 5.47 (2H, bs, CON<u>H</u>$_2$), 4.15 (2H, bs, C<u>H</u>$_2$NC<u>H</u>$_2$), 3.70 (3H, s, COOC<u>H</u>$_3$), 2.82 (2H, bt, *J* = 12.5 Hz, C<u>H</u>$_2$NC<u>H</u>$_2$), 2.35–2.28 (1H, m, $CH_2CH_2C\underline{H}CH_2CH_2$), 1.75 (2H, bd, *J* = 13.2 Hz, $CH_2C\underline{H}_2CHC\underline{H}_2CH_2$), 1.40–1.25 (2H, m, $CH_2C\underline{H}_2CHC\underline{H}_2CH_2$). MS: *m/z* 234.8 $[M+Na]^+$, 250.8 $[M+K]^+$.

2.2.4. Synthesis of 3-acetylsulfanyl-3-(1-methoxycarbonyl-4-piperidyl)propanamide (3)

To a suspension of compound **2** (4.24 g, 20 mmol) in CH_2Cl_2 (30 mL) was added thioacetic acid (1.67 mL, 22 mmol). The reaction mixture was stirred for 48 h at room temperature followed by evaporation under reduced pressure. The residue was recrystallized (EtOAc) to give **3** (5.1 g, 89%) as colorless crystals. mp 124–125 °C. ^{1}H NMR ($CDCl_3$): δ 5.73 (1H, bs, CON<u>H</u>$_2$), 5.34 (1H, bs, CON<u>H</u>$_2$), 4.16 (2H, bs, C<u>H</u>$_2$NC<u>H</u>$_2$), 3.85–3.78 (1H, m, CHC<u>H</u>SCH$_2$), 3.68 (3H, s, COOC<u>H</u>$_3$), 2.78–2.49 (4H, m, CHC<u>H</u>$_2$CO, C<u>H</u>$_2$NC<u>H</u>$_2$), 2.35 (3H, s, SCOC<u>H</u>$_3$), 1.95–1.62 (3H, m, $CH_2CH_2C\underline{H}CH_2CH_2$, $CH_2C\underline{H}_2CHC\underline{H}_2CH_2$), 1.38–1.11 (2H, m, $CH_2C\underline{H}_2CHC\underline{H}_2CH_2$). MS: *m/z* 310.9 $[M+Na]^+$, 326.8 $[M+K]^+$.

2.2.5. Synthesis of 5-(1-methoxycarbonyl-4-piperidyl)-3-isothiazolol (4)

A solution of NaOH (1.44 g, 36 mmol) in H_2O (10 mL) was added to compound **3** (5.2 g, 18 mmol), and the reaction was stirred for 4 h at room temperature. The pH was adjusted to 5 with 2 M H_2SO_4, and the acidic mixture was extracted with CH_2Cl_2 (3 × 20mL). The

combined organic phases were dried and evaporated under reduced pressure to afford a white solid. The solid was suspended in water (20 mL), heated to 50 °C, and H_2O_2 (35%, 1.5 mL, 13 mmol) was added dropwise. The reaction mixture was stirred for 24 h at 50 °C followed by evaporation under reduced pressure giving a white foam, which was dissolved in $ClCH_2CH_2Cl$ (15 mL). SO_2Cl_2 (0.73 mL, 9 mmol) was added slowly to the solution, and the reaction mixture was stirred for 24 h at room temperature before adding additional SO_2Cl_2 (0.36 mL, 4.5 mmol). Stirring was continued for 8 h after which additional SO_2Cl_2 (0.36 mL, 4.5 mmol) was added. The mixture was stirred for 16 h followed by evaporation under reduced pressure. To the residue was added water (30 mL), and the solution was extracted with EtOAc (5 × 30 mL). The combined organic phases were dried and evaporated under reduced pressure. Recrystallization (EtOAc) gave **5** (1.45g, 33%) as light brown crystals. mp 163–165 °C. ^{1}H NMR ($CDCl_3$): δ 6.33 (1H, s, Ar–H), 4.23 (2H, bs, C$\underline{H}_2$NC$\underline{H}_2$), 3.72 (3H, s, COOC$\underline{H}_3$), 3.04–2.81 (3H, m, C$\underline{H}_2$NC$\underline{H}_2$, $CH_2CH_2C\underline{H}CH_2CH_2$), 2.00 (2H, bd, J = 13.6 Hz, $CH_2C\underline{H}_2CHC\underline{H}_2CH_2$), 1.63 (2H, dq, J = 12.7, 3.8 Hz, $CH_2C\underline{H}_2CHC\underline{H}_2CH_2$). MS: *m/z* 242.1 $[M]^+$.

2.2.6. Synthesis of 3-isopropoxy-5-(1-methoxycarbonyl-4-piperidyl)isothiazole (5)

To a solution of **4** (1.1 g, 4.6 mmol) in dry DMF (30 mL) was added K_2CO_3 (0.7 g, 5.1 mmol), and the mixture was stirred at 60 °C for 30 min. Isopropyl bromide (0.65 mL, 6.9 mmol) was added to the mixture, and stirring was continued at 70 °C for 16 h. The reaction mixture was added to H_2O (30 mL) and extracted with *n*-hexane (4 × 30 mL). The combined organic phases were dried and evaporated under reduced pressure. Column chromatography

afforded **5** (1.07 g, 82%) as a pale yellow oil. ^{1}H NMR ($CDCl_3$): δ 6.31 (1H, s, Ar–H), 5.14 (1H, h, *J* = 6.2 Hz, $CH_3C\underline{H}CH_3$), 4.20 (2H, bs, $C\underline{H}_2NC\underline{H}_2$), 3.71 (3H, s, $COOC\underline{H}_3$), 3.04–2.81 (3H, m, $C\underline{H}_2NC\underline{H}_2$, $CH_2CH_2C\underline{H}CH_2CH_2$), 1.99 (2H, bd, *J* = 11.7 Hz, $CH_2C\underline{H}_2CHC\underline{H}_2CH_2$), 1.71–1.54 (2H, m, $CH_2C\underline{H}_2CHC\underline{H}_2CH_2$), 1.36 (6H, d, *J* = 6.3 Hz, $C\underline{H}_3CHC\underline{H}_3$). MS: *m/z* 284.1 $[M]^+$.

2.2.7. Synthesis of 4-iodo 3-isopropoxy-5-(1-methoxycarbonyl-4-piperidyl)isothiazole (6)

To a solution of compound **5** (625 mg, 2.2 mmol) in HOAc (5 mL), a solution of ICl in HOAc (5.9 mL, 4.4 mmol) was added dropwise followed by addition of H_2O (20 mL). The reaction mixture was stirred at 80 °C for 16 h. The reaction mixture was added to $Na_2S_2O_4$ (s) and evaporated under reduced pressure. The residue was dissolved in H_2O (40 mL) and extracted with Et_2O (3 × 40 mL). The combined organic phases were washed with 2% aqueous $Na_2S_2O_4$ (3 × 50 mL), dried, and evaporated under reduced pressure. Column chromatography afforded **6** (720 mg, 80%) as a light yellow oil. ^{1}H NMR ($CDCl_3$): δ 5.15 (1H, h, *J* = 6.1 Hz, $CH_3C\underline{H}CH_3$), 4.27 (2H, bs, $C\underline{H}_2NC\underline{H}_2$), 3.72 (3H, s, $COOC\underline{H}_3$), 3.08 (1H, tt, *J* = 12.0, 3.7 Hz, $CH_2CH_2C\underline{H}CH_2CH_2$), 2.90 (2H, bt, *J* = 11.5 Hz, $C\underline{H}_2NC\underline{H}_2$), 2.03 (2H, bd, *J* = 12.2 Hz, $CH_2C\underline{H}_2CHC\underline{H}_2CH_2$), 1.71–1.54 (2H, m, $CH_2C\underline{H}_2CHC\underline{H}_2CH_2$), 1.40 (6H, d, *J* = 5.9 Hz, $C\underline{H}_3CHC\underline{H}_3$). MS: *m/z* 410.0 $[M]^+$.

2.2.8. General procedure for the synthesis of 4-aryl/alkyl-3-isopropoxy-5-(1-methoxy-carbonyl-4-piperidyl)isothiazole (7b–k)

A mixture of **6**, an appropriate aryl/alkyl boronic acid, DMF, and aqueous potassium

carbonate was stirred at 90 °C for 24 h (Scheme 2.2). The reaction mixture was filtrated through celite. The organic phase was washed with water, aqueous NaOH, and brine, dried, and evaporated. Column chromatography gave the product **7b**–**k**.

Scheme 2.2 Synthesis of 4-substituted 5-(4-piperidyl)-3-isothiazolols[a]

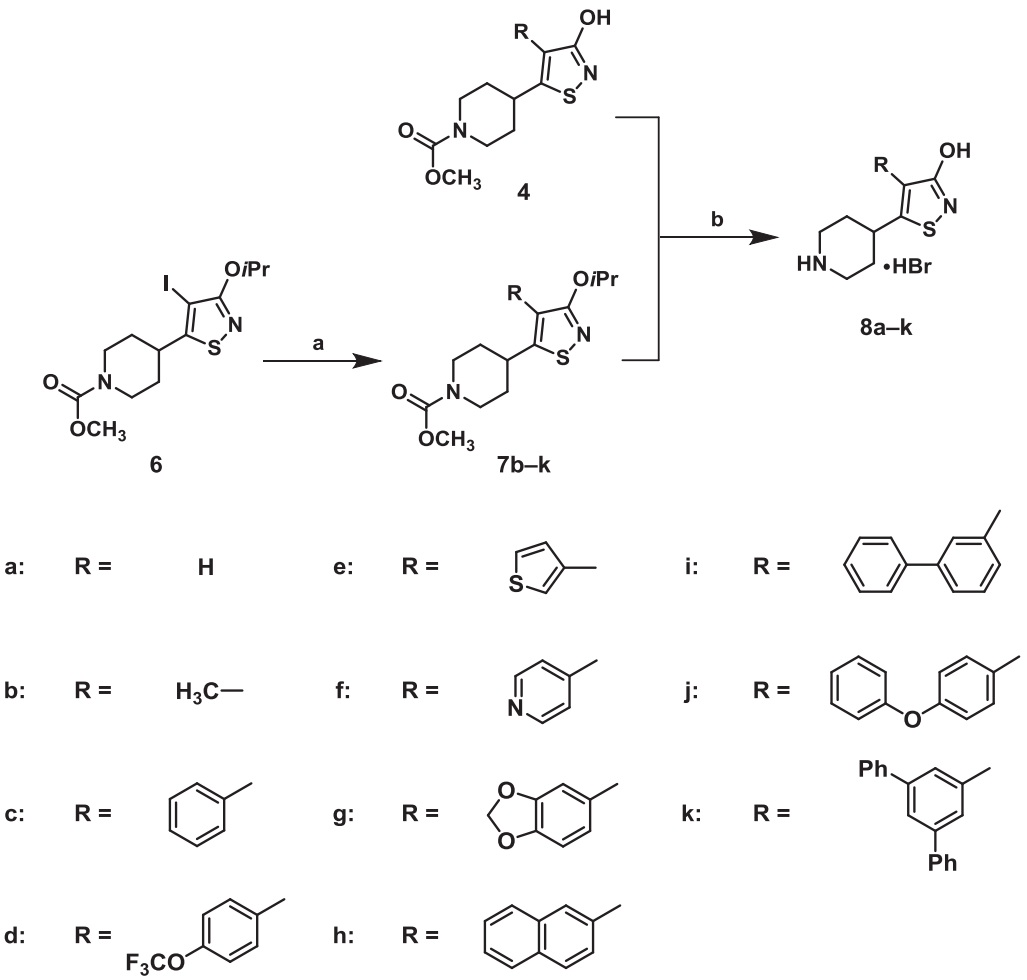

[a]Reagents and conditions: (a) $RB(OH)_2$, $Pd(PPh_3)_2Cl_2$, aq. K_2CO_3, DMF, 90 °C; (b) 33% HBr, CH_3COOH.

2.2.8.1. 3-Isopropoxy-5-(1-methoxycarbonyl-4-piperidyl)-4-methylisothiazole (7b)

Yield (67%). ^{1}H NMR (400 MHz, $CDCl_3$): δ 5.15 (1H, h, J = 6.3 Hz, $CH_3C\underline{H}CH_3$), 4.21 (2H, bs, $C\underline{H}_2NC\underline{H}_2$), 3.71 (3H, s, $COOC\underline{H}_3$), 2.98 (1H, tt, J = 12.2, 3.7 Hz,

$CH_2CH_2C\underline{H}CH_2CH_2$), 2.87 (2H, bt, *J* = 13.2 Hz, $C\underline{H}_2NC\underline{H}_2$), 1.98 (3H, s, Ar–$C\underline{H}_3$), 1.96–1.85 (2H, m, $CH_2C\underline{H}_2CHC\underline{H}_2CH_2$), 1.65–1.55 (2H, m, $CH_2C\underline{H}_2CHC\underline{H}_2CH_2$), 1.36 (6H, d, *J* = 6.3 Hz, $C\underline{H}_3CHC\underline{H}_3$). MS: *m*/z 298.1 $[M]^+$.

2.2.8.2. 3-Isopropoxy -5-(1-methoxycarbonyl-4-piperidyl)-4-phenylisothiazole (7c)

Yield (95%). ^{1}H NMR (400 MHz, $CDCl_3$): δ 7.46–7.25 (5H, m, Ar–H), 5.19 (1H, h, *J* = 6.2 Hz, $CH_3C\underline{H}CH_3$), 4.18 (2H, bs, $C\underline{H}_2NC\underline{H}_2$), 3.69 (3H, s, $COOC\underline{H}_3$), 3.10 (1H, tt, *J* = 12.0, 3.6 Hz, $CH_2CH_2C\underline{H}CH_2CH_2$), 2.73 (2H, bt, *J* = 12.4 Hz, $C\underline{H}_2NC\underline{H}_2$), 1.88 (2H, bd, *J* = 12.2 Hz, $CH_2C\underline{H}_2CHC\underline{H}_2CH_2$), 1.66–1.52 (2H, m, $CH_2C\underline{H}_2CHC\underline{H}_2CH_2$), 1.32 (6H, d, *J* = 6.3 Hz, $C\underline{H}_3CHC\underline{H}_3$). MS: *m*/*z* 360.1 $[M]^+$.

2.2.8.3 3-Isopropoxy-5-(1-methoxycarbonyl-4-piperidyl)-4-(4-trifluoromethoxy)phenyl-isothiazole (7d)

Yield (84%). ^{1}H NMR (400 MHz, $CDCl_3$): 7.35–7.24 (4H, m, Ar–H), 5.19 (1H, h, *J* = 6.3 Hz, $CH_3C\underline{H}CH_3$), 4.21 (2H, bs, $C\underline{H}_2NC\underline{H}_2$), 3.70 (3H, s, $COOC\underline{H}_3$), 3.07 (1H, tt, *J* = 12.0, 3.7 Hz, $CH_2CH_2C\underline{H}CH_2CH_2$), 2.76 (2H, bt, *J* = 12.4 Hz, $C\underline{H}_2NC\underline{H}_2$), 1.88 (2H, bd, *J* = 12.7 Hz, $CH_2C\underline{H}_2CHC\underline{H}_2CH)_2$, 1.68–1.52 (2H, m, $CH_2C\underline{H}_2CHC\underline{H}_2CH_2$), 1.33 (6H, d, *J* = 6.3 Hz, $C\underline{H}_3CHC\underline{H}_3$). MS: *m*/*z* 444.1 $[M]^+$.

2.2.8.4. 3-Isopropoxy-5-(1-methoxycarbonyl-4-piperidyl)-4-(3-thienyl)isothiazole (7e)

Yield (87%). ^{1}H NMR (400 MHz, $CDCl_3$): δ 7.41–7.15 (3H, m, Ar–H), 5.21 (1H, h, *J* = 6.0 Hz, $CH_3C\underline{H}CH_3$), 4.20 (2H, bs, $C\underline{H}_2NC\underline{H}_2$), 3.71 (3H, s, $COOC\underline{H}_3$), 3.23 (1H, tt, *J* = 12.0,

3.6 Hz, $CH_2CH_2C\underline{H}CH_2CH_2$), 2.80 (2H, bt, *J* = 12.7 Hz, $C\underline{H}_2NC\underline{H}_2$), 1.93 (2H, bd, *J* = 12.2 Hz, $CH_2C\underline{H}_2CHC\underline{H}_2CH_2$, 1.67–1.50 (2H, m, $CH_2C\underline{H}_2CHC\underline{H}_2CH_2$), 1.36 (6H, d, *J* = 6.3 Hz, $C\underline{H}_3CHC\underline{H}_3$). MS: *m*/*z* 366.1 $[M]^+$.

2.2.8.5. 3-Isopropoxy-5-(1-methoxycarbonyl-4-piperidyl)-4-(4-pyridinyl)isothiazole (7f)

Yield (81%). ^{1}H NMR (400 MHz, $CDCl_3$): δ 8.68 (2H, d, *J* = 5.9, Ar–H), 7.72–7.62 (2H, m, Ar–H), 5.20 (1H, h, *J* = 6.3 Hz, $CH_3C\underline{H}CH_3$), 4.22 (2H, bs, $C\underline{H}_2NC\underline{H}_2$), 3.70 (3H, s, $COOC\underline{H}_3$), 3.11 (1H, tt, *J* = 12.1, 3.7 Hz, $CH_2CH_2C\underline{H}CH_2CH_2$), 2.76 (2H, bt, *J* = 12.7 Hz, $C\underline{H}_2NC\underline{H}_2$), 1.89 (2H, bd, *J* = 12.7 Hz, $CH_2C\underline{H}_2CHC\underline{H}_2CH_2$, 1.70–1.55 (2H, m, $CH_2C\underline{H}_2CHC\underline{H}_2CH_2$), 1.33 (6H, d, *J* = 6.3 Hz, $C\underline{H}_3CHC\underline{H}_3$). MS: *m*/*z* 361.2 $[M]^+$.

2.2.8.6. 3-Isopropoxy-5-(1-methoxycarbonyl-4-piperidyl)-4-(3,4-methylenedioxyphenyl)-isothiazole (7g)

Yield (88%). ^{1}H NMR (400 MHz, $CDCl_3$): 6.90–6.64 (3H, m, Ar–H), 6.02 (2H, s, O–$C\underline{H}_2$–O), 5.19 (1H, h, *J* = 6.3 Hz, $CH_3C\underline{H}CH_3$), 4.17 (2H, bs, $C\underline{H}_2NC\underline{H}_2$), 3.70 (3H, s, $COOC\underline{H}_3$), 3.09 (1H, tt, *J* = 12.0, 3.7 Hz, $CH_2CH_2C\underline{H}CH_2CH_2$), 2.75 (2H, bt, *J* = 12.4 Hz, $C\underline{H}_2NC\underline{H}_2$), 1.88 (2H, bd, *J* = 12.2 Hz, $CH_2C\underline{H}_2CHC\underline{H}_2CH_2$), 1.65–1.52 (2H, m, $CH_2C\underline{H}_2CHC\underline{H}_2CH_2$), 1.33 (6H, d, *J* = 6.3 Hz, $C\underline{H}_3CHC\underline{H}_3$). MS: *m*/*z* 404.1 $[M]^+$.

2.2.8.7. 3-Isopropoxy-5-(1-methoxycarbonyl-4-piperidyl)-4-(2-naphthyl)isothiazole (7h)

Yield (86%). ^{1}H NMR (400 MHz, $CDCl_3$): δ 7.92–7.72 (4H, m, Ar–H), 7.55–7.39 (3H, m, Ar–H), 5.22 (1H, h, *J* = 6.2 Hz, $CH_3C\underline{H}CH_3$), 4.17 (2H, bs, $C\underline{H}_2NC\underline{H}_2$), 3.68 (3H, s,

COOC$\underline{H}_3$), 3.17 (1H, tt, *J* = 12.0, 3.7 Hz, $CH_2CH_2C\underline{H}CH_2CH_2$), 2.70 (2H, bt, *J* = 12.4 Hz, $C\underline{H}_2NC\underline{H}_2$), 1.91 (2H, bd, *J* = 12.2 Hz, $CH_2C\underline{H}_2CHC\underline{H}_2CH_2$), 1.67–1.58 (2H, m, $CH_2C\underline{H}_2CHC\underline{H}_2CH_2$), 1.32 (6H, d, *J* = 5.9 Hz, $C\underline{H}_3CHC\underline{H}_3$). MS: *m*/*z* 411.1 $[M+H]^+$, 433.1 $[M+Na]^+$.

2.2.8.8. 4-(3-Biphenylyl)-3-isopropoxy-5-(1-methoxycarbonyl-4-piperidyl)isothiazole (7i)

Yield (76%). ^{1}H NMR (400 MHz, $CDCl_3$): δ 7.63–7.25 (9H, m, Ar–H), 5.22 (1H, h, *J* = 6.0 Hz, $CH_3C\underline{H}CH_3$), 4.19 (2H, bs, $C\underline{H}_2NC\underline{H}_2$), 3.69 (3H, s, COOC$\underline{H}_3$), 3.17 (1H, tt, *J* = 12.2, 3.6 Hz, $CH_2CH_2C\underline{H}CH_2CH_2$), 2.76 (2H, bt, *J* = 12.4 Hz, $C\underline{H}_2NC\underline{H}_2$), 1.92 (2H, bd, *J* = 12.2 Hz, $CH_2C\underline{H}_2CHC\underline{H}_2CH_2$), 1.69–1.57 (2H, m, $CH_2C\underline{H}_2CHC\underline{H}_2CH_2$), 1.35 (6H, d, *J* = 6.3 Hz, $C\underline{H}_3CHC\underline{H}_3$). HRMS: *m*/*z* calcd for $C_{25}H_{29}N_2O_3S$ $[M+H]^+$ 437.1899, found 437.1920.

2.2.8.9. 3-Isopropoxy-5-(1-methoxycarbonyl-4-piperidyl)-4-(4-phenoxyphenyl)isothiazole (7j)

Yield (73%). ^{1}H NMR (400 MHz, $CDCl_3$): δ 7.42–7.25 (5H, m, Ar–H), 7.19–7.00 (4H, m, Ar–H), 5.19 (1H, h, *J* = 6.1 Hz, $CH_3C\underline{H}CH_3$), 4.19 (2H, bs, $C\underline{H}_2NC\underline{H}_2$), 3.70 (3H, s, COOC$\underline{H}_3$), 3.11 (1H, tt, *J* = 12.0, 3.7 Hz, $CH_2CH_2C\underline{H}CH_2CH_2$), 2.76 (2H, bt, *J* = 12.5 Hz, $C\underline{H}_2NC\underline{H}_2$), 1.89 (2H, bd, *J* = 13.2 Hz, $CH_2C\underline{H}_2CHC\underline{H}_2CH_2$), 1.67–1.60 (2H, m, $CH_2C\underline{H}_2CHC\underline{H}_2CH_2$), 1.33 (6H, d, *J* = 6.3 Hz, $C\underline{H}_3CHC\underline{H}_3$). HRMS: *m*/*z* calcd for $C_{25}H_{29}N_2O_4S$ $[M+H]^+$ 453.1848, found 453.1833.

2.2.8.10. 3-Isopropoxy-5-(1-methoxycarbonyl-4-piperidyl)-4-(5'-*m*-terphenylyl)isothiazole (7k)

Yield (91%). ^{1}H NMR (400 MHz, $CDCl_3$): δ 7.82–7.32 (13H, m, Ar–H), 5.25 (1H, h, J = 6.1 Hz, $CH_3C\underline{H}CH_3$), 4.22 (2H, bs, $C\underline{H}_2NC\underline{H}_2$), 3.69 (3H, s, $COOC\underline{H}_3$), 3.23 (1H, tt, J = 12.0, 3.6 Hz, $CH_2CH_2C\underline{H}CH_2CH_2$), 2.78 (2H, bt, J = 12.7 Hz, $C\underline{H}_2NC\underline{H}_2$), 1.96 (2H, bd, J = 12.7 Hz, $CH_2C\underline{H}_2CHC\underline{H}_2CH_2$), 1.72–1.58 (2H, m, $CH_2C\underline{H}_2CHC\underline{H}_2CH_2$), 1.38 (6H, d, J = 6.3 Hz, $C\underline{H}_3CHC\underline{H}_3$). MS: m/z 513.2 $[M+H]^+$.

2.2.9. General procedure for the synthesis of 4-aryl/alkyl-5-(1-methoxycarbonyl-4-piperidyl)-3-isothiazolol (8a–k)

Compounds **4** and **7b–k** was dissolved in a solution of HBr in AcOH (10 mL, 33%), and the mixture was stirred at 70 °C for 48 h (Scheme 2.2). The reaction mixture was evaporated followed by azeotropy with MeOH-toluene (1:1) three times, and the residue was recrystallized (MeOH/Et_2O) to give **8a–k**.

2.2.9.1. 5-(4-Piperidyl)-3-isothiazolol hydrobromide (8a, thio-4-PIOL)

Yield (83%), mp 216–218 °C. ^{1}H NMR (400 MHz, CD_3OD): δ 6.44 (1H, s, Ar–H), 3.48 (2H, bd, J = 13.2 Hz, $C\underline{H}_2NC\underline{H}_2$), 3.28–3.22 (1H, m, $CH_2CH_2C\underline{H}CH_2CH_2$), 3.21–3.08 (2H, m, $C\underline{H}_2NC\underline{H}_2$), 2.26 (2H, bd, J = 13.2 Hz, $CH_2C\underline{H}_2CHC\underline{H}_2CH_2$), 1.96–1.80 (2H, m, $CH_2C\underline{H}_2CHC\underline{H}_2CH_2$). ^{13}C NMR (100 MHz, CD_3OD): δ 172.25, 170.76, 110.19, 44.89, 35.15, 30.85. HRMS: m/z calcd for $C_8H_{13}N_2OS$ $[M–Br]^+$ 185.0749, found 185.0731.

2.2.9.2. 4-Methyl-5-(4-piperidyl)-3-isothiazolol hydrobromide (8b)

Yield (65%), mp 263–264 °C (dec). ^{1}H NMR (400 MHz, CD_3OD): δ 3.52–3.45 (2H, m, C$\underline{H}_2$NC$\underline{H}_2$), 3.43–3.33 (1H, m, $CH_2CH_2C\underline{H}CH_2CH_2$), 3.23-3.10 (2H, m, C$\underline{H}_2NC\underline{H}_2$), 2.19 (2H, bd, *J* = 14.1 Hz, $CH_2C\underline{H}_2CHC\underline{H}_2CH_2$), 2.03 (3H, s, Ar–C$\underline{H}_3$) 1.82 (2H, dq, *J* = 13.7, 3.5 Hz, $CH_2C\underline{H}_2CHC\underline{H}_2CH_2$). ^{13}C NMR (100 MHz, CD_3OD): δ 170.45, 163.27, 119.10, 45.09, 34.86, 30.14, 10.21. HRMS: *m*/*z* calcd for $C_9H_{15}N_2OS$ $[M–Br]^+$ 199.0905, found 199.0906.

2.2.9.3. 4-Phenyl-5-(4-piperidyl)-3-isothiazolol hydrobromide (8c)

Yield (84%), mp 244–245 °C (dec). ^{1}H NMR (400 MHz, CD_3OD): δ 7.49–7.30 (5H, m, Ar–H), 3.41–3.33 (3H, m, C$\underline{H}_2$NC$\underline{H}_2$, $CH_2CH_2C\underline{H}CH_2CH_2$), 3.08–2.95 (2H, m C$\underline{H}_2NC\underline{H}_2$), 2.15 (2H, bd, *J* = 14.1 Hz, $CH_2C\underline{H}_2CHC\underline{H}_2CH_2$), 1.95–1.75 (2H, m, $CH_2C\underline{H}_2CHC\underline{H}_2CH_2$). ^{13}C NMR (100 MHz, CD_3OD): δ 168.82, 166.68, 133.82, 130.74, 129.76, 129.02, 124.74, 44.96, 35.12, 30.89. HRMS: *m*/*z* calcd for $C_{14}H_{17}N_2OS$ $[M–Br]^+$ 261.1062, found 261.1063.

2.2.9.4. 5-(4-Piperidyl)-4-(4-trifluoromethoxyphenyl)-3-isothiazolol hydrobromide (8d)

Yield (76%), mp 249–250 ºC. ^{1}H NMR (400 MHz, CD_3OD): δ 7.52-7.32 (4H, m, Ar–H), 3.46–3.34 (3H, m, C$\underline{H}_2$NC$\underline{H}_2$, $CH_2CH_2C\underline{H}CH_2CH_2$), 3.06 (2H, dt, *J* = 13.4, 2.9 Hz, C$\underline{H}_2$NC$\underline{H}_2$), 2.16 (2H, bd, *J* = 14.1 Hz, $CH_2C\underline{H}_2CHC\underline{H}_2CH_2$), 1.86 (2H, dq, *J* = 13.6, 3.9 Hz, $CH_2C\underline{H}_2CHC\underline{H}_2CH_2$). ^{13}C NMR (100 MHz, CD_3OD): δ 168.38, 163.27, 139.29, 132.89, 132.60, 131.12, 123.13, 122.81, 122.20, 44.90, 35.02, 31.01. HRMS: *m*/*z* calcd for $C_{15}H_{16}F_3N_2O_2S$ $[M–Br]^+$ 345.0885, found 345.0887.

2.2.9.5. 5-(4-Piperidyl)-4-(3-thienyl)-3-isothiazolol hydrobromide (8e)

Yield (74%), mp 254–256 °C. ^{1}H NMR (400 MHz, CD_3OD): δ 7.56–7.48 (2H, m, Ar–H), 7.29–7.25 (1H, m, Ar–H), 3.53 (1H, tt, *J* = 12.2, 3.7 Hz, $CH_2CH_2C\underline{H}CH_2CH_2$), 3.48–3.40 (2H, m $C\underline{H}_2NC\underline{H}_2$), 3.09 (2H, dt, *J* = 12.9, 2.9 Hz, $C\underline{H}_2NC\underline{H}_2$), 2.20 (2H, bd, *J* = 14.1 Hz, $CH_2C\underline{H}_2CHC\underline{H}_2CH_2$), 1.92–1.78 (2H, dq, *J* = 13.2, 3.4 Hz, $CH_2C\underline{H}_2CHC\underline{H}_2CH_2$). ^{13}C NMR (100 MHz, CD_3OD): δ 168.84, 166.20, 133.38, 129.26, 126.66, 125.36, 119.66, 45.03, 35.28, 30.86. HRMS: *m*/*z* calcd for $C_{12}H_{15}N_2OS_2$ $[M–Br]^+$ 267.0626, found 267.0630.

2.2.9.6. 5-(4-Piperidyl)-4-(4-pyridinyl)-3-isothiazolol hydrobromide (8f)

Yield (86%), mp 240–242 °C (dec). ^{1}H NMR (400 MHz, CD_3OD): δ 8.93–8.88 (2H, m, Ar–H), 8.27–8.05 (2H, m, Ar–H), 3.73 (1H, tt, *J* = 12.0, 3.5 Hz, $CH_2CH_2C\underline{H}CH_2CH_2$), 3.52-3.40 (2H, m, $C\underline{H}_2NC\underline{H}_2$), 3.28–3.18 (2H, m, $C\underline{H}_2NC\underline{H}_2$), 2.26 (2H, bd, *J* = 14.1 Hz, $CH_2C\underline{H}_2CHC\underline{H}_2CH_2$), 1.92 (2H, dq, *J* = 13.6, 3.6 Hz, $CH_2C\underline{H}_2CHC\underline{H}_2CH_2$). ^{13}C NMR (100 MHz, CD_3OD): δ 167.43, 163.22, 152.52, 142.79, 128.81, 118.75, 44.87, 34.92, 31.30. HRMS: *m*/*z* calcd for $C_{13}H_{16}N_3OS$ $[M–Br]^+$ 267.1014; found 267.1025.

2.2.9.7. 4-(3,4-Methylenedioxyphenyl)-5-(4-piperidyl)-3-isothiazolol hydrobromide (8g)

Yield (54%), mp 236–238 ºC (dec). ^{1}H NMR (400 MHz, CD_3OD): δ 6.92–6.65 (3H, m, Ar–H), 5.99 (2H, s, O–$C\underline{H}_2$–O), 3.46–3.36 (3H, m, $C\underline{H}_2NC\underline{H}_2$, $CH_2CH_2C\underline{H}CH_2CH_2$), 3.04 (2H, dt, *J* = 13.2, 2.4 Hz, $C\underline{H}_2NC\underline{H}_2$), 2.15 (2H, bd, *J* = 14.1 Hz, $CH_2C\underline{H}_2CHC\underline{H}_2CH_2$), 1.84 (dq, *J* = 13.2, 3.9 Hz, $CH_2C\underline{H}_2CHC\underline{H}_2CH_2$). ^{13}C NMR (100 MHz, CD_3OD): δ 169.00, 164.28,

150.66, 148.66, 124.87, 123.56, 109.51, 104.94, 103.69, 44.94, 38.21, 30.79. HRMS: *m*/*z* calcd for $C_{15}H_{17}N_2O_3S$ $[M–Br]^+$ 305.0960, found 305.0957.

2.2.9.8. 4-(2-Naphthyl)-5-(4-piperidyl)-3-isothiazolol hydrobromide (8h)

Yield (90%), mp 205–206 ºC. ^{1}H NMR (400 MHz, CD_3OD): δ 7.97-7.82 (4H, m, Ar–H), 7.57–7.46 (3H, m, Ar–H), 3.50–3.35 (3H, m, C<u>H</u>$_2$NC<u>H</u>$_2$, CH_2CH_2C<u>H</u>CH_2CH_2), 2.99 (2H, dt, *J* = 13.2, 3.2 Hz, C<u>H</u>$_2$NC<u>H</u>$_2$), 2.18 (2H, bd, *J* = 14.1 Hz, CH_2C<u>H</u>$_2CHC$<u>H</u>$_2CH_2$), 1.86 (2H, dq, *J* = 13.6, 3.7 Hz, CH_2C<u>H</u>$_2CHC$<u>H</u>$_2CH_2$). ^{13}C NMR (100 MHz, CD_3OD): δ 166.98, 163.30, 131.38, 129.80, 129.31, 129.12, 128.71, 128.42, 127.51, 124.74, 44.95, 35.20, 30.94. HRMS: *m*/*z* calcd for $C_{18}H_{19}N_2OS$ $[M–Br]^+$ 311.1218, found 311.1219.

2.2.9.9. 4-(3-Biphenylyl)-5-(4-piperidyl)-3-isothiazolol hydrobromide (8i)

Yield (86%), mp 242–244 ºC. ^{1}H NMR (400 MHz, CD_3OD): δ 7.66–7.31 (9H, m, Ar–H), 3.50–3.37 (3H, m, C<u>H</u>$_2$NC<u>H</u>$_2$, CH_2CH_2C<u>H</u>CH_2CH_2), 3.03 (2H, dt, *J* = 13.2, 2.6 Hz, C<u>H</u>$_2$NC<u>H</u>$_2$), 2.19 (2H, bd, *J* = 13.7 Hz, CH_2C<u>H</u>$_2CHC$<u>H</u>$_2CH_2$), 1.86 (2H, dq, *J* = 13.6, 3.5 Hz, CH_2C<u>H</u>$_2CHC$<u>H</u>$_2CH_2$). ^{13}C NMR (100 MHz, CD_3OD): δ 168.84, 166.88, 142.99, 141.97, 134.48, 130.33, 129.98, 129.63, 129.30, 128.63, 128.10, 127.68, 124.67, 44.95, 35.20, 30.97. HRMS: *m*/*z* calcd for $C_{20}H_{21}N_2OS$ $[M–Br]^+$ 337.1375, found 337.1380.

2.2.9.10. 4-(4-Phenoxyphenyl)-5-(4-piperidyl)-3-isothiazolol hydrobromide (8j)

Yield (71%), mp 188–189 ºC. ^{1}H NMR (400 MHz, CD_3OD): δ 7.42–7.31 (4H, m, Ar–H), 7.18–7.00 (5H, m, Ar–H), 3.45–3.36 (3H, m, C<u>H</u>$_2$NC<u>H</u>$_2$, CH_2CH_2C<u>H</u>CH_2CH_2), 3.05 (2H, dt,

J = 13.2, 3.1 Hz, C$\underline{H_2}$NC$\underline{H_2}$), 2.17 (2H, bd, *J* = 14.1 Hz, CH$_2$C$\underline{H_2}$CHC$\underline{H_2}$CH$_2$), 1.85 (2H, dq, *J* = 13.2, 3.9 Hz, CH$_2$C$\underline{H_2}$CHC$\underline{H_2}$CH$_2$). ^{13}C NMR (100 MHz, CD$_3$OD): δ 168.80, 166.44, 158.71, 132.24, 130.97, 128.52, 124.81, 124.06, 120.30, 119.53, 44.95, 35.10, 31.02. HRMS: *m*/*z* calcd for $C_{20}H_{21}N_2O_2S$ $[M–Br]^+$ 353.1324, found 353.1328.

2.2.9.11. 5-(4-piperidyl)-4-(5'-m-terphenyly)-3-isothiazolol hydrobromide (8k)

Yield (86%), mp 263–265 ºC (dec). ^{1}H NMR (400 MHz, CD$_3$OD): δ 7.90–7.31 (13H, m, Ar–H), 3.52-3.35 (3H, m, C$\underline{H_2}$NC$\underline{H_2}$, CH$_2$CH$_2$C$\underline{H}$CH$_2$CH$_2$), 3.05 (2H, dt, *J* = 13.2, 2.7 Hz, C$\underline{H_2}$NC$\underline{H_2}$), 2.23 (2H, bd, *J* = 13.7 Hz, CH$_2$C$\underline{H_2}$CHC$\underline{H_2}$CH$_2$), 1.95–1.82 (2H, m, CH$_2$C$\underline{H_2}$CHC$\underline{H_2}$CH$_2$). ^{13}C NMR (100 MHz, CD$_3$OD): δ 164.42, 163.30, 143.68, 141.90, 137.50, 130.05, 128.80, 128.25, 126.59, 126.43, 124.61, 44.90, 35.27, 30.97. HRMS: *m*/*z* calcd for $C_{26}H_{25}N_2OS$ $[M–Br]^+$ 413.1688, found 413.1700.

2.2.10. FMP assays

The antagonist activities of the synthesized analogues were examined against cloned SBP (DDBJ accession No. AB253526, Narusuye et al., 2007) and CC (DDBJ accession No. DD171257, Nakao et al., 2013) RDL_{bd} GABARs, using the FMP assay as previously described (Nakao et al., 2010). In brief, the *Drosophila* cell lines expressing SBP or CC RDLRs were washed and dispersed in buffered saline (120 mM NaCl, 5 mM KCl, 2 mM $CaCl_2$, 8 mM $MgCl_2$, 10 mM HEPES, and 32 mM sucrose, adjusted to pH 7.2 with an NaOH solution), and aliquots (100 μL each) of this cell suspension (5×10^5 cells) were added to 96-well microplates for the fluorescent assay. After 10 min, the cells were spun down at 1400

rpm for 5 min and loaded with the FMP blue dye reagent (Molecular Devices, Sunnyvale, CA) 10-fold diluted with the saline (100 μL) at room temperature for 20 min. The synthesized analogues were first dissolved in dimethyl sulfoxide (DMSO) and diluted with the saline. The solution (25 μL) containing the test compounds and 1% DMSO was then added to the cells in each well and incubated with for 74 s. Subsequently, GABA in saline (25 μL) was added to each well. After the subsequent addition of 10 μM or 25 μM GABA in the saline (25 μL) to each well, the fluorescent intensity at 560 nm when excited at 530 nm was measured using a Flex-Station II plate reader (Molecular Devices). The GABA concentrations used in these experiments were the half maximal effective concentration (EC_{50}) for SBP (1 μM) and CC (2.5 μM) RDLRs. The inhibition percentage was determined based on changes in fluorescence before (the average value for 20 s) and after (the maximal value after 10–60 s) the addition of GABA. Each assay was repeated twice, unless otherwise noted.

2.2.11. Electrophysiology

2.2.11.1. Preparation of HF RDL cRNA

The linear template cDNA encoding the HF RDL_{ac} subunit (DDBJ accession Nos.: AB177547, complete cds of RDL_{bd}; AB824728, partial cds of exon 3a version; AB824729, partial cds of exon 6c version) was obtained by amplifying the plasmid pBluescript KS(–)–*MdRdl*$_{ac}$ by polymerase chain reaction (PCR) using KOD plus polymerase (Toyobo, Tokyo, Japan), a forward primer, 5'-TGTAAAACGACGGCCAGT-3', and a reverse primer, 5'-CAGGAAACAGCTATGACC-3'. The PCR products were purified using the illustra GFX PCR DNA and Gel Band Purification Kit (GE Healthcare UK, Ltd., Little Chalfont, UK), and

the integrity of amplified cDNAs was confirmed by sequence analysis. The capped cRNAs were synthesized using T7 polymerase (mMessage mMachine T7 Ultra Kit; Ambion, Austin, TX). The cRNAs were precipitated with LiCl, redissolved in sterile RNase-free water, diluted to a concentration of 543 ng/μL, and divided into portions that were stored at -80 °C until use.

2.2.11.2. TEVC

Ovarian lobes were surgically removed from mature female African clawed frogs (*Xenopus laevis*), which had been anaesthetized by immersion in 0.1% tricaine methylate for 30 min. The ovarian lobes were then treated with 2 mg/ml collagenase type I (Sigma-Aldrich Japan, Tokyo, Japan) in Ca^{2+}-free standard oocyte solution (SOS) (100 mM NaCl, 2 mM KCl, 1 mM $MgCl_2$, 5 mM HEPES, pH 7.6) for 90–120 min at room temperature. Stage V-VI oocytes were defolliculated manually. The oocytes were then gently washed with sterile SOS (100 mM NaCl, 2 mM KCl, 1.8 mM $CaCl_2$, 1 mM $MgCl_2$, 5 mM HEPES, pH 7.6) containing gentamycin (50 μg/mL, Life Technologies, Thermo Fisher Scientific Inc., Waltham, MA), penicillin (100 U/mL, Life Technologies), streptomycin (100 μg/mL, Life Technologies), and sodium pyruvate (2.5 mM, Sigma-Aldrich). Each oocyte was injected cytoplasmically with 5 ng of cRNA dissolved in RNase-free water (9.2 nL), and then the oocytes were incubated in sterile SOS for 48 h at 16 °C.

Electrophysiological experiments were performed as previously reported (Eguchi et al., 2006). Briefly, GABA-induced currents were recorded at a holding potential of –80 mV using an Oocyte Clamp OC-725C amplifier (Warner Instruments, Hamden, CT) and

Data-Trax2 software (World Precision Instruments Inc., Sarasota, FL). The glass capillary electrodes were fabricated using a micropipette puller (P-97, Sutter Instrument, Novato, CA) and filled with 2 M KCl (resistance ranging from 0.5 to 2.0 MΩ). Oocytes were placed in a recording bath that was continuously perfused with SOS at 18–22 °C.

GABA dissolved in SOS was applied to oocytes for 3 s, at intervals of 30–60 s to ensure a full recovery from desensitization. Dose–response curves were determined by sequential applications of increasing concentrations of GABA. Test compounds were dissolved in DMSO and then diluted with SOS to a final DMSO concentration of 0.1%, which did not induce any response in oocytes. The test compound solution was added to the perfusate after two successive control applications of GABA and was then applied consecutively for the remainder of the experiments. To ensure complete binding, antagonist solutions were perfused alone for 60 s before their coapplication with GABA. Then, GABA (10 μM) used at the approximate EC_{50} was coapplied with the antagonist for 3 s and was repeated at 30–60 s intervals to obtain the highest constant inhibition. All experiments were performed on at least four different oocytes obtained from at least two different frogs. EC_{50} and half maximal inhibitory concentration (IC_{50}) values were obtained from concentration–response data by nonlinear regression analysis using OriginPro 8J (OriginLab, Northampton, MA).

2.2.12. Insecticidal assays

The WHO/SRS strain of HFs was used in the present study. A solution of each test compound (**8h** and **8i**) dissolved in DMSO (0.1 μl) at various concentrations was injected into the dorsal side of the thorax of the HFs. This volume of DMSO solution alone did not

affect the viability of HFs. Twelve to fifteen HFs were used at each concentration. The HFs were maintained with sugar and water and were kept at 25 °C. The number of dead and/or paralyzed flies was counted after 24 h, and the experiments were repeated five times.

2.2.13. Homology modeling and ligand docking studies

The crystal structure of homopentameric *C. elegans* GluCl (PDB: 3RIF, Hibbs and Gouaux, 2011) was chosen as a template for building a HF RDL_{ac} GABAR model. A sequence alignment of the *C. elegans* GluCl α subunit and the HF RDL_{ac} subunit was carried out using ClustalW software and used to model all five subunits simultaneously using MOE 2011.10 software (Chemical Computing Group, Montreal, Canada). The created ligands were docked into the potential binding site of the generated model using ASEDock program (2011.01.27, Chemical Computing Group), which is a novel docking program based on a shape similarity assessment between a concave portion on a protein and a ligand (Goto et al., 2008). The energy of the receptor and ligands was minimized using the MMFF94x force field. The potential docking sites were searched using the Site Finder of MOE. The stable conformations of ligands were obtained by the conformational search. Tether weight was added to all receptor backbone atoms within 4.5 Å from a ligand, while others were free. The binding mode with the highest score was chosen for the final representation.

2.3. Results and discussion

2.3.1. Chemistry

In this chapter, a series of 4-substituted 5-(4-piperidyl)-3-isothiazolols were synthesized

as shown in Scheme 2.2. The intermediates **4** and **6** were synthesized in four and six steps, respectively, according to a reported method (Scheme 2.1; Krehan et al., 2006). Thio-4-PIOL (**8a**) was synthesized by removing the methoxycarbonyl group of **4** by treatment with hydrobromic acid in acetic acid. Compounds **7b**–**k** were derived from **6** by the Suzuki cross-coupling reaction using the appropriate aryl- or alkylboronic acid and $Pd(PPh_3)_2Cl_2$ in 67–95% yields. Thio-4-PIOL analogues **8b**–**k** were prepared by removing the methoxycarbonyl and isopropyl protecting groups of **7b**–**k** by treatment with hydrobromic acid in acetic acid.

2.3.2. Antagonism of SBP and CC GABARs

To investigate the functional characteristics of synthesized compounds in the GABARs of agricultural pest insects, I used *Drosophila* S2 cell lines that stably express RDL_{bd} GABARs cloned from SBPs and CCs, which cause serious damage to crops. The inhibition of GABA-induced membrane potential changes by synthesized analogues was examined using the FMP assays (Figs. 2.1 and 2.2).

Thio-4-PIOL (**8a**) was found to be a weak antagonist of SBP and CC RDLRs, with 34.4% and 8.8% inhibition of GABA-induced responses at 100 μM, respectively (Figs. 2.1 and 2.2). Thio-4-PIOL exhibited no agonist activity in either insect RDLR at 100 μM, whereas it was a partial agonist of human extrasynaptic subtypes of $GABA_A$Rs and showed marginal agonism at the synaptic subtypes of $GABA_A$Rs (Hoestgaard-Jensen et al., 2013). These findings indicate that a pharmacological difference exists between insect and mammalian GABARs. In order to examine whether the introduction of alkyl substituents or

monocyclic aromatic rings at the 4-position of the isothiazole ring increases the antagonistic activity, the methyl (**8b**), the phenyl (**8c**), the 4-trifluoromethoxylphenyl (**8d**), the 3-thienyl (**8e**), and the 4-pyridyl (**8f**) analogues were examined for their antagonistic activity. However, these compounds failed to exert pronounced effects, with less than 30% inhibition of GABA-induced responses in both SBP and CC RDLRs. These findings indicate that a small alkyl substituent and monocyclic aromatic rings at the 4-position are not beneficial for the antagonistic activity. Meanwhile, the 3,4-methylenedioxy substitution on the benzene ring of **8c** to give **8g** resulted in an increased antagonistic activity in SBP and CC RDLRs, with more than 50% inhibition at 100 μM, suggesting that the bicyclic system might be favorable for increasing the activity.

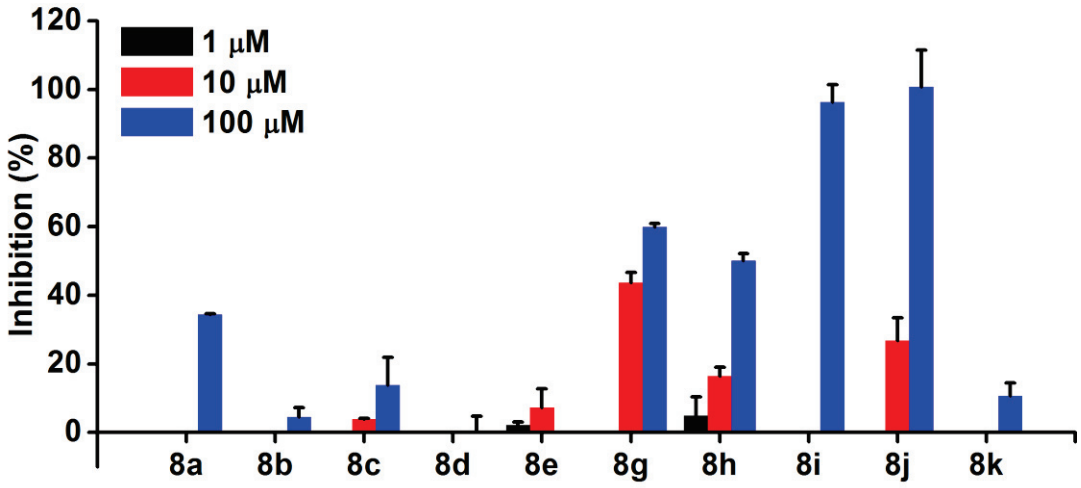

Figure 2.1 Inhibition of GABA-induced membrane potential changes by thio-4-PIOL analogues in SBP RDLRs expressed in *Drosophila* S2 cells. The EC_{50} (1.0 μM) of GABA was used to induce membrane potential changes. Data represent the means of two experiments with bars indicating the range of duplicates. Compound **8f** was omitted, as it had no effect.

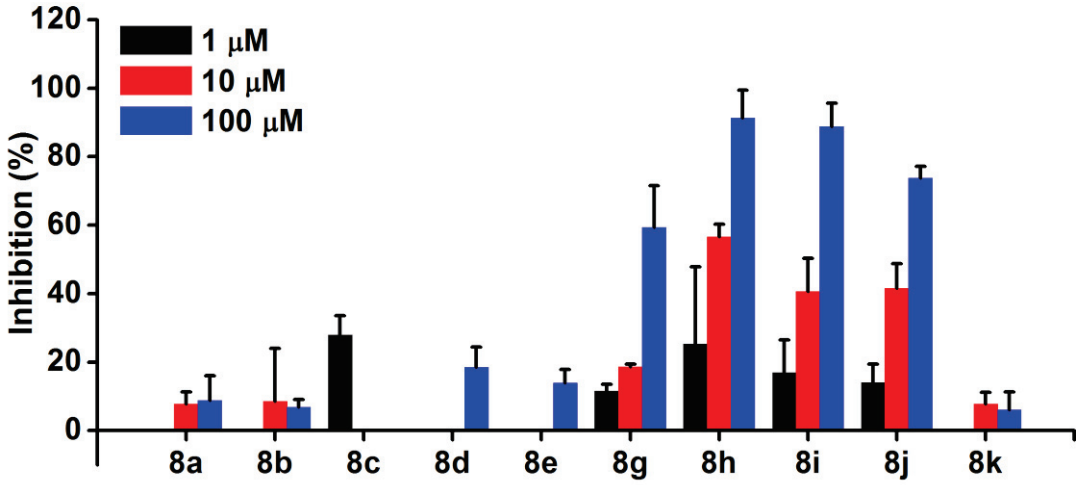

Figure 2.2 Inhibition of GABA-induced membrane potential changes by thio-4-PIOL analogues in CC RDLRs expressed in *Drosophila* S2 cells. The EC_{50} (2.5 μM) of GABA was used to induce membrane potential changes. Data represent the means of two experiments with bars indicating the range of duplicates. Compound **8f** was omitted, as it had no effect.

I next examined analogues with a bicyclic aromatic ring system at the 4-position. Replacement of the phenyl group of **8c** with a 2-naphthyl group to give **8h** markedly increased the activity in CC RDLRs, with 91.3% inhibition at 100 μM (Fig. 2.2), although no significant change in activity was observed in SBP RDLRs (Fig. 2.1). Compound **8h** showed 16.4% and 56.7% inhibition at 10 μM in SBP and CC RDLRs, respectively. Further increase in antagonistic activity in SBP RDLRs was observed in **8i** and **8j**, in which the 2-naphthyl group of **8h** has been replaced with a 3-biphenyl and a 4-phenoxyphenyl group, respectively, with approximately 96.3% and complete inhibition of GABA-induced responses at 100 μM, respectively (Fig. 2.1). As in SBP RDLRs, these compounds (**8h**, **8i,** and **8j**) showed high potencies as antagonists in CC RDLRs (Fig. 2.2). The IC_{50} values of **8h**, **8i,** and **8j** were estimated to be approximately 5.2 (3.6–7.8) μM, 10.6 (7.5–15.2) μM, and 18.0 (11.9–28.6) μM, (95% confidence interval in parentheses), respectively, using Probit analysis. These

findings indicate that analogues with bicyclic aromatic groups at the 4-position of the isothiazole ring are well tolerated at the binding site and that they are effective in antagonizing GABA-mediated receptor activation in SBP and CC RDLRs. However, introduction of 5'-*m*-terphenylyl group into the 4-position to give **8k** failed to increase the activity in both RDLRs, indicating that a substituent with three benzene rings is too bulky to fit into the binding site (Figs. 2.1 and 2.2).

2.3.3. Antagonism of HF GABARs

To study the pharmacological properties of synthesized compounds in the GABARs of a sanitary insect species HF, the antagonism of HF RDL_{ac} GABARs by synthesized analogues was examined using the *Xenopus* oocyte expression system. The inhibition of GABA-induced currents was recorded using the TEVC technique. A current trace in Figure 2.3A shows that GABA-induced currents were attenuated by the 2-naphthyl analog (**8h**). After confirmation of the constant amplitude of GABA-induced currents, the oocytes were perfused with an external solution containing 100 μM **8h**. During the perfusion, GABA (10 μM) was repeatedly applied at least three times. This analog attenuated the currents progressively, and a maximum inhibition of 88.4% was attained after the third application. The GABA-induced currents were recovered after washout of **8h**. The other analogues were also tested in a similar fashion. Figure 2.3B illustrates the inhibition of GABA-induced currents by synthesized antagonists at 100 μM.

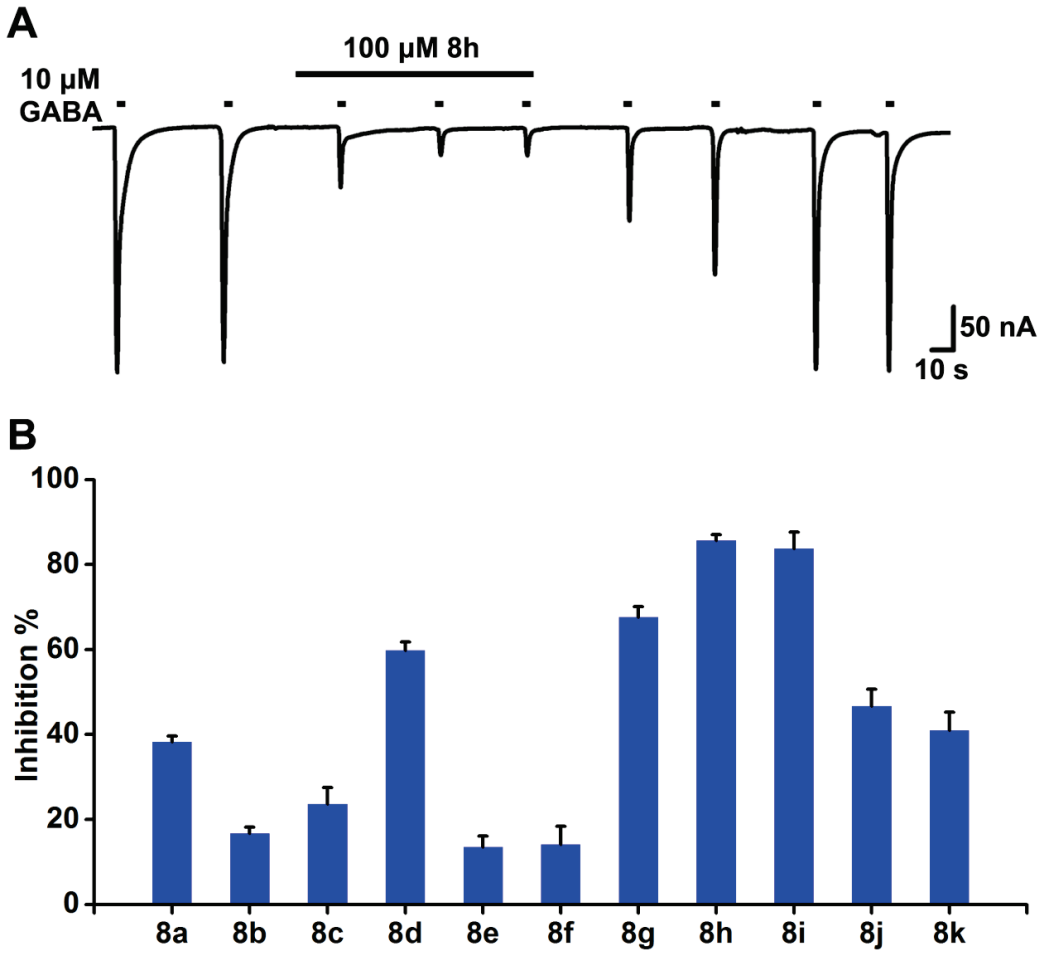

Figure 2.3 Inhibition of GABA-induced currents by thio-4-PIOL analogues in HF RDLRs expressed in *Xenopus* oocytes. (A) Progressive inhibition of currents by 100 µM **8h** and current recovery by washout. (B) Inhibition of currents by 100 µM of analogues. The EC_{50} (10 µM) of GABA was used to induce currents. Data represent means ± SEM (n = 4–6).

Thio-4-PIOL (**8a**) showed 38.2% inhibition of GABA-induced currents, which is in contrast to its partial agonist action at human $GABA_A$Rs (Mortensen et al., 2002; Hoestgaard-Jensen et al., 2013). As in SBP and CC RDLRs, analogues with a small alkyl substituent or a monocyclic aromatic ring (**8b**, **8c**, **8e**, and **8f**) had low activities, with less than 30% inhibition, whereas analogues with a substituted phenyl group (**8d** and **8g**) and a bicyclic aromatic ring (**8h**, **8i**, and **8j**) showed high antagonistic activities. The 2-naphthyl analog (**8h**) and the 3-biphenyl analog (**8i**) reduced GABA-activated currents by 85.6% and

83.7%, respectively, at 100 μM in HF RDLRs; the IC_{50} values of **8h** and **8i** were 29.6 ± 1.7 μM and 20.4 ± 1.4 μM, respectively (Fig. 2.4A). In contrast to the cases in SBP and CC RDLRs, introduction of a bulky substituent, such a 5'-*m*-terphenylyl group, into the 4-position, as shown in **8k**, did not cause a drastic reduction in antagonistic activity. This contrasting result in **8k** indicates that structural differences in the orthosteric site may exist between different insect species or variants. It remains to be investigated whether the information can be utilized for the development of insecticides with species-specificity.

The GABA concentration–response relationships in the presence and absence of **8h** were examined in order to determine whether synthesized compounds act as CAs. The result showed that the GABA concentration–response curve in the presence of **8h** was shifted parallel to the right relative to that in its absence (Fig. 2.4B); the EC_{50}s of GABA were 10.1 ± 1.6 μM and 24.9 ± 3.1 μM (mean ± SEM, n = 6) in the absence and presence of **8h**, respectively. A concentration-dependent reduction in GABA-induced currents in the presence of 8h was clearly observed (Figs. 2.4C and D). The potency of GABA in inducing currents was decreased approximately 2-fold in the presence of 30 μM **8h**, but the efficacy of GABA remained unchanged, indicating that **8h** competes with GABA for the orthosteric site but does not open the channel.

Given that noncompetitive GABAR antagonists include currently used insecticides, the synthesized CAs are assumed to exhibit insecticidal effects. Hence, I investigated the insecticidal activities of **8h** and **8i** by injecting them into adult female HFs. Compound **8h** produced convulsions in HFs, and showed 12.2 ± 2.2% and 19.4 ± 3.3% mortality at doses of 1 μg/HF and 10 μg/HF, respectively. Compound **8i** produced similar toxic symptoms and

exhibited 24.5 ± 2.4% and 44.0 ± 1.7% mortality at 1 μg/HF and 10 μg/HF, respectively. As the optimum hydrophobicity is needed for insecticidal compounds to reach the target site, the low insecticidal activities of these compounds may in part due to their high polarity.

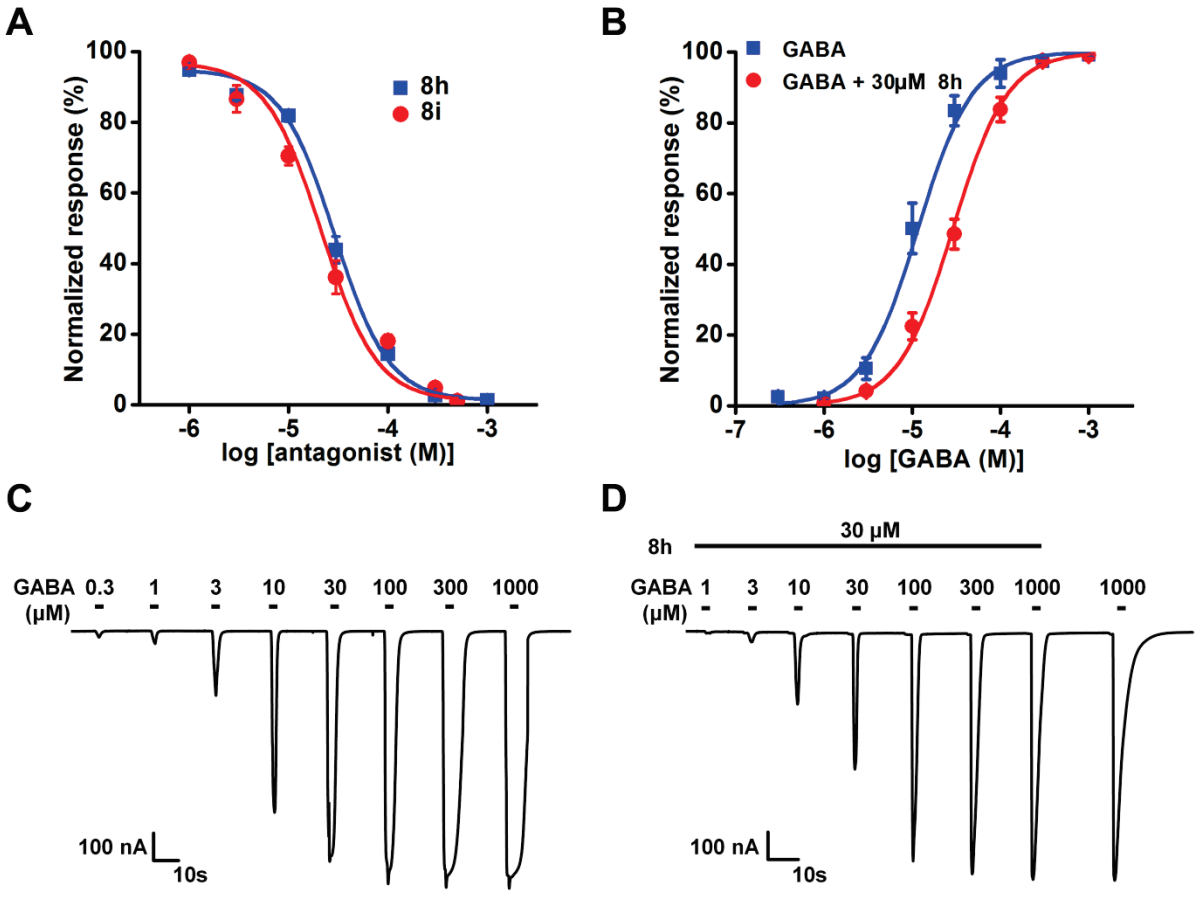

Figure 2.4 Effects of thio-4-PIOL analogues on GABA-induced currents in HF RDLRs expressed in *Xenopus* oocytes. (A) GABA response in the presence of various concentrations of **8h** (blue squares) and **8i** (red circles). Responses were normalized relative to currents induced by 10 μM GABA. Data points represent means ± SEM (n = 4–6). (B) GABA concentration-response curves in the presence (red circles) and absence (blue squares) of 30 μM **8h**. Responses were normalized relative to the maximum current induced by 1 mM GABA. Data points represent means ± SEM (n = 4–6). (C) Representative traces of currents induced by various concentrations of GABA in the absence of **8h**. (D) Representative traces of currents induced by various concentrations of GABA in the presence of 30 μM **8h**.

2.3.4. Homology modeling and ligand docking

To investigate the mechanisms of the interaction between 3-isothiazolols and insect GABARs, GABA, the 2-naphthyl analogue (**8h**), and the 3-biphenyl analogue (**8i**) were docked into the orthosteric site of a constructed HF RDLR homology model based on the crystal structure of the *C. elegans* GluCl (PDB: 3RIF, Hibbs and Gouaux, 2011). As known in Cys-loop receptors, the orthosteric site of this model is formed by residues from loops A–C on the principle subunit and loops D–F on the complementary subunit.

GABA was first docked into the orthosteric site of the HF RDLR model (Fig. 2.5A). The docking simulation shows that Glu202 of loop B and Arg109 of loop D electrostatically interact with a positively charged protonated amino group and a negatively charged carboxyl group, respectively. The backbone carbonyl oxygen atom of Ser203 of loop B was predicted to function as a hydrogen bond acceptor for the protonated amino group of GABA. In addition, Arg109 of loop D and Ser174 of loop E serve as hydrogen bond donors for the carboxylate anion of GABA. This orientation is consistent with those in the *Drosophila* RDLRs (Ashby et al., 2012). It is important to note that the so-called "aromatic box" formed by residues in loops A, B, C, and D was predicted in this model, as recently suggested for the human $GABA_CR$ and the *Drosophila* RDLR (Ashby et al., 2012; Lummis et al., 2012). Four aromatic residues, Phe144 (loop A), Phe204 (loop B), Tyr252 (loop C), and Tyr107 (loop D), exist near the protonated amino group of GABA in the docking model. Of these surrounding amino acid residues, two residues equivalent to Phe204 and Tyr252 have been identified in the *Drosophila* RDLR as making predominant contributions to cation/π interactions with the protonated amino group of GABA (Ashby et al., 2012; Lummis et al., 2011).

As shown in Figures 2.5B, C, and D, the piperidylisothiazole scaffold of **8h** and **8i** lies between Glu202 (loop B) and Arg109 (loop D). These two residues might interact with the protonated nitrogen atom of the piperidine ring and the deprotonated hydroxyl group (or the ring) of 3-isothiazolols, respectively. Furthermore, the backbone carbonyl oxygen atom of Ser203 of loop B is predicted to play a role as a hydrogen bond acceptor for the protonated nitrogen atom of the piperidine ring. It has been recently reported that two arginines of loops B and E are involved in binding gabazine in $\alpha_1\beta_2$ $GABA_A$Rs, whereas two arginines in loop C and D are critical residues in binding agonists (Goldschen-Ohm et al., 2011). More studies are needed to elucidate the roles of these arginines in RDLRs. Docked **8h** and **8i** overlapped one another in the orthosteric site (Fig. 2.5D), suggesting that thio-4-PIOL analogues might interact with HF RDLRs in an identical mode. The docking results show that spacious cavities exist on both sides of the core scaffold connecting the key residues Glu202 and Arg109 to accommodate bulky aromatic substituents at the 4-position of thio-4-PIOL analogues, which is in agreement with a $GABA_A$R model (Sander et al., 2011). In our docking simulation, both **8h** and **8i** are oriented with the 4-substituents pointed inward in the binding pocket, thereby most likely forming CH-π interactions with Tyr252 of loop C or Phe162 of loop E. The piperidine ring lies within the aromatic pocket created by Phe144, Phe204, Tyr252, and Tyr107. The orientation of 4-substituted thio-4-PIOLs is analogous to that of a 4-substituted 4-PIOL docked in a $GABA_A$R model based on molecular dynamics simulation (Sander et al., 2011). However, whether the 4-substituent points inward or outward in the pocket remains unclear.

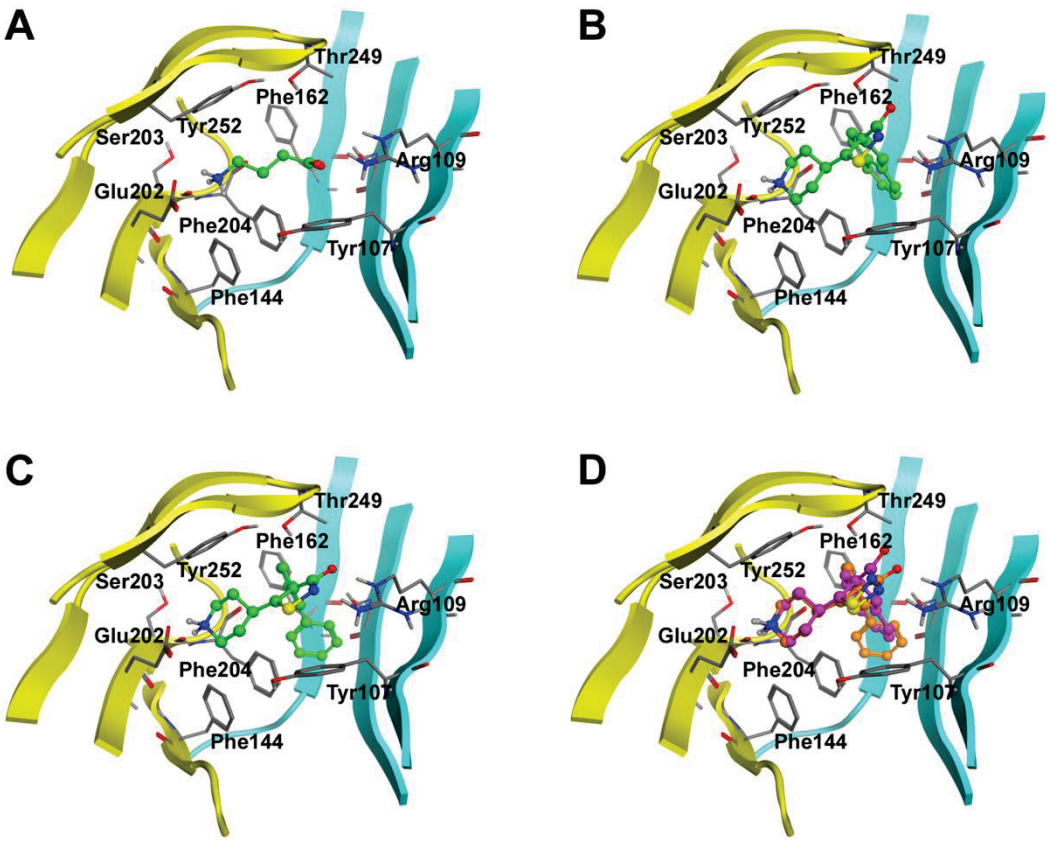

Figure 2.5 Simulation of the dockings of GABA and thio-4-PIOL analogues into the orthosteric site of a HF RDLR homology model. (A) GABA (green). (B) **8h** (green). (C) **8i** (green). (D) The alignment of **8h** (purple) and **8i** (orange).

2.4. Conclusion

I have synthesized a series of thio-4-PIOL analogues with substituents, including bulky aromatic groups, at the 4-position of the isothiazole ring and examined their antagonism of insect RDLRs. These analogues exhibited competitive antagonistic activity against three insect RDLRs. In particular, analogues with relatively large aromatic groups at the 4-position showed high potencies at insect RDLRs with IC_{50} values in the low micromolar range. Ligand docking studies using a HF RDLR homology model predicted that the binding site contains two cavities large enough to accommodate bicyclic aromatic 4-substituents of

thio-4-PIOL analogues. Although the potencies of the analogues against insect RDLRs are lower than the reported low nanomolar potencies of 4-aryl-4-PIOL analogues (Frølund et al., 2007) and 4-arylalkyl-thio-4-PIOL analogues (Krehan et al., 2006) in $\alpha_1\beta_3\gamma_{2S}$ $GABA_A$Rs, the findings described in this chapter should provide useful information for designing and developing novel CAs with higher potencies for insect GABARs. The ρ_1 GABARs are also of low sensitive to competitive $GABA_A$R antagonists, such as bicuculline and gabazine. The amino acid residues responsible for the low sensitivity have been identified in ρ_1 GABARs (Zhang et al., 2008). As three of the four identified amino acids are conserved in SBP, CC, and HF GABARs, structural moieties that overcome this low sensitivity most likely should add to compounds to further enhance the potencies of CAs in insect GABARs.

Chapter 3

Competitive antagonism of housefly GABA receptor variants by 4,5-disubstituted 3-isoxazolols

3.1. Introduction

In insects, GABARs are predominantly expressed in the central nervous system and play important physiological roles in sleep, olfaction, and learning/memory (Ozoe et al., 2009; Ozoe, 2013). Because vertebrate and invertebrate GABARs have different pharmacological properties, insect GABARs are an important target for safe insecticides, such as phenylpyrazoles (Buckingham and Sattelle, 2010; Ozoe et al., 2009; Ozoe, 2013). Whereas 19 constitutive subunits are present in mammalian GABARs, RDL is the only subunit that constitutes inhibitory GABARs in insects (Buckingham and Sattelle, 2010; Ozoe et al., 2009; Ozoe, 2013). However, the RDL-encoding gene *Rdl* undergoes alternative splicing of exons 3 and 6 to generate four variants (ac, ad, bc, and bd) in the *Drosophila* and other insect species (Fig. 1.4, ffrench-Constant and Rocheleau, 1993; Ozoe, 2013). The *Drosophila* variants of RDLRs have been reported to exhibit differential agonist sensitivity when expressed in *Xenopus* oocytes (Hosie et al., 1996, 2001; Jones et al., 2009). The alternative splicing may also increase the pharmacological diversity of insect RDLRs. However, the physiology and pharmacology of these variants of RDLRs have yet to be characterized.

CAs that act at the orthosteric binding site of RDLRs have the potential to become novel insecticides. In Chapter 2 and our previous studies (Liu et al., 2014; Rahman et al., 2014),

thio-4-PIOL and gabazine analogues were synthesized and examined for their antagonism of RDLRs cloned from three insect species. Subsequently, we found that introducing bicyclic aromatic groups into the 4-position of the isothiazole ring of thio-4-PIOL or into the 3-position of the dihydropyridazine ring of gabazine enhances the antagonism of insect RDLRs by these analogues. These analogues also showed insecticidal activity, though this activity was moderate. These findings prompted further exploration of potentially novel insecticides acting as competitive GABAR antagonists. Here, I synthesized a series of 4,5-disubstituted 3-isoxazolols (Fig. 1.10) and examined their differential antagonism of four splice variants of HF RDLRs.

3.2. Materials and methods

3.2.1. General methods for chemistry

Reagents and solvents were purchased from Wako Pure Chemical Industries, Ltd. (Osaka, Japan), Tokyo Chemical Industry Co., Ltd. (Tokyo, Japan), and Sigma-Aldrich Co., LLC. (Tokyo, Japan), unless otherwise noted. All air- and moisture-sensitive reactions were performed under an argon atmosphere using oven-dried glassware. Reactions were monitored by thin layer chromatography (TLC Silica gel 60 F254 plates, Merck KGaA, Darmstadt, Germany) using UV light or a $KMnO_4$ spray reagent. Column chromatography was performed using silica gel (Wakogel C-200, 75−150 μm, Wako). Melting points were determined using a YANACO MP-500D micro melting point apparatus and are uncorrected. ^{1}H (400 MHz) and ^{13}C (100 MHz) NMR spectra were recorded on a JEOL JNM A-400 spectrometer. Chemical shifts are reported in parts per million (ppm) on the δ scale, and

coupling constants (*J*) are in Hertz (Hz). Spin multiplicities are abbreviated as follows: s (singlet), bs (broad singlet), d (doublet), t (triplet), and m (multiplet). MS were measured using an ESI+ mode on a Waters XEVO mass spectrometer, and HRMS were obtained using an ESI+ mode on a Waters SYNAPT G2 spectrometer.

3.2.2. Synthesis of methyl 3-hydroxy-5-isoxazolecarboxylate (9)

Dimethyl acetylenedicarboxylate (1.4 g, 10.0 mmol) was added to a solution of 1,8-diazabicyclo[5.4.0]undec-7-ene (1.8 g, 12.0 mmol) and *N*-hydroxyurea (760 mg, 10.0 mmol) in methanol (15 mL) at 0 °C under argon. The solution was stirred at 0 °C for 30 min and then at room temperature for 12 h. After the solvent was evaporated, the residue was dissolved in water (25 mL) and acidified to pH 1 with conc. HCl. The product was extracted with Et_2O (3 × 30 mL), and the combined organic phases were washed with brine, dried over Na_2SO_4, and evaporated under reduced pressure. The obtained solid was recrystallized from chloroform to give **9** as a light yellow solid (840 mg, 59% yield). ^{1}H NMR (400 MHz, DMSO-d_6): δ 11.97 (1H, s, OH), 6.76 (1H, s, Ar–H), 3.87 (3H, s, $COOCH_3$).

3.2.3. Synthesis of 3-benzyloxy-5-methoxycarbonylisoxazole (10)

A mixture of **9** (2.1 g, 15 mmol) and K_2CO_3 (3.1 g, 22.5 mmol) in acetone (30 mL) was heated at 70 °C for 1 h. Benzyl bromide (3.8 g, 22.5 mmol) was added dropwise, and the mixture was stirred at 50 °C for 12 h. The mixture was filtered, and the filtrate was concentrated under reduced pressure. Water (30 mL) was added to the filtrate, and the product was extracted with Et_2O (3 × 30 mL). The combined organic phases were washed

with brine, dried over Na_2SO_4, and evaporated under reduced pressure. Column chromatography (hexane/EtOAc 15:1) gave **10** as a colorless oil (3.1 g, 87% yield). ^{1}H NMR (400 MHz, $CDCl_3$): δ 7.54–7.28 (5H, m, Ar–H), 6.57 (1H, s, Ar–H), 5.32 (2H, s, OCH_2), 3.95 (3H, s, $COOCH_3$). MS: *m*/*z* 255.9 $[M+Na]^+$.

3.2.4. Synthesis of 3-benzyloxy-5-carbamoylisoxazole (11)

A mixture of **10** (466 mg, 2.0 mmol) and aqueous ammonia (5 mL, 28%) was stirred at room temperature for 12 h. The mixture was concentrated to dryness under reduced pressure. Water (15 mL) was added to the residue, and the mixture was extracted with EtOAc (3 × 15 mL). The combined organic phases were washed with brine, dried over Na_2SO_4, and evaporated under reduced pressure to afford **11** as a white solid (395 mg, 91% yield). mp 162–164 °C. ^{1}H NMR (400 MHz, $CDCl_3$): δ 7.48–7.32 (5H, m, Ar–H), 6.59 (1H, s, Ar–H), 6.43 (1H, bs, $CONH_2$), 5.87 (1H, bs, $CONH_2$), 5.31 (2H, s, OCH_2). MS: *m*/*z* 241.1 $[M+Na]^+$.

3.2.5. Synthesis of muscimol hydrobromide (12a)

Borane in THF (1 M, 5 mL, 5.0 mmol) was slowly added to a solution of **11** (480 mg, 2.2 mmol) in dry THF (15 mL) at 0 °C. The solution was stirred at room temperature for 16 h. After acidification (pH 1) with 4 M HCl, the solution was stirred for 1 h and concentrated under reduced pressure. The residue was suspended in water, and the solution was made basic (pH 10) with 4 M NaOH. The product was extracted with EtOAc (3 × 30 mL); the combined organic phases were washed with brine, dried over Na_2SO_4, and evaporated under reduced pressure to afford a light yellow oil. The oil was dissolved in a solution of HBr in AcOH (10

mL, 30%), and the mixture was stirred at room temperature for 24 h. The reaction mixture was concentrated with a subsequent azeotropic treatment of MeOH/toluene (1:1) three times, and the residue was recrystallized (MeOH/Et_2O) to give **12a** as a light brown solid (179 mg, 42% yield). ^{1}H NMR (400 MHz, DMSO-d_6): δ 11.25 (1H, bs, OH), 8.45 (3H, bs, NH_2·HBr), 6.18 (1H, s, Ar–H), 4.14 (2H, s, CH_2). ^{13}C NMR (100 MHz, DMSO-d_6): δ 170.14, 165.22, 96.04, 34.29. HRMS: *m*/*z* calcd for $C_4H_7N_2O_2$ $[M–Br]^+$ 115.0508, found 115.0502.

3.2.6. Synthesis of 5-carbamoyl-3-isoxazolol (13a)

Compound **11** (349 mg, 1.6 mmol) was suspended in a solution of HBr in AcOH (10 mL, 30%), and the mixture was stirred at room temperature for 24 h. The reaction mixture was concentrated with a subsequent azeotropic treatment of MeOH/toluene (1:1) three times, and the residue was recrystallized (MeOH/EtOAc) to give **13a** as a white solid (152 mg, 74% yield). mp 236–239 °C (dec). ^{1}H NMR (400 MHz, DMSO-d_6): δ 11.61 (1H, bs, OH), 8.15 (1H, bs, $CONH_2$), 7.81 (1H, bs, $CONH_2$), 6.54 (1H, s, Ar–H). ^{13}C NMR (100 MHz, DMSO-d_6): δ 170.40, 163.58, 157.39, 97.69. HRMS: *m*/*z* calcd for $C_4H_5N_2O_3$ $[M+H]^+$ 129.0295, found 129.0290.

3.2.7. Synthesis of 3-benzyloxy-5-carbamoyl-4-iodoisoxazole (14)

A mixture of **11** (1.1 g, 5 mmol), $Pd(OAc)_2$ (112 mg, 0.5 mmol), CsOAc (2.3 g, 12 mmol), $NaHCO_3$ (420 mg, 5 mmol), I_2 (3.8 g, 15 mmol), 4 Å molecular sieves (150 mg), and *N*-methylformamide (30 mL) was stirred at 75 °C for 16 h. After cooling, the reaction mixture was added to $Na_2S_2O_4$ (solid) until the color stopped changing, and then it was

filtered through celite, which was thoroughly washed with EtOAc. The combined organic phases were washed with water twice and then with brine, dried over Na_2SO_4, and evaporated under reduced pressure. Column chromatography (hexane/EtOAc 10:1) gave **14** as a light yellow solid (980 mg, 57% yield). mp 179–182 °C. ^{1}H NMR (400 MHz, $CDCl_3$): δ 7.50–7.35 (5H, m, Ar–H), 6.43 (1H, bs, $CONH_2$), 5.94 (1H, bs, $CONH_2$), 5.37 (2H, s, OCH_2). MS: *m*/*z* 366.9 $[M+Na]^+$.

3.2.8. General procedure for the synthesis of 4-aryl-3-benzyloxy-5-carbamoylisoxazole (15b–g)

A mixture of **14** (1 mmol), an arylboronic acid (1.5 mmol), $Pd(PPh_3)_2Cl_2$ (0.08 mmol), DMF (5 mL), and aqueous K_2CO_3 (0.5 mL, 3 M, 1.5 mmol) was stirred at 80 °C for 24 h. After cooling, the reaction mixture was filtered through celite and diluted using Et_2O. The organic phase was washed with water and brine, dried over Na_2SO_4, and evaporated under reduced pressure. Column chromatography (hexane/EtOAc) gave **15b**–**g**.

3.2.8.1. 3-Benzyloxy-4-(3-biphenylyl)-5-carbamoylisoxazole (15b)

A white solid, yield 82%, mp 145–147 °C. ^{1}H NMR (400 MHz, $CDCl_3$): δ 7.93 (1H, s, Ar–H), 7.70–7.26 (13H, m, Ar–H), 6.40 (1H, bs, $CONH_2$), 5.78 (1H, bs, $CONH_2$), 5.42 (2H, s, OCH_2). ^{13}C NMR (100 MHz, $CDCl_3$): δ 169.88, 157.95, 156.60, 141.09, 140.78, 135.39, 129.03, 128.83, 128.74, 128.60, 128.56, 128.09, 127.58, 127.37, 127.20, 126.59, 114.21, 72.27. MS: *m*/*z* 371.0 $[M+H]^+$, 393.0 $[M+Na]^+$.

3.2.8.2. 3-Benzyloxy-5-carbamoyl-4-(2-naphthyl)isoxazole (15c)

A white solid, yield 69%, mp 138–140 °C. ^{1}H NMR (400 MHz, $CDCl_3$): δ 8.14 (1H, s, Ar–H), 7.88–7.73 (4H, m, Ar–H), 7.72–7.26 (7H, m, Ar–H), 6.39 (1H, bs, $CONH_2$), 5.84 (1H, bs, $CONH_2$), 5.43 (2H, s, OCH_2). ^{13}C NMR (100 MHz, $CDCl_3$): δ 169.90, 157.95, 156.60, 135.33, 133.21, 132.90, 129.75, 129.58, 128.49, 128.37, 127.90, 127.74, 127.63, 127.26, 126.74, 126.23, 123.56, 114.31, 72.17. MS: *m*/*z* 367.0 $[M+Na]^+$.

3.2.8.3. 3-Benzyloxy-4-(4-biphenylyl)-5-carbamoylisoxazole (15d)

A white solid, yield 90%, mp 164–167 °C. ^{1}H NMR (400 MHz, $CDCl_3$): δ 7.80–7.28 (14H, m, Ar–H), 6.39 (1H, bs, $CONH_2$), 5.75 (1H, bs, $CONH_2$), 5.42 (2H, s, OCH_2). ^{13}C NMR (100 MHz, $CDCl_3$): δ 169.98, 158.03, 156.59, 141.72, 140.66, 135.48, 132.23, 132.13, 130.49, 128.84, 128.67, 128.60, 128.47, 128.08, 127.59, 127.19, 126.95, 125.21, 114.11, 72.34. MS: *m*/*z* 371.0 $[M+H]^+$.

3.2.8.4. 3-Benzyloxy-5-carbamoyl-4-(1-naphthyl)isoxazole (15e)

A white solid, yield 77%, mp 154–156 °C. ^{1}H NMR (400 MHz, $CDCl_3$): δ 7.95–7.25 (12H, m, Ar–H), 6.05 (1H, bs, $CONH_2$), 5.72 (1H, bs, $CONH_2$), 5.34 (2H, s, OCH_2). ^{13}C NMR (100 MHz, $CDCl_3$): δ 170.35, 158.09, 157.37, 135.23, 133.66, 131.57, 129.83, 128.97, 128.52, 128.41, 128.05, 126.56, 126.25, 125.26, 125.19, 123.84, 112.32, 72.02. MS: *m*/*z* 367.1 $[M+Na]^+$.

3.2.8.5. 3-Benzyloxy-5-carbamoyl-4-(6-methoxy-2-naphthyl)isoxazole (15f)

A light yellow solid, yield 67%, mp 124–126 °C. ^{1}H NMR (400 MHz, $CDCl_3$): δ 8.07 (1H, s, Ar–H), 7.78–7.65 (3H, m, Ar–H), 7.46–7.30 (5H, m, Ar–H), 7.18–7.10 (2H, m, Ar–H), 6.40 (1H, bs, $CONH_2$), 6.06 (1H, bs, $CONH_2$), 5.42 (2H, s, OCH_2), 3.91 (3H, s, OCH_3). ^{13}C NMR (100 MHz, $CDCl_3$): δ 169.92, 158.40, 158.21, 156.39, 135.41, 134.54, 129.90, 129.50, 128.55, 128.45, 127.86, 127.79, 126.57, 121.23, 119.11, 114.35, 105.61, 72.12, 55.32. MS: *m*/*z* 397.1 $[M+Na]^+$.

3.2.8.6. 3-Benzyloxy-5-carbamoyl-4-(6-hydroxy-2-naphthyl)isoxazole (15g)

A light yellow solid, yield 43%, mp 177–179 °C. ^{1}H NMR (400 MHz, DMSO-d_6): δ 9.73 (1H, s, Ar–OH), 8.11 (1H, bs, $CONH_2$), 7.97 (1H, s, Ar–H), 7.85 (1H, bs, $CONH_2$), 7.75–7.05 (10H, m, Ar–H), 5.41 (2H, s, OCH_2). ^{13}C NMR (100 MHz, DMSO-d_6): δ 169.11, 158.67, 158.25, 155.96, 135.67, 134.12, 129.56, 128.60, 128.37, 128.24, 127.93, 127.31, 127.06, 125.49, 120.77, 118.98, 111.59, 108.54, 71.63. MS: *m*/*z* 383.1 $[M+Na]^+$.

3.2.9. Synthesis of 5-aminomethyl-4-(3-biphenylyl)-3-isoxazolol hydrobromide (12b)

Compound **12b** was prepared from **15b** (185 mg, 0.5 mmol) according to the procedure described for **12a**. Recrystallization (MeOH/Et_2O) gave **12b** as a white solid (69 mg, 40%). mp 220–222 °C. ^{1}H NMR (400 MHz, CD_3OD): δ 7.75–7.30 (9H, m, Ar–H), 4.36 (2H, s, CH_2). ^{13}C NMR (100 MHz, CD_3OD): δ 163.30, 160.88, 143.29, 141.79, 130.50, 129.95, 129.33, 128.72, 128.66, 128.38, 128.07, 128.02, 111.90, 35.40. HRMS: *m*/*z* calcd for $C_{16}H_{15}N_2O_2$ $[M–Br]^+$ 267.1134, found 267.1143.

3.2.10. Synthesis of 5-aminomethyl-4-(2-naphthyl)-3-isoxazolol hydrobromide (12c)

Compound **12c** was prepared from **15c** (196 mg, 0.57 mmol) according to the procedure described for **12a**. Recrystallization (MeOH/Et_2O) gave **12c** as a brown solid (85 mg, 47%). mp 226–228 °C. ^{1}H NMR (400 MHz, CD_3OD): δ 8.01–7.86 (4H, m, Ar–H), 7.65–7.50 (3H, m, Ar–H), 4.41 (2H, s, CH_2). ^{13}C NMR (100 MHz, CD_3OD): δ 170.22, 160.92, 134.85, 134.37, 129.63, 129.09, 128.77, 127.69, 127.20, 126.21, 112.05, 35.56. HRMS: *m*/*z* calcd for $C_{14}H_{13}N_2O_2$ $[M–Br]^+$ 241.0977, found 241.0989.

3.2.11. Synthesis of 4-(3-biphenylyl)-5-carbamoyl-3-isoxazolol (13b)

Compound **13b** was prepared from **15b** (333 mg, 0.9 mmol) according to the procedure described for **13a**. Recrystallization (MeOH/EtOAc) gave **13b** as a white solid (210 mg, 83%). mp 193–195 °C. ^{1}H NMR (400 MHz, DMSO-d_6): δ 12.03 (1H, bs, OH), 8.09 (1H, bs, $CONH_2$), 7.90 (1H, s, Ar–H), 7.82 (1H, bs, $CONH_2$), 7.71–7.27 (8H, m, Ar–H). ^{13}C NMR (100 MHz, DMSO-d_6): δ 168.62, 158.59, 158.30, 140.04, 139.77, 128.87, 128.42, 128.35, 128.05, 127.43, 126.62, 126.19, 111.31. HRMS: *m*/*z* calcd for $C_{16}H_{13}N_2O_3$ $[M+H]^+$ 281.0921, found 281.0914.

3.2.12. Synthesis of 5-carbamoyl-4-(2-naphthyl)-3-isoxazolol (13c)

Compound **13c** was prepared from **15c** (189 mg, 0.55 mmol) according to the procedure described for **13a**. Recrystallization (MeOH/EtOAc) gave **13c** as a light yellow solid (95 mg, 68%). mp 221–223 °C. ^{1}H NMR (400 MHz, DMSO-d_6): δ 12.02 (1H, bs, OH), 8.10 (1H, s, Ar–H), 8.06 (1H, bs, $CONH_2$), 7.95–7.88 (3H, m, Ar–H), 7.79 (1H, bs, $CONH_2$), 7.66 (1H, d,

J = 8.3 Hz, Ar–H), 7.58–7.47 (2H, m, Ar–H). ^{13}C NMR (100 MHz, DMSO-d_6): δ 168.58, 158.39, 158.28, 132.33, 132.19, 128.35, 127.80, 127.25, 126.92, 126.23, 126.02, 124.96, 111.33. HRMS: m/z calcd for $C_{14}H_{11}N_2O_3$ $[M+H]^+$ 255.0770, found 255.0785.

3.2.13. Synthesis of 4-(4-biphenylyl)-5-carbamoyl-3-isoxazolol (13d)

Compound **13d** was prepared from **15d** (222 mg, 0.6 mmol) according to the procedure described for **13a**. Recrystallization (MeOH/EtOAc) gave **13d** as a white solid (112 mg, 67%). mp 278–280 °C (dec). ^{1}H NMR (400 MHz, DMSO-d_6): δ 12.03 (1H, bs, OH), 8.09 (1H, bs, $CONH_2$), 7.82 (1H, bs, $CONH_2$), 7.80–7.50 (6H, m, Ar–H), 7.48–7.34 (3H, m, Ar–H). ^{13}C NMR (100 MHz, DMSO-d_6): δ 168.61, 158.56, 158.20, 139.65, 139.58, 129.96, 128.86, 127.48, 126.61, 126.54, 126.04, 110.98. HRMS: m/z calcd for $C_{16}H_{12}N_2O_3Na$ $[M+Na]^+$ 303.0740, found 303.0738.

3.2.14. Synthesis of 5-carbamoyl-4-(1-naphthyl)-3-isoxazolol (13e)

Compound **13e** was prepared from **15e** (330 mg, 0.96 mmol) according to the procedure described for **13a**. Recrystallization (MeOH/EtOAc) gave **13e** as a white solid (128 mg, 52%). mp 189–191 °C. ^{1}H NMR (400 MHz, DMSO-d_6): δ 11.77 (1H, bs, OH), 7.96 (2H, d, J = 7.8 Hz, Ar–H), 7.92 (1H, bs, $CONH_2$), 7.68 (1H, bs, $CONH_2$), 7.59–7.41 (5H, m, Ar–H). ^{13}C NMR (100 MHz, DMSO-d_6): δ 169.34, 159.28, 157.69, 133.03, 131.46, 128.66, 128.44, 128.07, 126.08, 125.76, 125.39, 125.15, 110.58. HRMS: m/z calcd for $C_{14}H_{11}N_2O_3$ $[M+H]^+$ 255.0770, found 255.0785.

3.3.15. Synthesis of 5-carbamoyl-4-(6-methoxy-2-naphthyl)-3-isoxazolol (13f)

Compound **13f** was prepared from **15f** (243 mg, 0.65 mmol) according to the procedure described for **13a**. Recrystallization (MeOH/EtOAc) gave **13f** as a white solid (115 mg, 62%). mp 242–244 °C (dec). ^{1}H NMR (400 MHz, DMSO-d_6): δ 11.99 (1H, bs, OH), 8.03 (2H, bs, $CONH_2$), 7.85–7.70 (4H, m, Ar–H), 7.63 (1H, dd, J = 8.8, 2.0 Hz, Ar–H), 7.32 (1H, d, J = 2.4 Hz, Ar–H), 7.17 (1H, dd, J = 8.8, 2.4 Hz, Ar–H), 3.89 (3H, s, OCH_3). ^{13}C NMR (100 MHz, DMSO-d_6): δ 168.72, 158.58, 158.05, 157.71, 133.70, 129.52, 128.31, 127.89, 127.83, 125.99, 122.60, 118.64, 111.58, 105.90, 55.21. HRMS: m/z calcd for $C_{15}H_{12}N_2O_4Na$ $[M+Na]^+$ 307.0695, found 307.0691.

3.2.16. Synthesis of 5-carbamoyl-4-(6-hydroxy-2-naphthyl)-3-isoxazolol (13g)

Compound **13g** was prepared from **15g** (90 mg, 0.25 mmol) according to the procedure described for **13a**. Recrystallization (MeOH/EtOAc) gave **13g** as a white solid (52 mg, 77%). mp 210–213 °C. ^{1}H NMR (400 MHz, DMSO-d_6): δ 11.94 (1H, bs, OH), 9.70 (1H, bs, OH), 8.05–7.50 (6H, m, Ar–H and $CONH_2$), 7.36–7.05 (2H, m, Ar–H). ^{13}C NMR (100 MHz, DMSO-d_6): δ 168.73, 158.61, 157.91, 155.78, 129.56, 128.37, 128.12, 127.56, 127.11, 125.29, 121.64, 118.81, 111.69, 108.51. HRMS: m/z calcd for $C_{14}H_{11}N_2O_4$ $[M+H]^+$ 271.0719, found 271.0714.

3.2.17. Preparation of cRNAs of HF RDL variants and their expression *in Xenopus* oocytes

The cRNAs of four HF RDL variants (ac, bc, ad, and bd; DDBJ accession Nos.: AB177547, complete cds of RDL_{bd}; AB824728, partial cds of exon 3a version; AB824729, partial cds of exon 6c version) were prepared as previously described in Chapter 2.2.11.1 using plasmids pBluescript KS(-)-$MdRdl_{ac}$, -$MdRdl_{bc}$, -$MdRdl_{ad}$, and -$MdRdl_{bd}$. The cRNAs were precipitated with LiCl, dissolved in sterile RNase-free water, and stored at –20 °C until use. The *Xenopus* oocytes were obtained as previously described in Chapter 2.2.11.2. Each oocyte was injected with 5 ng of cRNA and then incubated in sterile SOS for 48 h at 16 °C.

3.2.18. TEVC electrophysiology

Electrophysiological experiments were performed as previously described in Chapter 2.2.11.2. Briefly, for agonist assays, GABA and muscimol dissolved in SOS was applied to oocytes for 3 s, at intervals of 30–60 s to ensure a full recovery from desensitization. Concentration–response curves were generated by sequential applications of increasing concentrations of agonists.

For antagonist assays, 3-isoxazolols were dissolved in DMSO and then diluted with SOS to the desired concentrations [DMSO, ≤ 0.1% (v/v)]. The test compound solution was added to the perfusate after two successive control applications of GABA and was then applied consecutively for the remainder of the experiments. Antagonist solutions were perfused alone for 30 s before their co-application with GABA. GABA, at a concentration corresponding to the EC_{50} for each variant, was then co-applied with an antagonist for 3 s, and the

co-application was repeated at 30–60 s intervals to obtain the highest constant inhibition. All experiments were performed using at least four different oocytes obtained from at least two different frogs. EC_{50} and IC_{50} values were obtained from concentration–response data by nonlinear regression analysis using OriginPro 8J (OriginLab, Northampton, MA). Statistical significance was assessed using one-way analysis of variance (ANOVA) followed by Duncan's multiple range test.

3.2.19. Insecticidal assays

The WHO/SRS strain of HFs was used to examine the insecticidal activity of **13b**. The experiments were replicated five times according to the same procedure described in Chapter 2.2.12. The median lethal dose (LD_{50}) was calculated from the mean values of mortality at three dosages using the Probit method.

3.2.20. Homology modeling and ligand docking studies

A recently published X-ray crystal structure of the homopentameric human β3 GABAR (PDB: 4COF, Miller and Aricescu, 2014) was used as a template to construct a HF RDL_{ac} GABAR homology model. A sequence alignment of the RDL_{ac} and β subunits was carried out using ClustalW software, and this was used to build all five subunits simultaneously using MOE 2011.10 software (Chemical Computing Group, Montreal, Canada). The obtained pentamer model was optimized geometrically using the AMBER99 force field. GABA and muscimol were created in the zwitterionic forms, and compound **13b** was created in a deprotonated hydroxyl form using MOE Builder. The docking studies were performed in the

same manner as descried in Chapter 2.2.14 using the ASEDock program (2011.01.27, Chemical Computing Group) with default parameters. The binding mode with the highest score was chosen for the final representation. Structural images were visualized using PyMOL Ver. 1.3 (Schrödinger, Tokyo, Japan).

3.3. Results and discussion

3.3.1. Chemistry

A new, convenient strategy to synthesize 4-aryl-substituted muscimols and 4-aryl-5-carbamoyl-3-isoxazolols starting from dimethyl acetylenedicarboxylate was established and is outlined in Scheme 3.1. 3-Isoxazolol **9** was synthesized from dimethyl acetylenedicarboxylate according to a reported method (Frey and Jäger, 1985), and the hydroxyl group was protected to give 3-benzyloxyisoxazole **10** (Riess et al., 1998). Ammonolysis of ester **10** to amide **11** was followed by reduction with borane and deprotection with hydrobromic acid to afford muscimol hydrobromide (**12a**). Treatment of **11** with 30% hydrobromic acid in acetic acid afforded 5-carbamoyl-3-isoxazolol (**13a**). To introduce aromatic groups into the 4-position of the isoxazole ring, **11** was first iodinated at this position using iodine and $Pd(OAc)_2$ as a catalyst to give **14** (Wang et al., 2013). The Suzuki-Miyaura cross-coupling reaction of **14** with the appropriate arylboronic acids in the presence of a palladium catalyst afforded analogues **15b**–**g** in 43–90% yields, the hydroxyl groups of which were deprotected with hydrobromic acid to give **13b**–**g**. Compounds **12b**–**c** were obtained by reduction and subsequent deprotection of **15b**–**c**, as described for **12a**.

Scheme 3.1 Synthesis of muscimol and target 4,5-disubstituted 3-isoxazolols[a]

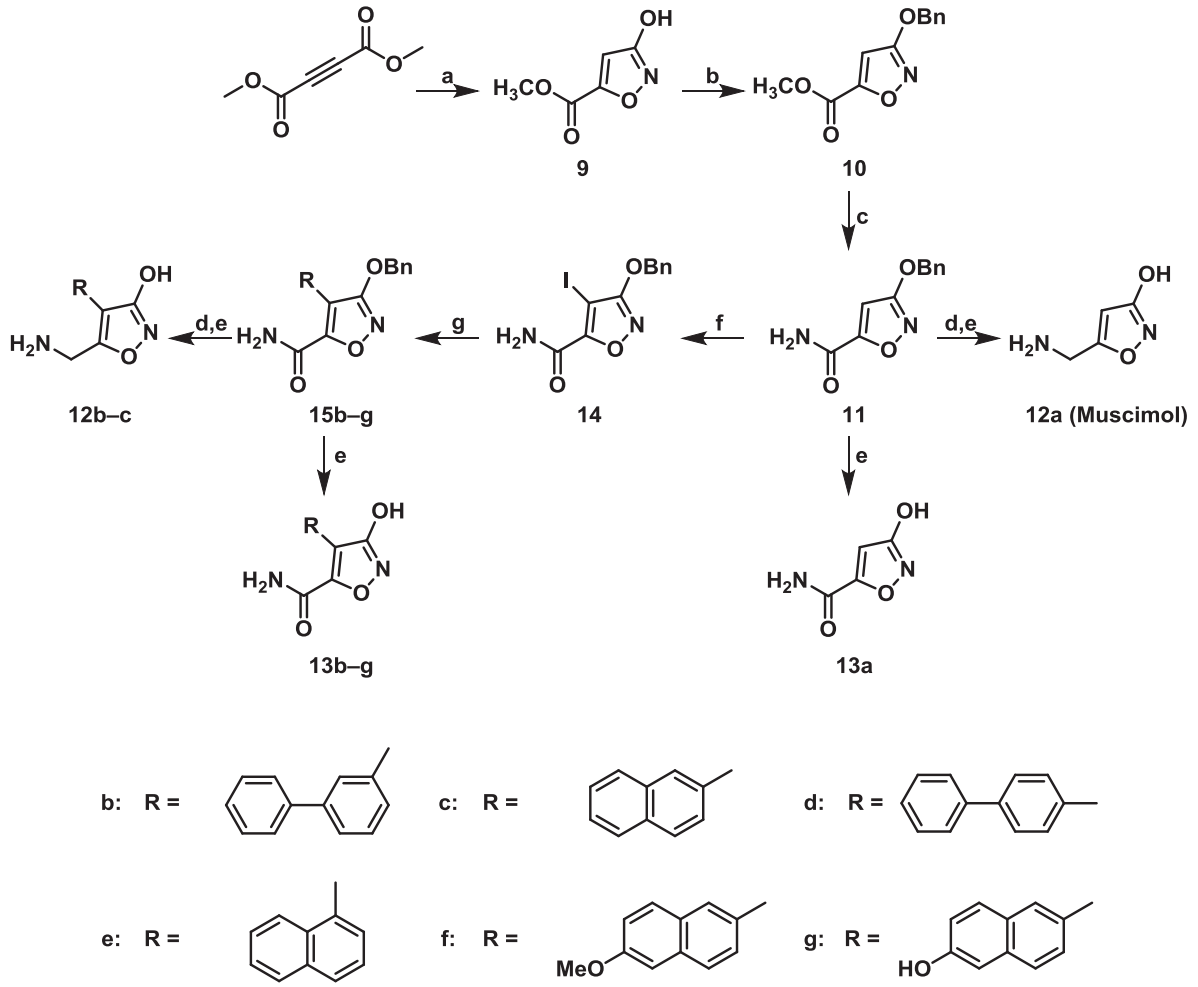

[a]Reagents and conditions: (a) *N*-hydroxyurea, 1,5-diazabicyclo[5.4.0]undec-5-ene, MeOH, 0 °C; (b) benzyl bromide, K_2CO_3, acetone, 70 °C; (c) aqueous NH_3, room temperature; (d) BH_3, THF, room temperature; (e) 30% HBr in AcOH, room temperature; (f) I_2, $Pd(OAc)_2$, CsOAc, $NaHCO_3$, DMF, 75 °C; (g) $RB(OH)_2$, $PdCl_2(PPh_3)_2$, K_2CO_3, DMF, 80 °C.

3.3.2. Differential sensitivity of HF RDLR variants to GABA and muscimol

Similar to the case of *D. melanogaster* (ffrench-Constant and Rocheleau, 1993), four splice variants (ac, ad, bc, and bd) of RDL are endogenously generated by alternatively splicing exons 3 (a and b) and 6 (c and d) of *Rdl* in HFs. The two amino acid residues that

differ between the sequences encoded by exons 3a and 3b are located upstream of the agonist-interacting region of the RDL subunit, and the ten residues that differ between the sequences encoded by exons 6c and 6d are located in a region including loops F and C (Fig. 1.4), which are predicted to be generally involved in the interaction with agonists in Cys-loop receptors (Buckingham et al., 2005). In the present study, the four variants of HF RDL were expressed in *Xenopus* oocytes, and their responses to the agonists GABA and muscimol were first investigated using the TEVC method.

Application of GABA to the oocytes expressing HF RDLRs induced concentration-dependent inward currents in all four variants when the voltage was clamped at –80 mV. The GABA concentration–response curves show that the order of variants giving higher sensitivity to GABA is $RDL_{ac} \approx RDL_{bc} > RDL_{ad} \approx RDL_{bd}$ (Fig. 3.1A); the EC_{50} values are given in Table 3.1. The finding that the alternative splicing of exon 3 did not affect the sensitivity to GABA suggests that the two variable residues in exon 3 may not be involved in the interaction with GABA. RDL_{ac} GABARs showed ~6-fold higher sensitivity to GABA than RDL_{ad} GABARs, and RDL_{bc} GABARs had ~5-fold higher sensitivity than RDL_{bd} GABARs. This finding indicates that the alternative splicing of exon 6 significantly influences GABA potency in the HF RDLR variants. Similarly, muscimol (**12a**) was a more potent full agonist in the ac and bc variants than in the ad and bd variants (Fig. 3.1, Table 3.1). These different potencies of GABA and muscimol in the four variants are similar to those in *Drosophila* RDLR variants (Hosie et al., 1996, 2001; Jones et al., 2009). The changes of agonist potencies may be due to the residue difference in loop(s) F and/or C in the orthosteric binding site.

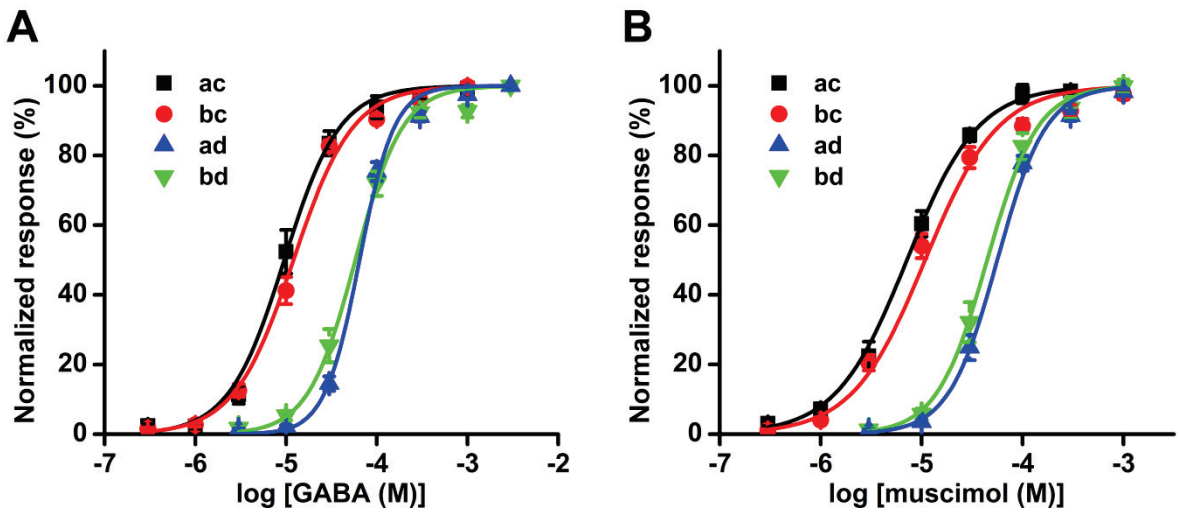

Figure 3.1 Agonist responses of the four splice variants of HF RDLRs expressed in *Xenopus* oocytes. Responses were normalized relative to the maximum currents induced by 1 mM GABA in the ac and bc variants and by 3 mM GABA in the ad and bd variants. No significant differences were observed in the maximum currents induced by muscimol and GABA in each variant, indicating that muscimol is a full agonist. Data represent means ± SEM (n = 6–9). (A) GABA concentration–response curves of the four variants. (B) Muscimol concentration–response curves of the four variants.

Table 3.1 Potencies of GABA and muscimol in the four splice variants of HF RDLRs

Variant	GABA		Muscimol	
	EC_{50} (μM)	n_H	EC_{50} (μM)	n_H
RDL_{ac}	10.6 ± 1.6[a]	1.74 ± 0.23	7.1 ± 0.7[a]	1.25 ± 0.16
RDL_{bc}	12.2 ± 0.7[a]	1.62 ± 0.24	10.2 ± 1.0[a]	1.18 ± 0.10
RDL_{ad}	64.1 ± 3.8[b]	2.29 ± 0.10	54.1 ± 2.2[b]	1.98 ± 0.26
RDL_{bd}	59.0 ± 5.7[b]	1.77 ± 0.21	45.8 ± 4.7[b]	1.76 ± 0.16

Data are means ± SEM (n = 6–9). n_H is the Hill coefficient. The different superscript letters within a column indicate statistically significant difference with $p < 0.01$.

3.3.3. Antagonism of HF RDLR variants by synthesized analogues

I examined the activity of synthesized compounds against RDLRs from three insect species. The compounds were first tested against CC and SBP RDLRs expressed in *Drosophila* S2 cells using the FMP assays. Unexpectedly, synthesized analogues other than muscimol failed to show significant activity at 100 μM in both insect receptors (data not shown). In contrast to these results, significant results were obtained against HF RDLRs, prompting further investigation described below. These contrasting results suggest that structural differences in the orthosteric binding sites of RDLRs might exist between different insect species.

As agonist potencies vary by the variant, synthesized analogues were assessed for their functional characteristics in the four variants of HF RDLRs expressed in *Xenopus* oocytes using a TEVC method. Analogues were first tested at 100 μM in the absence and in the presence of the EC_{50} of GABA to determine if they are agonists or antagonists. Unlike muscimol, all synthesized analogues showed no agonism but exhibited antagonism at 100 μM in the four RDL variants.

In Chapter 2, I found that the 4-(2-naphthyl)-thio-4-PIOL (**8h**) and 4-(3-biphenylyl)-thio-4-PIOL (**8i**) showed competitive antagonism in HF RDL_{ac} GABARs and CC RDL_{bd} GABARs, indicating that the 3-biphenylyl and 2-naphthyl groups are beneficial for CAs of insect GABARs (Liu et al., 2014). Thus, these groups were introduced into the 4-position of muscimol (**12a**) to afford **12b** and **12c**. Both compounds showed antagonism at 100 μM in all four variants of HF RDLRs, albeit with less than 40% inhibition of GABA-induced currents (Fig. 3.2A). Although the potencies of these analogues were low, these results indicate that

the 3-isoxazolol scaffold may be useful for developing antagonists of HF RDLRs and that the bicyclic aromatic system at the 4-position of the isoxazole ring may be beneficial for antagonistic activity as it was in thio-4-PIOL analogues.

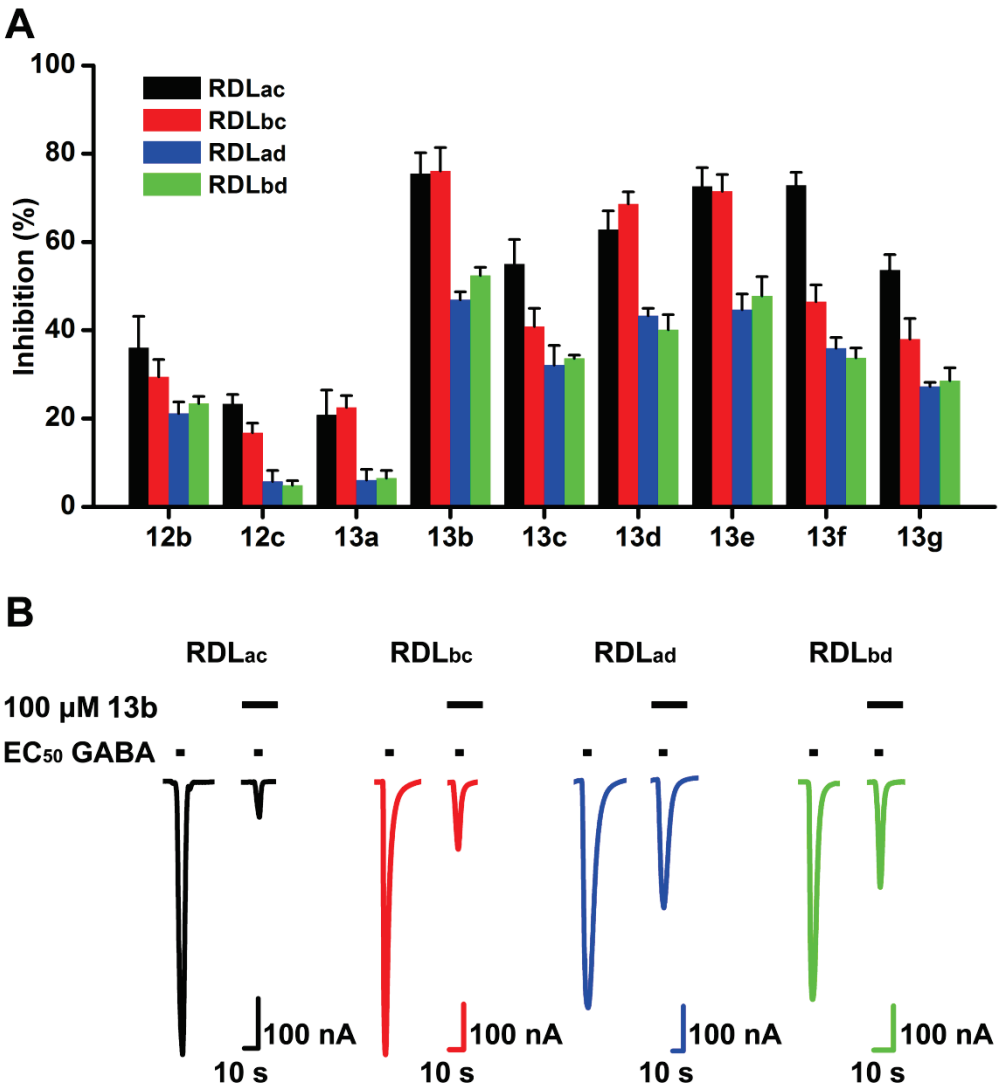

Figure 3.2 Inhibition of GABA-induced currents by the 3-isoxazolol analogues in the four splice variants of HF RDLRs expressed in *Xenopus* oocytes. The EC_{50} of GABA for each variant (Table 3.1) was used to induce control currents in each oocyte. (A) Inhibition of GABA-induced currents by synthesized analogues at 100 µM in the four variants. Data represent means ± SEM (n = 4–6). (B) Examples of GABA-induced currents inhibited by 100 µM **13b** in the four variants.

Replacement of the aminomethyl group of muscimol (**12a**) with a carbamoyl group to give **13a** changed the function of muscimol from an agonist to an antagonist in the four variants, with ~20% inhibition of GABA-induced currents at 100 μM in RDL_{ac} GABARs and RDL_{bc} GABARs and ~6% inhibition in RDL_{ad} GABARs and RDL_{bd} GABARs. These findings indicate that the protonated amino group is needed for agonist activity and that the carbamoyl group at the 5-position favors antagonism rather than agonism. The introduction of a 3-biphenylyl group at the 4-poisiton of **13a** to give **13b** markedly increased the antagonistic activity against the four variants, leading to 75.5, 76.1, 46.9, and 52.4% inhibition of GABA-induced currents in RDL_{ac}, RDL_{bc}, RDL_{ad}, and RDL_{bd} GABARs, respectively (Fig. 3.2A). Figure 3.2B shows that GABA-induced currents were inhibited by the 3-biphenylyl analog (**13b**) at 100 μM in the four RDL variants.

Compound **13c**, with a 2-naphthyl substitution at the 4-position of the isoxazole ring, also exhibited higher inhibition than **13a** in all four variants, but relatively lower inhibition compared with **13b**. Additionally, two different aromatic groups, 4-biphenylyl and 1-naphthyl, were introduced into the 4-position to yield **13d** and **13e**, respectively. The inhibition of GABA-induced currents by **13d** and **13e** in the four variants was comparable to the inhibition by **13b**. These findings indicate that analogues with bicyclic aromatic groups at the 4-position of the isoxazole ring are well tolerated at the binding site and that they are effective in inhibiting GABA-induced current in HF RDLRs. To investigate whether the electron-donating groups on the aromatic group at the 4-position increase activity, a methoxyl and a hydroxyl group were introduced to the 6-position of the 2-naphthyl group of **13c** to afford **13f** and **13g**, respectively. Compounds **13f** and **13g** were comparable in activity to **13c**

in the four variants, although inhibition by **13f** in the ac variant was higher than that of **13c** (Fig. 3.2A). Overall, the synthesized analogues **12b**–**c** and **13b**–**g** were more potent against RDL_{ac} and RDL_{bc} GABARs than RDL_{ad} and RDL_{bd} GABARs (Fig. 3.2A), with ~1.5- to ~4-fold higher inhibition in the former than in the latter. The different sensitivities of the four variants to the synthesized analogues are similar to those of the agonists GABA and muscimol, implying that the synthesized analogues bind to the same site as agonists.

Compounds **13b**–**g**, which exerted relatively greater inhibitory effects, were further evaluated in RDL_{ac} GABARs with the generation of antagonist concentration–response curves in the presence of 10 μM (EC_{50}) GABA (Fig. 3.3A). The 3-biphenylyl analog (**13b**), with an IC_{50} value of 30.0 μM, is among the analogues that displayed the greatest antagonism in the ac variant (Table 3.2). The replacement of the 3-biphenylyl group with a 2-naphthyl and a 4-biphenylyl group to yield **13c** and **13d** resulted in 2.3- and 1.8-fold increases in the IC_{50} value, respectively. The 1-naphthyl analog (**13e**) had a potency similar to that of **13b** in the ac variant. Thus, the 3-biphenyl group is advantageous compared with the 4-biphenyl group; the 1-naphthyl group is preferable to the 2-naphthyl group. The introduction of a methoxyl group into **13c** to yield **13f** led to a 1.9-fold increased potency in the ac variant, whereas the potency of **13g**, in which a hydroxyl group was introduced, was similar to that of **13c** in the ac variant. Compound **13b** was further examined for its potencies in other RDL variants of HF RDLRs. Figure 3.3B shows concentration–response curves for **13b** in the presence of the EC_{50} of GABA in the four variants. No significant differences were observed in the IC_{50} values of **13b** between the ac and bc variants or between the ad and bd variants, whereas the IC_{50} values of **13b** in the ad and bd variants were ~3-fold greater compared with

those in the ac and bc variants (Table 3.2). These findings were analogous to those in the EC_{50} values of GABA and muscimol in the four variants, indicating that **13b** most likely acts on the same site as agonists. The different amino acid residues in the region encoded by exon 6 in different variants may cause the difference in the sensitivity to CAs and agonists.

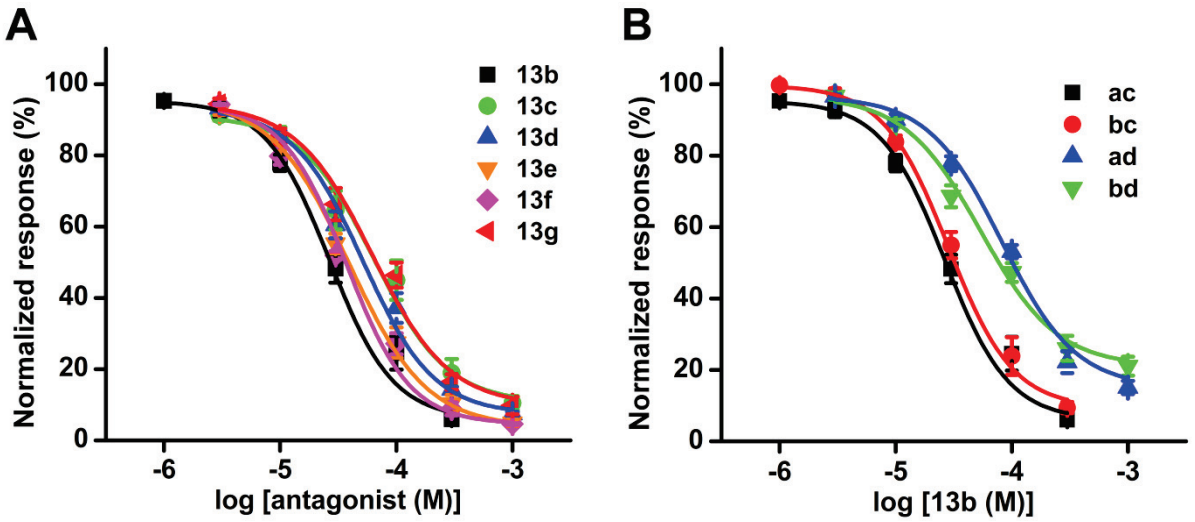

Figure 3.3 Effects of the 3-isoxazolol analogues on GABA-induced currents in HF RDLRs expressed in *Xenopus* oocytes. Data represent means ± SEM (n = 4–6). (A) Concentration–response inhibition curves of 4-aryl-5-carbamoyl-3-isoxazolols (**13b–g**) in the HF RDL_{ac} variant. The EC_{50} (10 μM) of GABA was used to induce the currents. (B) Concentration–response inhibition curves of **13b** in four GABAR variants. Responses were normalized relative to currents induced by the EC_{50} of GABA for each variant.

Table 3.2 Inhibition of GABA (EC_{50})-induced currents by 4-aryl-5-carbamoyl-3-isoxazolols (**13b**–**g**) in the four variants of HF RDLRs

Comp.	IC_{50} (μM)			
	RDL_{ac}	RDL_{bc}	RDL_{ad}	RDL_{bd}
13b	30.0 ± 2.6^{a}	34.3 ± 2.4^{a}	107.2 ± 8.1^{b}	96.0 ± 4.9^{b}
13c	67.7 ± 3.0^{c}	> 100	> 100	> 100
13d	53.3 ± 3.4^{d}	ND	> 100	> 100
13e	38.5 ± 4.9^{a}	ND	≈ 100	> 100
13f	36.0 ± 3.5^{a}	ND	> 100	> 100
13g	64.9 ± 2.7^{cd}	> 100	> 100	> 100

Data are means ± SEM (n = 4). The different superscript letters within a row and a column indicate statistically significant difference with $p < 0.01$ and $p < 0.05$, respectively. ND: not determined.

3.3.4. Mode of antagonism.

To determine whether synthesized 3-isoxazolols act as CAs, the GABA concentration–response relationships in the presence and absence of **13b** were examined in the ac variant. The GABA concentration–response curves made a parallel rightward shift with increasing **13b** concentrations, indicating a competitive mechanism (Fig. 3.4). The EC_{50} values of GABA in the absence and presence of 30 and 100 μM **13b** were 10.6, 27.2, and 55.6 μM, respectively. The potency of GABA was decreased 2.6- and 5.2-fold in the presence of 30 and 100 μM **13b**, respectively, whereas the efficacy of GABA remained unchanged. These results indicate that **13b** competes with GABA for the orthosteric site to stabilize the closed conformation of chloride channels.

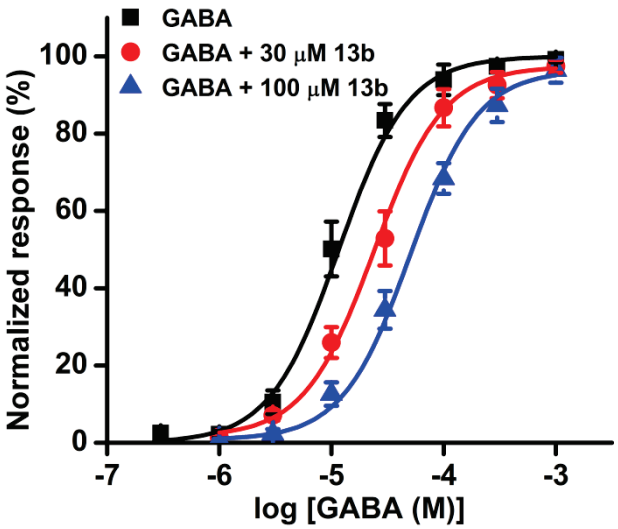

Figure 3.4 GABA concentration–response curves of HF RDL_{ac} GABARs in the presence and absence of 30 and 100 μM **13b**. Responses were normalized relative to the maximum current induced by 1 mM GABA in each oocyte. Data represent means ± SEM (n = 4–6).

3.3.5. Insecticidal activity

CAs stabilize the closed conformation of GABAR channels and should thus exert insecticidal effects when they act at insect GABARs. There is no information about the insecticidal action of CAs. I investigated whether **13b**, which showed the highest antagonism, has intrinsic insecticidal activity by injection into adult female HFs. The LD_{50} value of **13b** was estimated to be 5.6 (4.9–6.3) nmol/HF (95% confidence interval in parentheses). The finding that **13b** shows insecticidal activity by definition is somewhat encouraging, although the activity was not prominent and was observed by injection but not topical application.

3.3.6. Molecular interaction between ligands and HF RDLR

To understand the molecular mechanisms of the interaction between 3-isoxazolols and insect GABARs, GABA, muscimol, and the 3-biphenylyl analog (**13b**) were docked into the

orthosteric binding site of a HF RDL_{ac} GABAR homology model constructed based on the X-ray crystal structure of the human homopentameric β3 GABAR. The β3 subunit shares 38.7% amino acid identity with the RDL_{ac} subunit. The most likely binding poses were selected based on the score. The orthosteric site of Cys-loop receptors, which is located in the extracellular interface of two adjacent subunits (Fig. 3.5), is formed by loops A−C from the principal subunit and loops D−F from the complementary subunit (Miller and Smart, 2010). Similarly, the orthosteric binding pocket of the constructed model is basically formed by Phe144, Val146, Glu202, Ser203, Phe204, Gly205, Ile245, Leu247, and Arg254 from the principal subunit and by Tyr88, Leu90, Tyr107, Arg109, and Met224 from the complementary subunit. The distance between two key residues Glu202 and Arg109 is approximately 9.0 Å.

The docking simulation showed that the protonated amino groups of GABA and muscimol are located close to Glu202 of loop B and that they form an electrostatic interaction and hydrogen bonds with this residue (Figs. 3.6A and B). Arg109 of loop D electrostatically interacts with the deprotonated carboxyl group of GABA and the deprotonated hydroxyl group (or the isoxazole ring) of muscimol. In addition, Arg109 serves as a hydrogen bond donor for the carboxylate of GABA and the hydroxyl oxygen or the nitrogen atom of muscimol. These important interactions were observed in the docking simulation results using another HF RDLR homology model in our previous studies (Liu et al., 2014; Rahman et al., 2014) and are apparently conserved in *Drosophila* RDLRs (Ashby et al., 2012; Comitani et al., 2014; McGonigle et al., 2010). Tyr252 of loop C, which surrounds the protonated amino group of GABA and muscimol, may produce a cation-π interaction, as

proposed for *Drosophila* RDLRs (Ashby et al., 2012; Comitani et al., 2014; McGonigle et al., 2010). Similar orientations and interactions of GABA and muscimol in the binding site indicate that these two agonists interact with HF RDLRs in an identical mode.

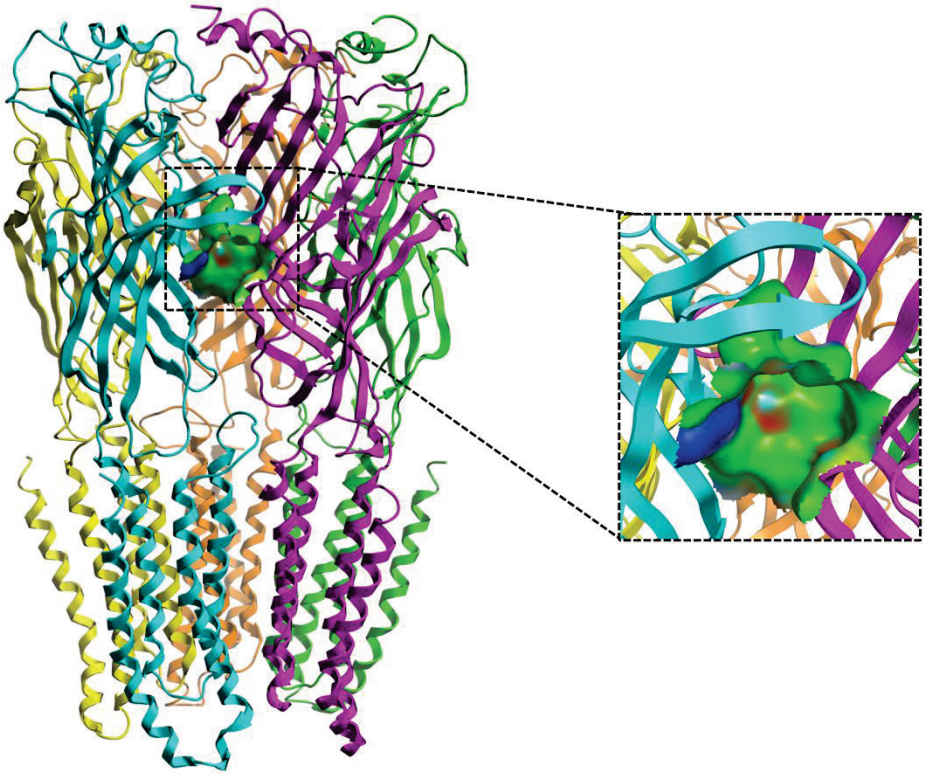

Figure 3.5 View of the orthosteric binding pocket in a HF RDL_{ac} GABAR homology model. The solvent-accessible surface of the binding cavity in a HF RDL_{ac} GABAR homology model was created using MOE 2011.10 software (Chemical Computing Group, Montreal, Canada). The surface map illustrates the location and the size of the orthosteric binding pocket, which was used for docking simulation. The solvent-accessible surface is shown in green for hydrophobic region, in blue for mildly polar region, and in purple for hydrogen bonding region.

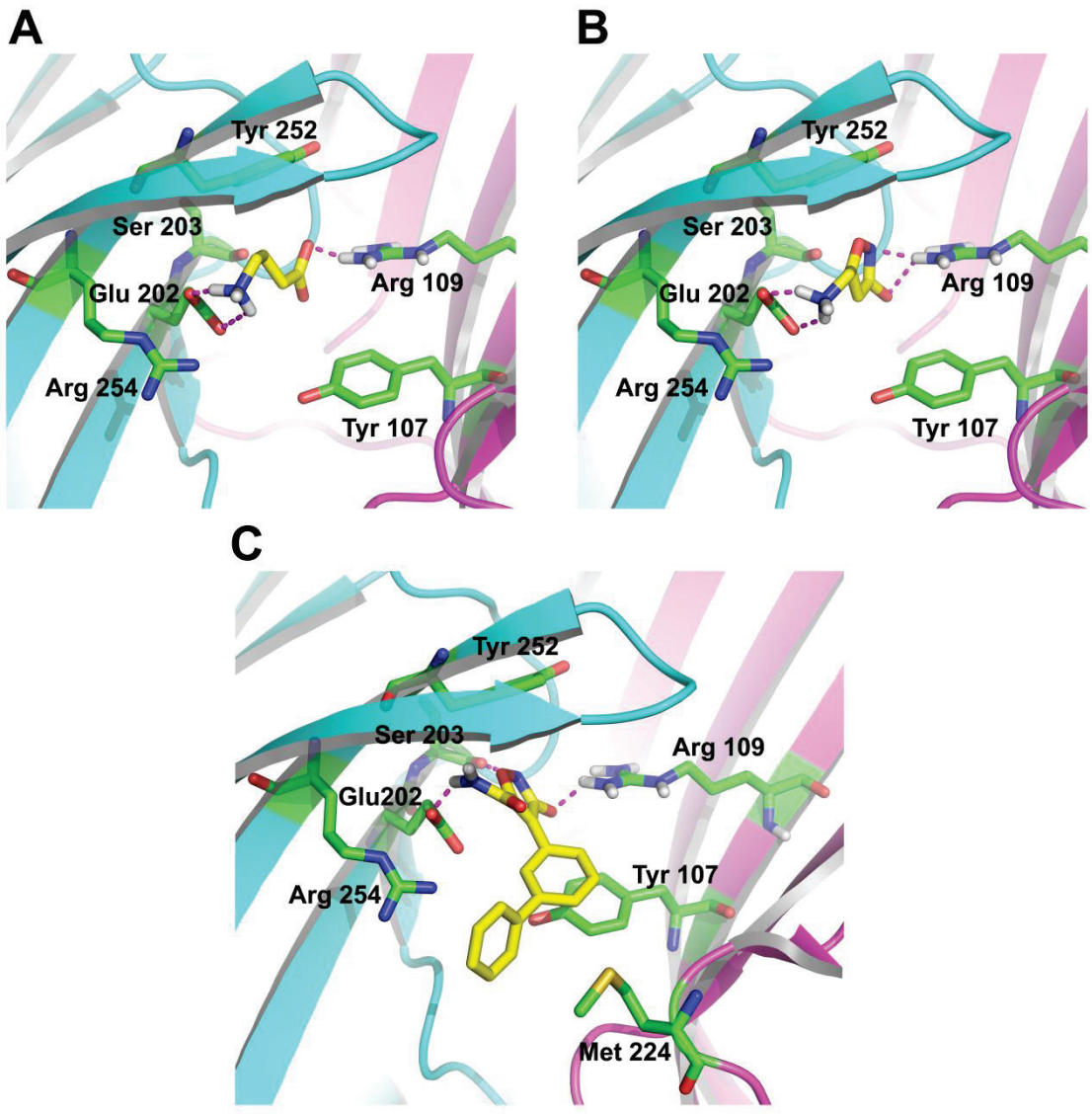

Figure 3.6 Simulation of the docking of GABA, muscimol, and **13b** into the orthosteric binding site of a HF RDL_{ac} GABAR homology model. The crystal structure of the homopentameric human β3 GABAR (PDB: 4COF) was used as a template to construct the model. (A) Docking of GABA into the orthosteric site. (B) Docking of muscimol. (C) Docking of **13b**.

Docking of the 4-(3-biphenylyl) analog (**13b**) to the homology model of the HF RDLR predicts that the 5-carbamoyl-3-isoxazolol scaffold of **13b** lies between Glu202 (loop B) and Arg109 (loop D) in the same orientation as muscimol (Figs. 3.6B and C). Similar to the cases of GABA and muscimol, the side chain of Arg109 electrostatically interacts with the

deprotonated hydroxyl group of **13b** and forms a hydrogen bond with the same group; the side chain of Glu202 functions as a hydrogen acceptor for the carbamoyl group of **13b**. Furthermore, the two amino acid residues, Arg254 of loop C and Tyr107 of loop D, surround the 3-biphenylyl group of **13b**. The present docking studies of **13b** predict that the 3-biphenylyl group points out of the binding site and may form a cation-π interaction with Arg254 and a π-π interaction with Tyr107. The orientation of the 3-biphenylyl group is in contrast with that of the 4-substitution of thio-4-PIOL analogues in Chapter 2 (Liu et al., 2014). This difference may be due to the different templates used in the homology modeling. It has yet to be elucidated which orientation is feasible.

3.4. Conclusion

I synthesized a novel class of competitive HF RDLR antagonists (**13b**–**g**) by replacing the aminomethyl group of muscimol with a carbamoyl group and simultaneously introducing bicyclic aromatic groups at the 4-position. All of the analogues exhibited antagonism of the four splice variants of HF RDLRs, the most potent compound being 4-(3-biphenylyl)-5-carbamoyl-3-isoxazolol (**13b**). The potencies of **13b** in RDL_{ac} and RDL_{bc} GABARs were ~3-fold greater than those in RDL_{ad} and RDL_{bd} GABARs, and this potency difference in these variants is similar to the potency difference of agonists. The identification of a novel series of competitive GABAR antagonists serves to widen the current scope for insecticidal chemicals competitively acting at the orthosteric sites beyond those of gabazine and thio-4-PIOL derivatives.

Chapter 4

Differential interactions of 5-(4-piperidyl)-3-isoxazolol analogues with insect GABA receptors leading to functional selectivity

4.1. Introduction

Insect RDLRs contain multiple binding sites located at the extracellular and transmembrane domains for a number of agonists, antagonists, and modulators (Buckingham and Sattelle, 2010; Casida, 2015; Casida and Durkin, 2015; Ozoe et al., 2009; Ozoe, 2013;). Conventional insecticides such as fipronil are NCAs of insect RDLRs that block the channels by interacting with channel-lining residues. In contrast to these well-known NCAs, the pharmacology of insect RDLR CAs is not well understood.

Several series of 4-substituted 4-PIOLs, 4-substituted thio-4-PIOLs, and 5-substituted 4-PHPs were recently developed as potent CAs of mammalian $GABA_A$Rs (Fig. 1.8; Frølund et al., 2002, 2005, 2007; Krehan et al., 2006; Møller et al., 2010). The studies in Chapter 2 revealed that thio-4-PIOL and its 4-aryl analogues exhibited competitive antagonism in insect RDLRs and moderate insecticidal activity (Liu et al., 2014). However, the analogues of 4-PIOL and 4-PHP have not been tested in insect RDLRs (Fig. 1.10). In an effort to identify potent CAs for insect RDLRs, I examined the effects of 4-(3-biphenylyl)-/4-arylalkly-substituted 4-PIOLs and 5-(3-biphenylyl)-4-PHP (Fig. 4.1) on three insect RDLRs in this chapter. Here, I describe that a cation-π interaction between the aromatic rings of analogues

and an Arg residue in the orthosteric site is the key interaction leading to the antagonism of RDLRs.

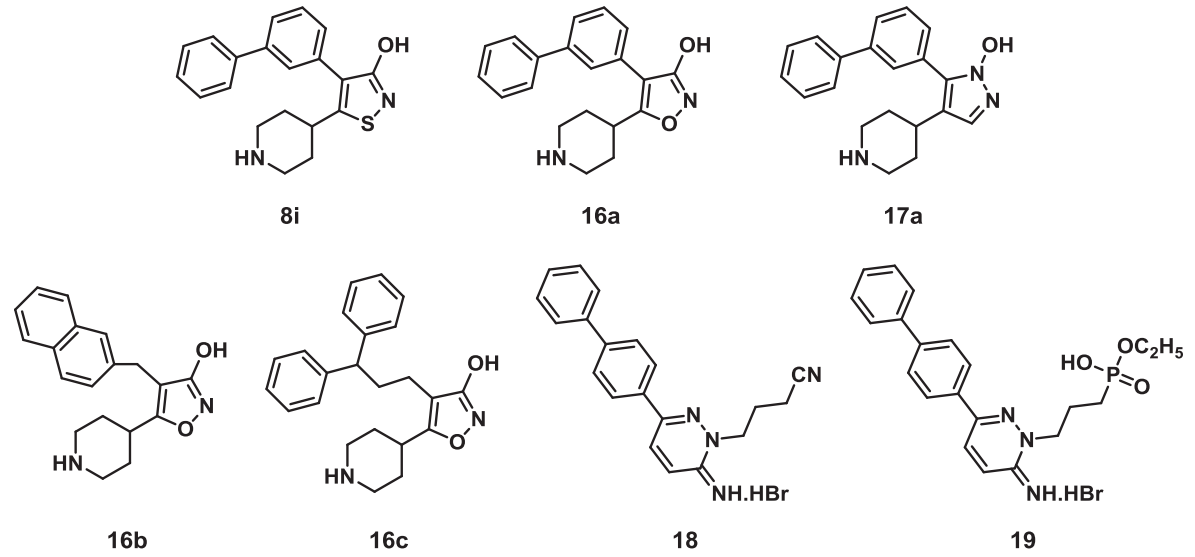

Figure 4.1 Chemical structures of 4-(3-biphenylyl)-thio-4-PIOL (**8i**), 4-(3-biphenylyl)-4-PIOL (**16a**), 4-(2-naphthylmethyl)-4-PIOL (**16b**), 4-(3,3-diphenylpropyl)-4-PIOL (**16c**), 5-(3-biphenylyl)-4-PHP (**17a**), and 1,3-disubstituted 1,6-dihydro-6-iminopyridazines (**18** and **19**).

4.2. Materials and methods

4.2.1. Chemicals

GABA and general reagents were purchased from Sigma-Aldrich Co., LLC. (Tokyo, Japan) or Life Technologies, Thermo Fisher Scientific Inc. (Waltham, MA, USA), unless otherwise noted. The thio-4-PIOL analogue (**8i**) was available from Chapter 2. The 4-PIOL analogues (**16a**, **16b**, and **16c**), the 4-PHP analogue (**17a**), and dihydroiminopyridazines (**18** and **19**) were available from earlier studies (Frølund et al., 2002, 2005, 2007; Møller et al., 2010; Rahman et al., 2014).

4.2.2. Preparation of cRNAs encoding three insect RDL subunits

The GABARs used in the present study are CC, HF, and SBP RDL_{bd} GABARs. The cRNA of HF RDL_{bd} subunits was synthesized as previously described in Chapter 3.2.17. The full-length cDNAs encoding the bd splice variants of the CC and SBP RDL subunits (DDBJ accession Nos.: DD171257 and AB253526, respectively) were cloned into the plasmid vectors pcDNA3 and pcDNA3.2, respectively, as previously described (Narusuye et al., 2007). The cDNA templates including the upstream RNA polymerase promoter site was amplified by PCR using specific primers and KOD-Plus-Ver.2 (Toyobo, Tokyo, Japan). The following primers were used: pcDNA3F (5'-CTTTCCAAAATGTCGTAACAACTCC-3') and pcDNA3R (5'-TCCAGGGTCAAGGAAGGCAC-3') for CC *Rdl*; and pcDNA3F and attB2R (5'-ACCACTTTGTACAAGAAAGCTG-3') for SBP *Rdl*. All PCR products were purified using the illustra GFX PCR DNA and Gel Band Purification Kit (GE Healthcare UK, Ltd., Little Chalfont, UK) and were validated by sequence analysis. The capped cRNAs were synthesized using T7 polymerase (mMessage mMachine T7 Ultra Kit; Ambion, Austin, TX) and dissolved in sterile RNase-free water at a concentration of 543 ng/nl.

4.2.3. Site-directed mutagenesis of RDL subunits

Point mutations were introduced into CC and HF RDL subunits using QuikChange site-directed mutagenesis kit (Stratagene, La Jolla, CA) according to the manufacturer's instruction. The designed oligonucleotide primers were used as follows: R150M 5'-GCAACGAATTCATC**ATG**ATTCATCATTCTGG-3' for CC *Rdl* and R254M 5'-GGAAATTATTCG**ATG**CTGGCTTGCGAG-3' for HF *Rdl* (mutations are bold and

underlined). The mutations were verified by sequence analysis. The cRNAs of the mutant RDL subunits were synthesized as previously described in Chapter 4.2.2.

4.2.4. TEVC electrophysiology

The effects of five 4-PIOL analogues (Fig. 4.1) on GABA-induced currents in the three RDLRs expressed in *Xenopus* oocytes were examined using TEVC electrophysiology as previously described in Chapter 2.2.11.2. The alignment of the amino acid sequences displays high sequence identity (>78%) among these RDLRs (Table 4.1). All experiments were performed using at least three different oocytes obtained from at least two different frogs. EC_{50} and IC_{50} values were obtained from concentration–response data by nonlinear regression analysis using OriginPro 8J (OriginLab, Northampton, MA) and are presented as the mean ± SEM.

Table 4.1 Percent identity matrix of three insect RDL amino acid sequences

	CC RDL	HF RDL	SBP RDL
CC RDL	100.0	81.0	78.1
HF RDL	81.0	100.00	81.5
SBP RDL	78.1	81.5	100.0

4.2.3. Homology modeling and ligand docking studies

The X-ray crystal structure of the homopentameric human β3 GABAR (PDB: 4COF) (Miller and Aricescu, 2014) was chosen as a template to construct three insect RDLR and a α1β2γ2 $GABA_AR$ homology models. The CC, HF, and SBP RDL subunits were aligned

individually to the β3 subunit using ClustalW software. These alignments were used to build the respective homopentameric RDL model using MOE 2014.09 software (Chemical Computing Group, Montreal, Canada). The human $GABA_AR$ α1, β2, and γ2 subunits (DDBJ accession Nos.: X14766, S77553, and X15376, respectively) were also aligned individually to the β3 subunit using ClustalW software. These alignments were used to build a heteropentameric $GABA_AR$ model assembly in a counterclockwise configuration of (β2)(α1)(β2)(α1)(γ2). The obtained models were optimized geometrically using the AMBER99 force field. Compound **16a** was created in a zwitterionic form and compound **13b** (Chapter 3.2.11) was created in a deprotonated hydroxyl form using MOE Builder. The docking studies were performed as previously descried in Chapter 2.2.14. The non-bonded interactions between ligands and receptors were analyzed using extended Hückel theory in MOE.

4.3. Results and discussion

4.3.1. Antagonism of CC GABARs

The previous FMP assays indicated that 4-(3-biphenylyl)-thio-4-PIOL (**8i**) is a CA with an IC_{50} value of 10.6 μM in CC RDLRs in Chapter 2. I first examined the antagonism of CC RDLRs by the analogue of **8i** (Fig. 4.1) using the TEVC assay with *Xenopus* oocytes. Consistent with the previous finding in Chapter 2, **8i** was a moderately potent antagonist of CC RDLRs, which inhibited 48 μM (EC_{50}) GABA-induced currents by 50.6% at 30 μM (Fig. 4.2A). 4-(3-Biphenylyl)-4-PIOL (**16a**) showed higher inhibition (89.8%) of GABA-induced currents at 30 μM (Fig. 4.2A), indicating that the 3-isoxazolol is preferable to the

3-isothiazolol for the antagonism of CC RDLRs. This result is in contrast to previous findings that thio-4-PIOL analogues showed higher affinity and potency in human $GABA_A$Rs than 4-PIOL analogues (Krehan et al., 2006). 4-(3-Biphenylyl)-4-PHP (**17a**) exhibited only 29.8% inhibition at 30 μM, indicating that the introduction of the 1-hydroxypyrazole is not beneficial for producing potent CAs against RDLRs (Fig. 4.2A). Thus, the heterocyclic moieties of these analogues greatly affect the antagonism of CC RDLRs.

Next, the effects of the 4-substituents of **16a** on antagonism were investigated. Replacement of the 3-biphenylyl group of **16a** with a 2-naphthylmethyl and a 3,3-diphenylpropyl group to give **16b** and **16c**, respectively, resulted in decreased inhibition of GABA-induced currents, indicating that the aromatic rings linked to the 4-position of the isoxazole ring with a methylene(s) are disadvantageous for antagonism. This is also in contrast to previous findings in human $GABA_A$Rs (Frølund et al., 2002), suggesting that the structure of the orthosteric binding site might be different between insect and mammalian GABARs and that this difference might be utilized for designing safe insecticides.

The antagonism of CC RDLRs by **16a** was further examined at various concentrations. As shown in current traces in Figure 4.2B, GABA-induced currents in CC RDLRs were greatly attenuated by repeated GABA applications with 30 μM **16a** being perfused. Compound **16a** inhibited the responses of CC RDLRs to GABA in a concentration-dependent manner, with an IC_{50} value of 3.4 ± 0.2 μM (mean ± SEM, n = 3) (Fig. 4.2C). To our knowledge, **16a** is the most potent CA reported to date against CC RDLRs.

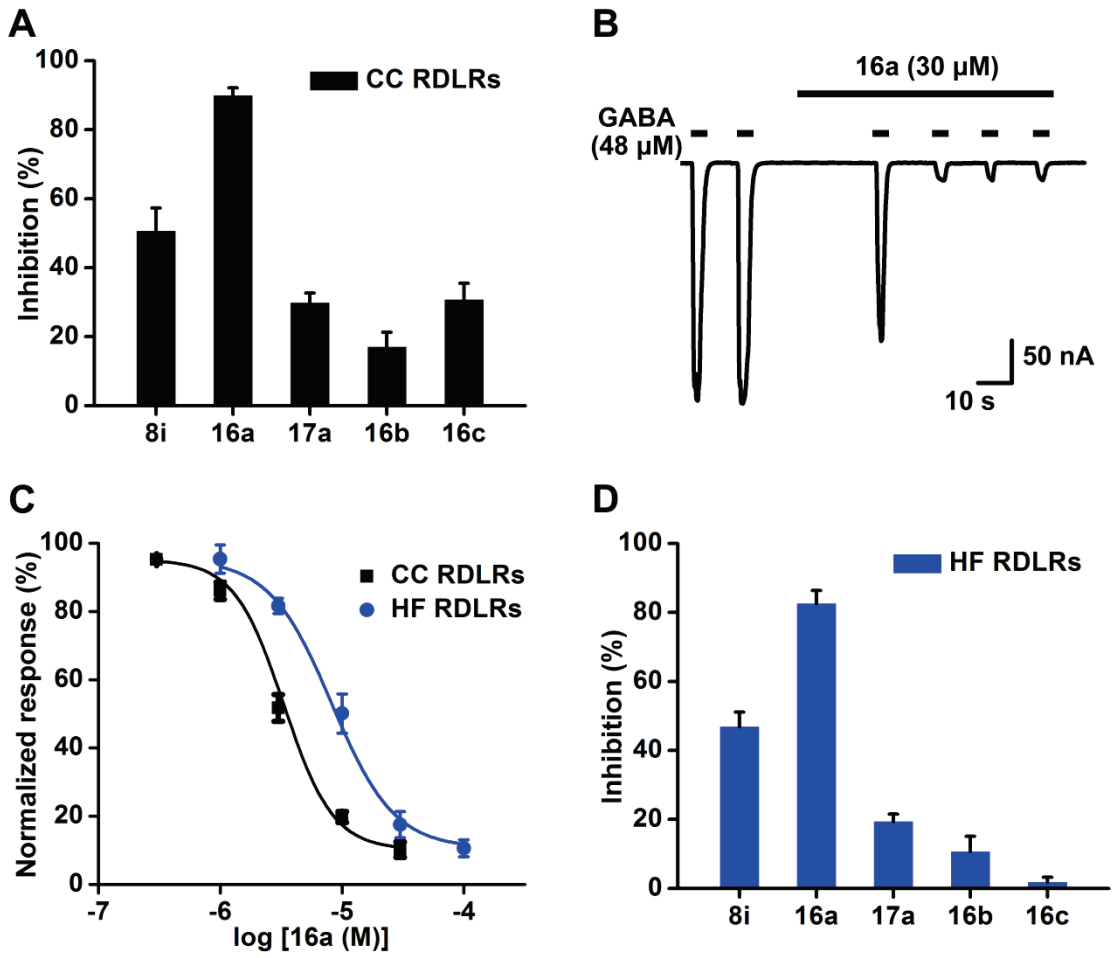

Figure 4.2 Effects of compounds **8i**, **16a**–**c**, and **17a** on GABA-induced currents in CC and HF RDLRs expressed in *Xenopus* oocytes. (A) Inhibition of GABA-induced currents by the title compounds (30 μM) in CC RDLRs. (B) Application protocol to test the inhibition of GABA-induced currents by 30 μM **16a** in CC RDLRs. (C) Concentration-response inhibition curves of **16a** in CC and HF RDLRs. Responses were normalized relative to currents induced by the EC_{50} of GABA for each receptor. (D) Inhibition of GABA-induced currents by the title compounds (30 μM) in HF RDLRs. The EC_{50} of GABA was used to induce currents for CC (48 μM) and HF (60 μM) RDLRs, respectively. Data points are the mean ± SEM of three to four independent assays.

4.3.2. Antagonism of HF GABARs

I next examined the antagonism of HF RDLRs by the same series of analogues. Compound **8i** at 30 μM showed 46.9% inhibition of 60 μM (EC_{50}) GABA-induced currents in HF RDLRs expressed in *Xenopus* oocytes, as previously observed in Chapter 2. As in CC RDLRs, **16a** exhibited the highest activity with 82.5% inhibition at 30 μM in HF RDLRs, whereas the other compounds (**16b–c** and **17a**) showed low activities with less than 30% inhibition (Fig. 4.2D). All the analogues showed slightly lower inhibitions in HF RDLRs than in CC RDLRs when compared at 30 μM. The IC_{50} value of **16a** in HF RDLRs was calculated from concentration–current inhibition relationships to be 10.2 ± 1.1 μM (mean ± SEM, n = 3, Fig. 4.2C), which is 3-fold greater than that in CC RDLRs, indicating that **16a** is a more potent antagonist in CC RDLRs than in HF RDLRs.

4.3.3. Antagonism and agonism of SBP GABARs

I subsequently investigated the abilities of the five analogues to inhibit 16 μM (EC_{50}) GABA-induced currents in SBP RDLRs using the TEVC assay. Compound **8i** at 30 μM inhibited GABA-induced currents by only approximately 20% in SBP RDLRs (Figs. 4.3A and B). This is in line with the previous FMP assay results in Chapter 2, which showed that **8i** displayed no antagonism at 10 μM in SBP RDLRs although it had 96.3% inhibition at 100 μM (Liu et al., 2014). All other compounds exhibited similar or even lower antagonistic activity in SBP RDLRs.

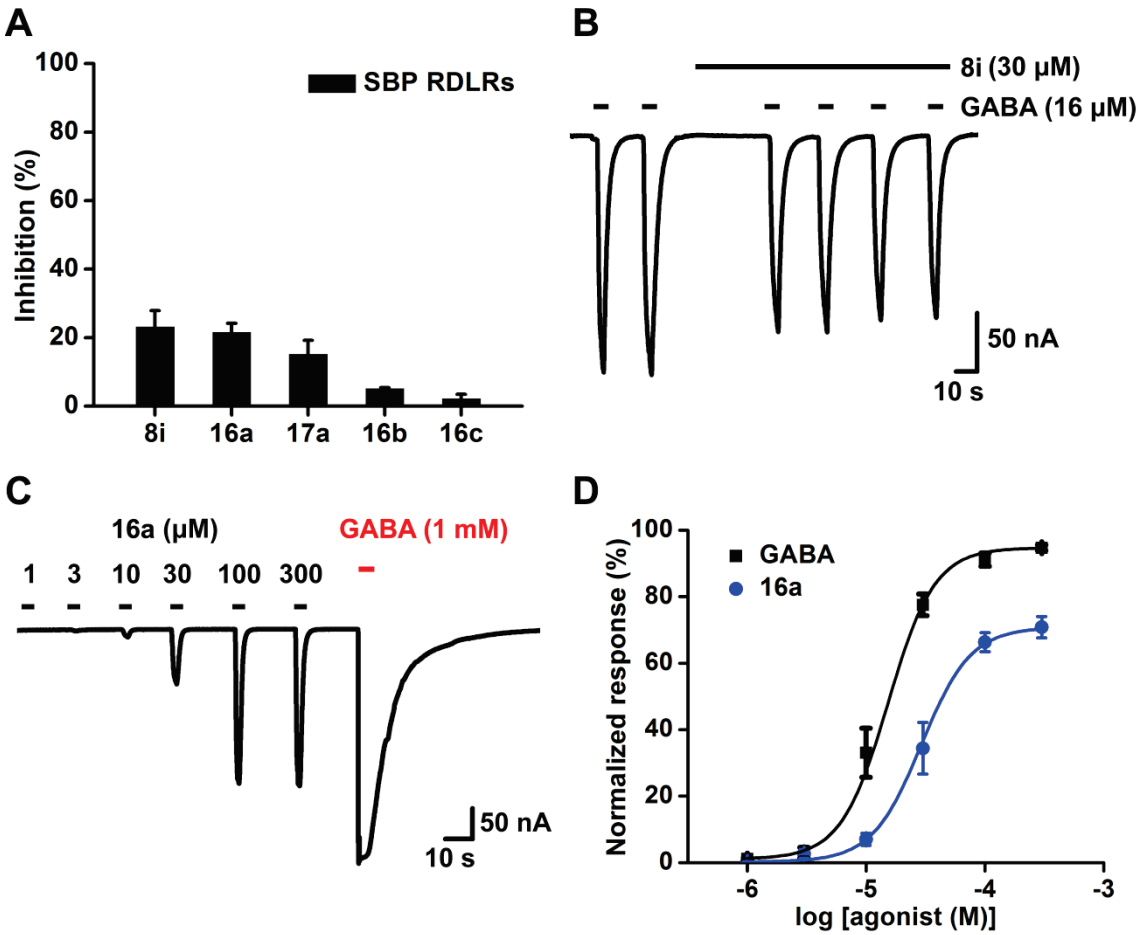

Figure 4.3 Effects of **8i**, **16a–c**, and **17a** on GABA-induced currents in SBP RDLRs expressed in *Xenopus* oocytes. (A) Inhibition of GABA-induced currents by the title compounds (30 μM). The EC_{50} (16μM) of GABA was used to induce currents. (B) An example of GABA-induced currents inhibited by 30 μM **8i**. (C) Representative traces showing the inward currents induced by various concentrations of **16a**. (D) Concentration-response curves of **16a** and GABA; responses were normalized relative to the maximum current induced by 1 mM GABA. Data points are the mean ± SEM of four to eight independent assays.

In contrast to other analogues, **16a** is interesting in that it alone induced concentration-dependent inward currents in SBP RDLRs (Fig. 4.3C). The EC_{50} value and the Hill coefficient of **16a** were determined to be 31.3 ± 3.4 μM (mean ± SEM, n = 4) and 2.5 ± 0.3 (mean ± SEM, n = 4), respectively. Although the current amplitude increased with increasing concentrations of **16a**, the maximal current was 70.8 ± 3.2% (mean ± SEM, n = 4) of those induced by GABA (Fig. 4.3D), indicating that **16a** is a partial agonist of SBP RDLRs. Given our previous result that 4-PIOL is a partial agonist in SBP RDLRs expressed in S2 cells (Narusuye et al., 2007), the common scaffold of **16a** and 4-PIOL, 5-(4-piperidyl)-3-isoxazolol, might be a structural feature that gives rise to partial agonism, although this assertion has yet to be determined.

Compound **16a** also inhibited GABA-induced currents by 21.6 ± 2.7% (mean ± SEM, n = 4) at 30 μM, while **16a** alone induced currents, with 55.3 ± 5.5% (mean ± SEM, n = 4) of currents induced by 16 μM GABA (Fig. 4.4A). As **16a** induced inward currents by acting at SBP RDLRs, I examined whether **8i**, the isothiazolol analogue of **16a**, also shows agonism at a higher concentration in SBP RDLRs. However, compound **8i** (100 μM) failed to induce currents but had an ability to inhibit GABA (EC_{50})-induced currents by 66.8 ± 2.0% (mean ± SEM, n = 4), indicating that **8i** is a pure antagonist unlike **16a** (Fig. 4.4B). I also examined whether the partial agonism by **16a** is suppressed by the CAs that we reported earlier (Rahman et al., 2014). The **16a**-induced currents were inhibited by the CAs dihydroiminopyridazines **18** and **19** (300 μM) by 79.9 ± 4.1% and 86.5 ± 1.3% (mean ± SEM, n = 3), respectively (Fig. 4.4C). Taken together, these findings indicate that **16a** acts as a partial orthosteric agonist in SBP RDLRs.

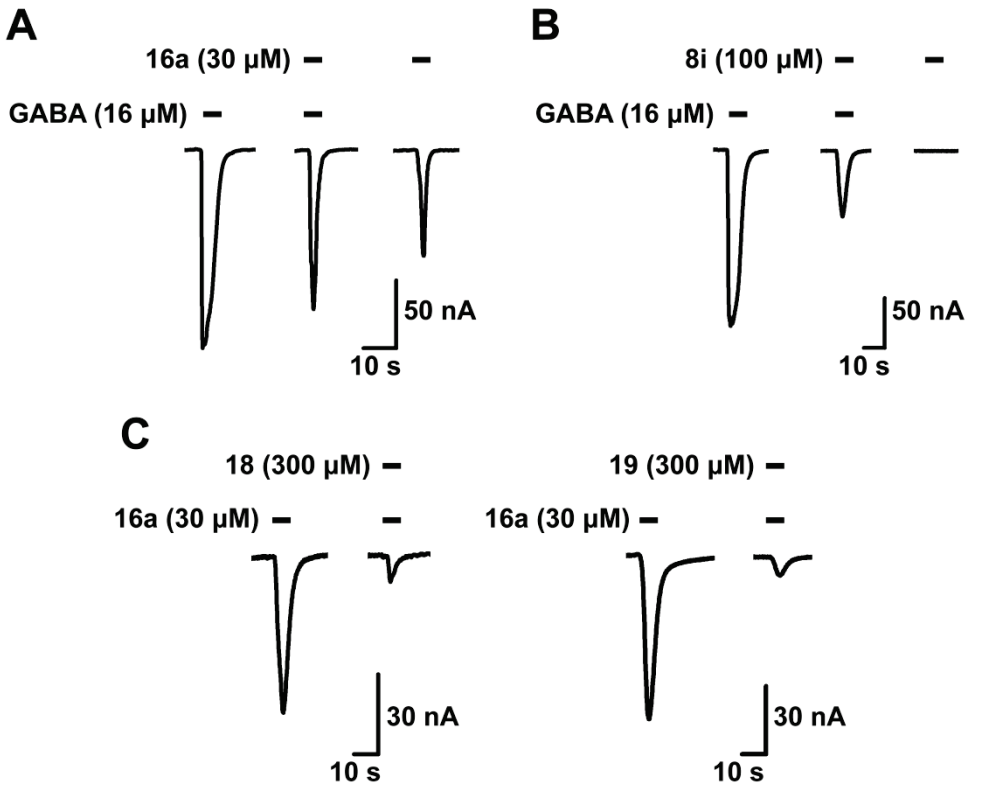

Figure 4.4 Effects of **8i** and **16a** on SBP RDLRs. (A) Representative current traces from an oocyte showing the application of the EC_{50} of GABA alone, the co-application of GABA (EC_{50}) and **16a** (30 μM), and the application of **16a** (30 μM) alone. (B) Representative current traces from an oocyte showing that **8i** (100 μM) inhibited the response induced by the EC_{50} of GABA. Compound **8i** alone failed to induce currents at 100 μM. (C) Representative traces of currents induced by **16a** in the absence and presence of 300 μM **18** or **19**.

4.3.4. Docking studies in insect RDLRs

To identify the mechanisms underlying the antagonism and agonism by the 4-PIOL analogues, I generated three RDLR homology models. The X-ray crystal structures of two ligand-gated chloride channels, the *C. elegans* GluCl and the β3 GABAR, have been published (Hibbs and Gouaux, 2011; Miller and Aricescu, 2014). The CC, HF, and SBP RDL subunits share 44.2, 44.2, and 44.5% identities with the β3 subunit, respectively, which are

higher than those (approximately 40%) with the *C. elegans* GluCl-α subunit. RDLRs share the agonist GABA with the β3 GABAR. RDLRs and the β3 GABAR have only one disulfide bond at the ECD of each subunit, whereas the GluCl has two disulfide bonds. The RDLR homology models were constructed based on the X-ray crystal structure of the human homopentameric β3 GABAR solved at 3 Å resolution (Miller and Aricescu, 2014). The employed β3 GABAR is in a desensitized state that binds an agonist benzamidine at the orthosteric site.

The orthosteric site of Cys-loop receptors, including GABARs, is formed by discontinuous regions termed "loops" in the extracellular interface between two neighboring subunits: loops A–C on the principal subunit and loops D–F on the complementary subunit. Previous studies indicated that GABA in the zwitterionic form interacts with two key amino acid residues, a Glu residue of loop B and an Arg residue of loop D in insect RDLRs (Ashby et al., 2012; Comitani et al., 2014; Liu et al., 2014). Both residues seem to play a critical role in the interaction of orthosteric ligands with insect RDLRs. I previously showed that the 5-(4-piperidyl)-3-isothiazolol scaffold of **8i** lies between Glu202 of loop B and Arg109 of loop D in an MdRDLR model in Chapter 2. Glu202 and Arg109 were predicted to interact with the protonated nitrogen atom of the piperidine ring and the deprotonated hydroxyl group, respectively.

In a HF RDLR model constructed in this chapter, **16a** was shown to have interactions similar to that of **8i** described above (Fig. 4.5A). As in the HF RDLR model, the 5-(4-piperidyl)-3-isoxazolol scaffold of **16a** lies between the equivalent amino acid residues (Glu188 of loop B and Arg95 of loop D) in the CC RDLR model, with electrostatic

interactions and hydrogen bonding (Fig. 4.5B). The 3-biphenylyl group of **16a** faces the inner side of the binding pocket in the CC RDLR model so that it can form a cation-π interaction with Arg150 of loop E (Fig. 4.5B), whereas the group faces the outer side of the binding pocket in the HF RDLR model so that it can form a cation-π interaction with Arg254 of loop C (Fig. 4.5A). Two corresponding Arg residues in loops C and E in human α1β2 $GABA_A$Rs were reported to stabilize the antagonist-bound state (Goldschen-Ohm et al., 2011). This suggests that the cation-π interaction between the biphenylyl group of **16a** and an Arg might be responsible for the antagonism of CC and HF RDLRs. The opposite orientations of the 3-biphenylyl group of **16a** in two models might account for the difference in its antagonistic activity in CC and HF RDLRs. The cavities that accommodate aromatic substituents might exist on both sides of the core region connecting the key residues, Glu and Arg, in insect GABARs in analogy with $GABA_A$Rs (Sander et al., 2011). In addition, the 3-biphenylyl group of **16a** forms a CH-π interaction with Phe130 of loop A in the CC RDLR model and with Tyr88 of loop D in the HF RDLR model. The equivalent aromatic residues, which constitute the so-called 'aromatic box', are conserved in the *Drosophila* RDLR and the human $GABA_C$R and are involved in the interaction with GABA (Ashby et al., 2012; Comitani et al., 2014; Lummis et al., 2011, 2012). In the *Drosophila* RDLRs, a Phe residue in loop B and a Tyr residue in loop C form cation-π interactions with the pronated amino group of GABA (Lummis et al., 2012). The corresponding residues in the CC and HF RDLR models were also found to contribute to the formation of the binding sites, but not to have direct interactions with the protonated nitrogen atom of **16a**. However, in the CC RDLR model, Tyr238 of loop C, which corresponds to the Tyr residue of the *Drosophila* RDLRs,

forms a CH-π interaction with the carbon atom next to the nitrogen atom of the piperidine ring.

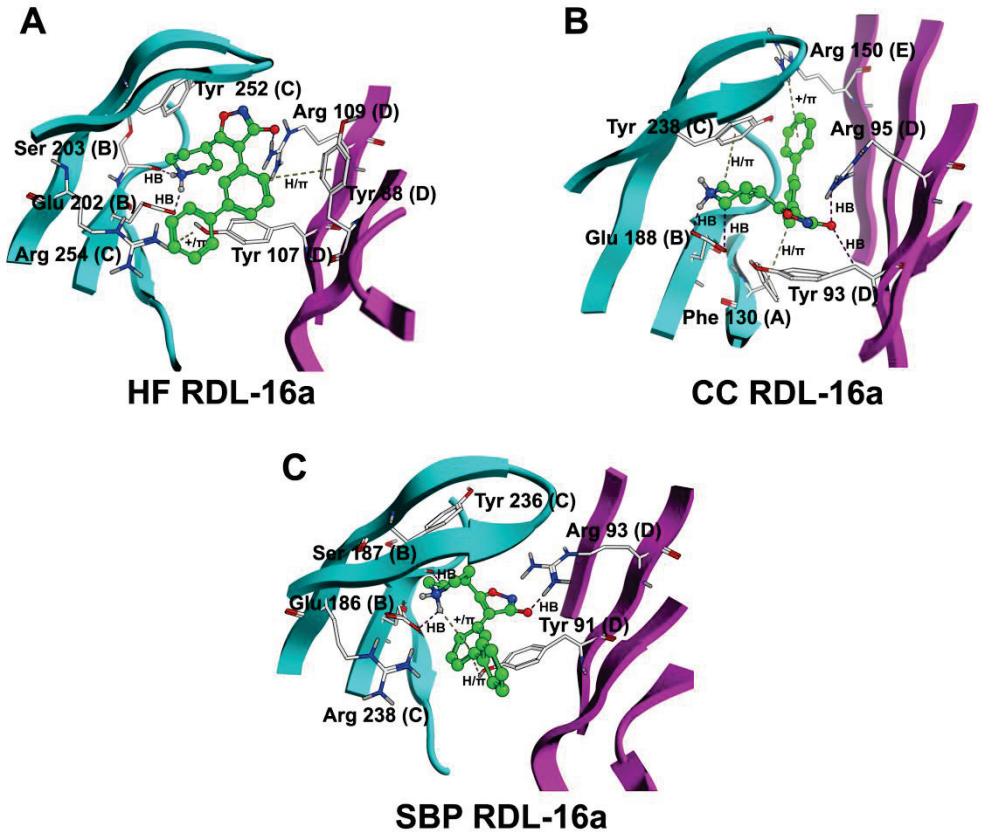

Figure 4.5 Simulation of the dockings of **16a** into the orthosteric binding sites of RDLRs. (A) HF RDLR. (B) CC RDLR. (C) SBP RDLR. The residues are labeled with loop names in parentheses. The interaction lines are labeled with HB (hydrogen bonding interactions), H/π (CH-π interactions), and +/π (cation-π interactions).

In the SBP RDLR model, Glu186 of loop B, which corresponds to Glu202 of MdRDLR, forms an electrostatic interaction and a hydrogen bond with the protonated nitrogen atom of the piperidine ring of **16a** (Fig. 4.5C). The side chain of Arg93 in loop D, which corresponds to Arg109 of the HF RDLR, electrostatically interacts with the 3-isoxazole nitrogen atom of **16a**. Arg93 also plays a role as a hydrogen-bond donor for the deprotonated oxygen of the

hydroxyl group. The docking pose of **16a** in the SBP RDLR model resembles that in the HF RDLR model. However, the protonated nitrogen atom of the piperidine ring of **16a** forms an intramolecular cation-π interaction with the 3-biphenylyl group (Fig. 4.5C). Due to this intramolecular interaction, **16a** fails to form a cation-π interaction with Arg238 of loop C. As it is postulated that a cation-π interaction between the 3-biphenylyl group of **16a** and Arg254 of HF RDLRs plays a critical role for the antagonism, the failure of the cation-π interaction with Arg238 in the SBP RDLR model might explain, in part, that **16a** shows agonism rather than antagonism in SBP RDLRs. Furthermore, the docking pose of **16a** in the SBP RDLR model seems to be in accord with a recent result in the partial agonist complexes of acetylcholine binding protein, in which the aromatic groups of the nicotinic partial agonists are extended out of the binding pocket and point to loop F of the complementary subunit (Hibbs et al., 2009). It is assumed that loop C caps the orthosteric site upon agonist binding to transmit the activation signal to the channel domain (Miller et al., 2010). The loop-C capping dictates whether a ligand is a full agonist, a partial agonist, or an antagonist. It has yet to be determined whether the orientation of **16a** in SBP RDLRs is associated with the capping.

The docking simulation revealed that the Arg residues in loops C and E play important roles for the binding of **16a** in CC and HF RDLRs. To obtain solid evidence for this finding, I constructed two mutants, R150M CC RDLRs and R254M HF RDLRs. However, when expressed in *Xenopus* oocytes, these mutants yielded no GABA (1 mM)-induced currents (Fig. 4.6), indicating that the Arg residues are critical for the GABA binding or function of both RDLRs. Mutation of the two corresponding Arg residues of the *Drosophila* RDLRs to Ala (R166A and R256A) also resulted in nonfunctional or defective receptors (Ashby et al.,

2012). These results indicate that alternative approaches are needed to prove the importance of the Arg residues in loops C and E for the antagonism of insect RDLRs by CAs.

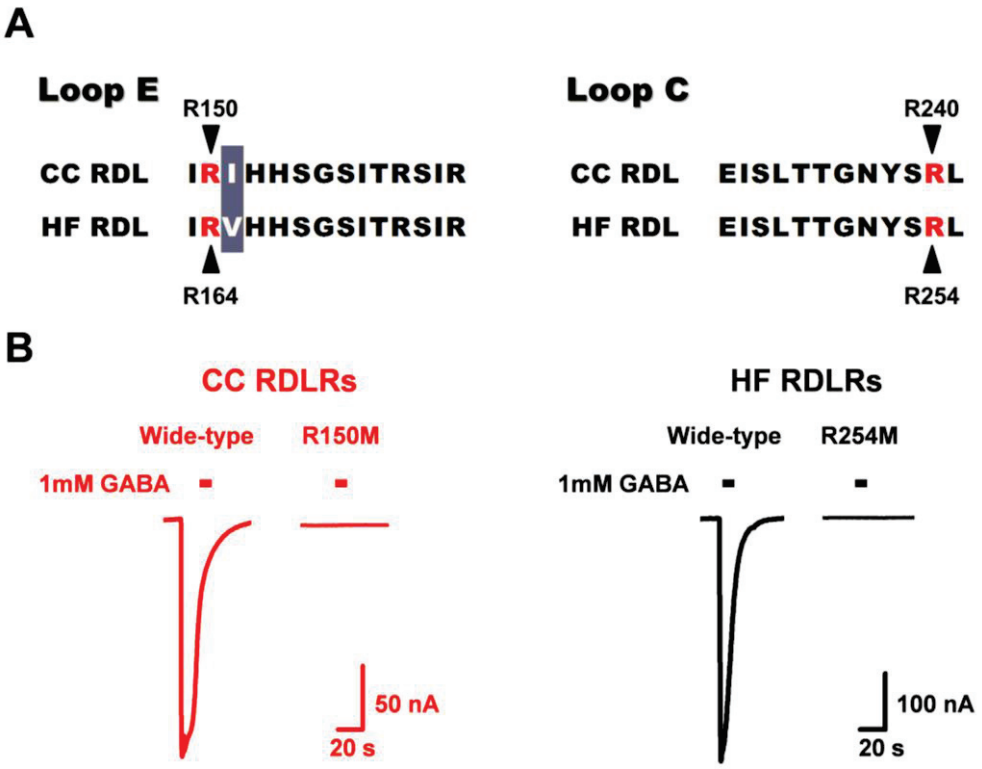

Figure 4.6 Site-directed mutations in CC and HF RDLRs. (A) Sequences alignments of putative loops E and C in the orthosteric site of CC and HF subunits. The residues pointed by arrowheads are the positions (CC R150 and HF R254) under investigation. (B) Representative current traces of 1 mM GABA in wide-type and mutant RDLRs. Mutant RDLRs, CC R150M and HF R254M, failed to show response to 1 mM GABA.

4.3.5. Docking studies in mammalian $GABA_A$Rs

Although compound **16a** was found to be the most potent CA of insect RDLRs, its micormolar potency in RDLRs is still much lower than its reported low nanomolar potency in mammalian $GABA_A$Rs. Structural insights into the interactions between **16a** and mammalian $GABA_A$Rs might provide helpful information for the further design and development of more

potent CAs for insect GABARs. Thus, I constructed an α1β2γ2 $GABA_AR$ model using the same template, the homopentameric human β3 $GABA_AR$ (PDB: 4COF), and docked **16a** into the orthosteric binding site of the model.

As shown in Figure 4.7A, the docking pose of **16a** in the $GABA_AR$ model resembles that in the CC RDLR model (Fig. 4.5B). The piperidylisoxazole scaffold of **16a** anchored between β2 Glu155 (loop B) and α1 R66 (loop D), which is excellent agreement with the docking results of 4-PIOL analogues in a previously reported $GABA_AR$ model (Sander et al., 2011). The residues Glu155 and R66 might interact with the protonated piperidine ring nitrogen and the deprotonated 3-hydroxyisoxazole, respectively. The 3-biphenylyl group of **16a** points inward in the binding pocket and may form a cation-π interaction with α1 Arg119 (loop E). This finding is consistent with the orientation of the 3-biphenylyl group in the CC RDLR model.

Four aromatic residues, β2 Tyr97 (loop A), Phe200 (loop C), Tyr205 (loop C), and α1 Phe64 (loop D), constitute the aromatic box to surround the piperidine ring, which is similar to the docking simulation of **8h** and **8i** in the HF RDLR model in Chapter 2. However, of these aromatic residues, only β2 Tyr205 was found to be conserved as Tyr 252 in HF RDLRs (Table 4.2; Fig. 4.8). The differences of the other aromatic residues between the $GABA_AR$ and the HF RDLR might affect the potency of **16a** as well as other CAs. β2 Phe200, which corresponds to HF RDL Leu247 (Table 4.2), forms a CH–π interaction with **16a** in the $GABA_AR$ model. However, Leu247 in the HF RDLR model was not found to contribute to the formation of the binding site (Fig. 4.5A). Thus, this non-conserved F–to–L mutation potentially eliminates a CH–π interaction, making the HF RDLR less sensitive to **16a**. In

addition, α1 Phe64 is equivalent to HF RDL Tyr107 as well as $GABA_C$ ρ1 Tyr102, and β2 Tyr97 is equivalent to HF RDL Phe144 as well as $GABA_C$ ρ1 Phe 138 (Table 4.2; Fig. 4.8). Zhang et al. (2008) reported that the gabazine insensitivity of the ρ1 $GABA_CR$ was mainly determined by Tyr102, Phe138, and Tyr106, which differ from those in the $GABA_AR$. In the HF RDLR model, the corresponding residues Tyr107 and Phe144 also have no direct interaction with **16a** (Fig. 4.5A). In some respects, RDLRs rather resemble $GABA_CRs$ because the recombinant ρ $GABA_CRs$ form functional homo-oligomers and are insensitive to bicuculline (Zhang et al., 2001; Buckingham and Sattelle, 2010). Therefore, it is plausible that residues Tyr107 and Phe144 in HF RDL also might not be beneficial for the sensitivity of gabazine and **16a**. Further mutation experiments are needed to verify the roles of these residues (Leu247, Tyr107, and Phe144) in insect RDLRs.

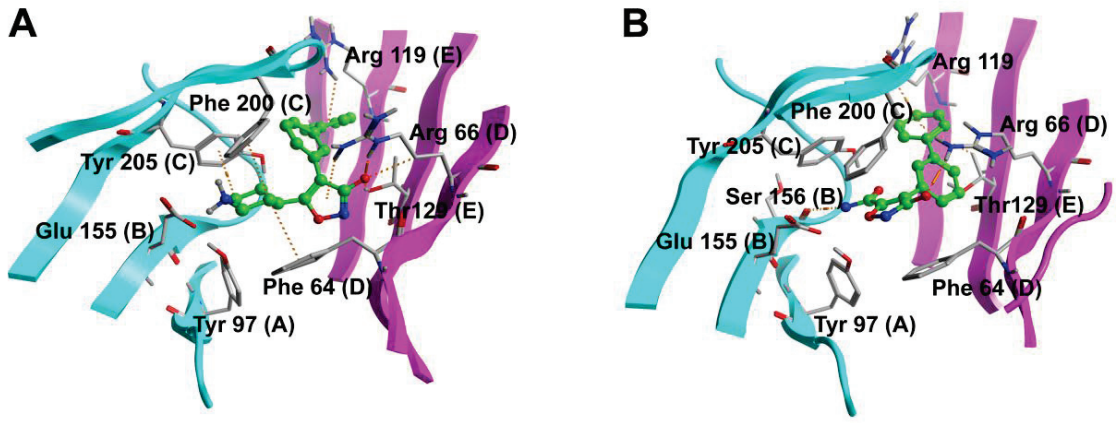

Figure 4.7 Simulation of the dockings of **16a** and **13b** into the orthostric binding site of an α1β2γ2 $GABA_AR$ model. The crystal structure of the homopentameric human β3 $GABA_AR$ (PDB: 4COF) was used as the template. (A) Docking of **16a**. (B) Docking of **13b**. The β2 and α1 subunits are colored in cyan and magenta, respectively.

Table 4.2 Alignment of four aromatic residues contributing to the aromatic box of the orthosteric binding site in different GABARs

Receptor	Loop A	Loop C		Loop D
$GABA_A$ (α1β2γ2)	Tyr 97 (β2)	Phe200 (β2)	Tyr205 (β2)	Phe64 (α1)
HF RDL	Phe144	Leu247	Tyr252	Tyr107
$GABA_C$ (ρ1)	Phe138	Tyr241	Tyr247	Tyr102

The residue numbers of $GABA_CR$ are from Zhang et al., 2008.

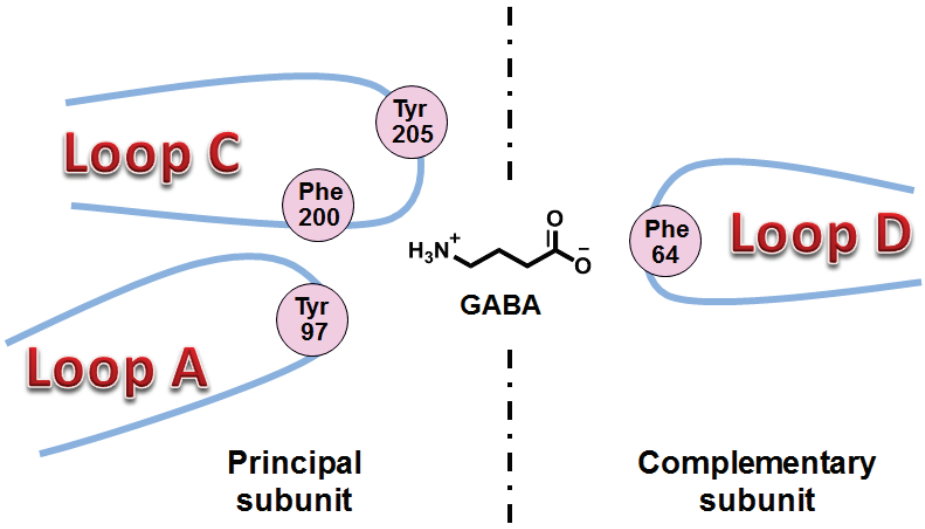

Figure 4.8 Schematic presentation of four aromatic residues contributing to the aromatic box of the orthosteric binding site in α1β2γ2 $GABA_AR$s.

I also docked compound **13b**, a CA of HF RDLRs mentioned in Chapter 3, into the orthosteric site of the α1β2γ2 $GABA_AR$ model (Fig. 4.7B). The 5-carbamoyl-3-isoxazolol scaffold of **13b** lies between β2 Glu155 (loop B) and α1 R66 (loop D). The similar cation-π interaction of the 3-biphenylyl group with α1 Arg119 (loop E) was also found. The side chains of α1 Phe64 and β2 Phe200 are parallel to the 3-isoxazole ring, forming π-π interactions. These sandwich π-stacking interactions seem to stabilize the binding of **13b**,

possibly increasing its affinity in $GABA_A$Rs. However, the activity of **13b** and other 4-substituted 5-carbamoyl-3-isoxazolols (**13c**–**g**) in mammalian GABARs has yet to be determined.

4.4. Conclusion

I examined the interaction of three 3-isoxazolols, a 3-isothiazolol, and a 1-hydroxypyrazole with insect RDLRs. The 3-isoxazolol was found to be a more efficient ring system for antagonism than the 3-isothiazolol and the 1-hydroxypyrazole in CC and HF RDLRs. 4-(3-Biphenylyl)-4-PIOL (**16a)** was a potent CA in CC and HF RDLRs with IC_{50} values of 3.4 and 10.2 μM, respectively. To our knowledge, **16a** is the most potent CA reported to date for CC and HF RDLRs. In contrast, **16a** was a partial orthosteric agonist in SBP RDLRs with an EC_{50} value of 31.3 μM. An Arg residue in loop E in CC RDLRs or loop C in HF RDLRs was predicted to form a cation-π interaction with the biphenylyl group of **16a**, respectively. This cation-π interaction, which most likely stabilizes the antagonist-bound receptor state, might be critical for the antagonism of **16a** in CC and HF RDLRs. The lack of this interaction might lead to the partial agonism of SBP RDLRs by **16a**. Although the complex interactions between **16a** and insect GABARs remain to be further clarified, the results described herein provide invaluable information for the ongoing development of novel insecticides targeting the orthosteric site of insect GABARs.

Chapter 5

Conclusion

Insect ionotropic GABARs are of interest as they are targets of highly effective insecticides such as fipronil. High-affinity CAs have potentials to be utilized for the development of novel GABAR-targeting insecticides because they inhibit GABARs by acting at the orthosteric site that is different from the sites of NCA insecticides. However, insect GABAR CAs have not been well studied. Therefore, several series of insect GABAR CAs, including thio-4-PIOL analogues, muscimol analogues, and 4-PIOL analogues, have been synthesized and pharmacologically characterized in the present study (Fig. 5.1). Most of the compounds exhibited the antagonism of insect GABARs in the micromolar range.

First, I synthesized a series of thio-4-PIOL analogues by introducing bulky aromatic groups into the 4-position of the 3-isothiazole ring and examined for their antagonism of SBP, CC, and HF RDLRs expressed in *Drosophila* S2 cells or *Xenopus* oocytes using the FMP or the TEVC assay. The analogues with bicyclic aromatic substituents at 100 μM exhibited high inhibition of GABA-induced response in three receptors. Particularly, the 2-naphthyl (**8h**) and the 3-biphenylyl (**8i**) analogues had antagonist potencies with IC_{50} values in the low micromolar range. Both compounds exhibited weak insecticidal activities when tested against HFs. In HF RDLRs, compound **8h** caused a parallel rightward shift of the GABA dose–response curve, suggesting competitive antagonism by these analogues. Ligand docking studies using a HF RDLR homology model predicted that the orthosteric site contains two cavities large enough to accommodate bicyclic aromatic 4-substituents of thio-4-PIOL

analogues. These findings indicate that the bicyclic system is effective for CAs of insect RDLRs in inhibiting GABA-mediated receptor activation, and that the orthosteric site of insect RDLRs might be a potential target site of insecticides.

According to the clues derived from the thio-4-PIOL analogues, I next introduced the 2-naphthyl and 3-biphenyl groups into the 4-position of muscimol. The obtained compounds (**12b** and **12c**) showed antagonism at 100 μM in four variants of HF RDLRs, indicating that the 3-isoxazolol scaffold might be useful for developing CAs of HF RDLRs and that the bicyclic aromatic system at the 4-position of the 3-isoxazole ring might also be beneficial for antagonistic activity. Subsequently, the replacement of the aminomethyl group with a carbamoyl group at the 5-position of muscimol and the simultaneous introduction of bicyclic aromatic groups at the 4-position resulted in six 4-aryl-5-carbamoyl-3-isoxazolols (**13b**–**g**), which exhibited significantly enhanced antagonism with IC_{50} values in the low micromolar range in the ac variant of HF RDLRs. The inhibition of GABA-induced currents by 100 μM analogues was approximately 1.5- to 4-fold greater in the ac and bc variants than in the ad and bd variants. 4-(3-Biphenylyl)-5-carbamoyl-3-isoxazolol (**13b**) displayed competitive antagonism, with IC_{50} values of 30, 34, 107, and 96 μM in the ac, bc, ad, and bd variants, respectively, and exhibited moderate insecticidal activity against HFs, with an LD_{50} value of 5.6 nmol/fly. These findings suggest that these 3-isoxazolol analogues are novel lead compounds for the design and development of insecticides that target the orthosteric site of HF RDLRs. The docking studies predicted that the 3-biphenylyl group of **13b** points out of the binding site and may form a cation-π interaction with an Arg residue. This interaction might be beneficial for competitive antagonism.

I further investigated the effects of three 4-aryl/arylalkyl-4-PIOLs, and a 5-(3-biphenylyl)-4-PHP on three insect RDLRs expressed in *Xenopus* oocytes using the TEVC method. The 3-isoxazolol was found to be a more efficient ring system for antagonism than the 3-isothiazolol and the 1-hydroxypyrazole in CC and HF RDLRs. 4-(3-Biphenylyl)-4-PIOL (**16a**) was found to be the most potent CA reported to date for CC and HF RDLRs, with IC_{50} values of 3.4 and 10.2 μM, respectively. Interestingly, **16a** was a partial orthosteric agonist in SBP RDLRs with an EC_{50} value of 31.3 μM. An Arg150 of loop E in CC RDLRs or an Arg254 of loop C in HF RDLRs was predicted to form a cation-π interaction with the biphenylyl group of **16a**, respectively. This cation-π interaction is most likely responsible for the antagonism of CC and HF RDLRs by **16a**. The lack of this interaction in SBP RDLRs might lead to the partial agonism of **16a**. The relative low potency of **16a** in RDLRs compared with that in mammalian $GABA_A$Rs indicated that structural differences in the orthosteric site might exist between insect RDLRs and mammalian $GABA_A$Rs. Further investigations are needed to determine the key residues for the competitive antagonism of insect RDLRs.

In conclusion, several series of 3-isothiazolols and 3-isoxazolols were synthesized and reported for the first time to show competitive antagonism of insect GABARs with low micromolar IC_{50} values, and some of them exhibited moderate insecticidal activity. The synthetic information and the proposed interaction mechanisms might prove useful for designing and developing novel CA type of GABAR-targeting insecticides.

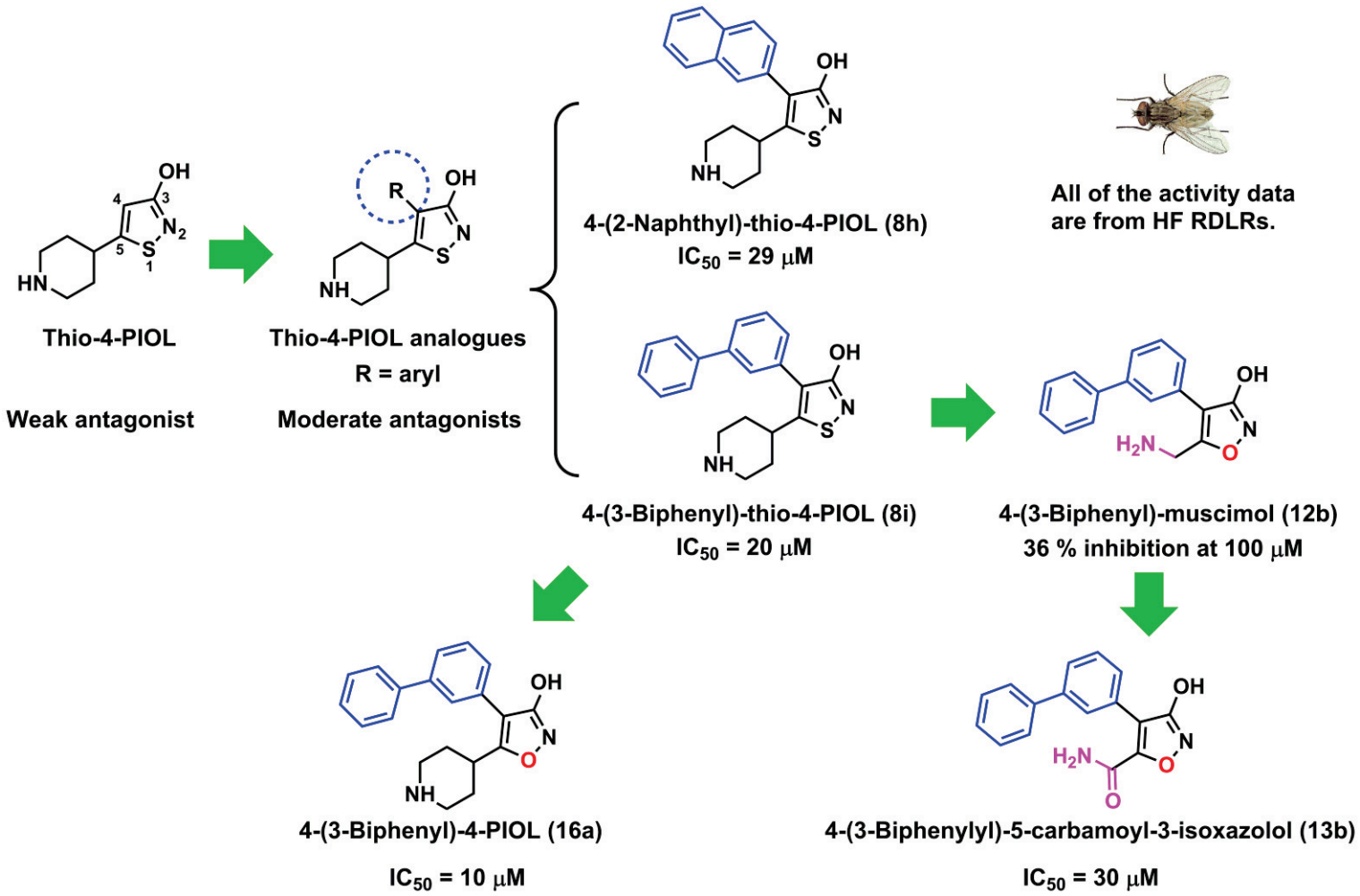

Figure 5.1 Graphical representation of the synthetic strategy for target CAs of insect RDLRs. Data represent the highest activities of the compounds in HF RDLRs.

References

Ashby, J. A.; McGonigle, I. V.; Price, K. L.; Cohen, N.; Comitani, F.; Dougherty, D. A.; Molteni, C.; Lummis, S. C. R. GABA binding to an insect GABA receptor: a molecular dynamics and mutagenesis study. *Biophys. J.* **2012**, 103, 2071–2081.

Awapara, J.; Landua, A. J.; Fuerst, R.; Seale, B. Free γ-aminobutyric acid in brain. *J. Biol. Chem.* **1950**, 187, 35–39.

Barbara, G. S.; Zube, C.; Rybak, J.; Gauthier, M.; Grünewald, B. Acetylcholine, GABA and glutamate induce ionic currents in cultured antennal lobe neurons of the honeybee, *Apis mellifera*. *J. Comp. Physiol. A.* **2005**, 191, 823–836.

Bazemore, A. W.; Elliott, K. A. C.; Florey, E. Isolation of factor I. *J. Neurochem.* **1957**, 1, 334–339.

Bettler, B.; Kaupmann, K.; Mosbacher, J.; Gassmann, M. Molecular structure and physiological functions of $GABA_B$ receptors. *Physiol. Rev.* **2004**, 84, 835–867.

Beugnet, F.; Liebenberg, J.; Halos, L. Comparative efficacy of two oral treatments for dogs containing either afoxolaner or fluralaner against *Rhipicephalus sanguineus* sensu lato and *Dermacentor reticulatus*. *Vet. Parasitol.* **2015**, 209, 142–145.

Bocquet, N.; Nury, H.; Baaden, M.; Le Poupon, C.; Changeux, J. P.; Delarue, M.; Corringer, P. J. X-ray structure of a pentameric ligand-gated ion channel in an apparently open conformation. *Nature* **2009**, 457, 111–114.

Bowery, N. G.; Bettler, B.; Froestl, W.; Gallagher, J. P.; Marshall, F.; Raiteri, M.; Bonner, T. I.; Enna, S. J. International union of pharmacology. XXXIII. Mammalian

γ-aminobutyric acid$_B$ receptors: structure and function. *Pharmacol. Rev.* **2002**, 54, 247–264.

Brejc, K.; van Dijk, W. J.; Klaassen, R. V.; Schuurmans, M.; van Der Oost, J.; Smit, A. B.; Sixma, T. K. Crystal structure of an ACh-binding protein reveals the ligand-binding domain of nicotinic receptors. *Nature* **2001**, 411, 269–276.

Buckingham, S. D.; Hosie, A. M.; Roush, R. L.; Sattelle, D. B. Actions of agonists and convulsant antagonists on a *Drosophila melanogaster* GABA receptor (Rdl) homo-oligomer expressed in *Xenopus* oocytes. *Neurosci. Lett.* **1994**, 181, 137–140.

Buckingham, S. D.; Biggin, P. C.; Sattelle, B. M.; Brown, L. A.; Sattelle, D. B. Insect GABA receptors: splicing, editing, and targeting by antiparasitics and insecticides. *Mol. Pharmacol.* **2005**, 68, 942–951.

Buckingham, S. D.; Sattelle, D. B. GABA receptors of insects. In *Insect Pharmacology: Channels, Receptors, Toxins and Enzymes*; Gilbert, L. I., Gill, S. S., Eds.; Academic Press: London, UK, **2010**; pp 29–64.

Casida, J. E. Golden age of RyR and GABA-R diamide and isoxazoline insecticides: common genesis, serendipity, surprises, selectivity, and safety. *Chem. Res. Toxicol.* **2015**, 28, 560–566.

Casida, J. E.; Durkin, K. A. Novel GABA receptor pesticide targets. *Pestic. Biochem. Physiol.* **2015**, 121, 22–30.

Celie, P. H. N.; Klaassen, R. V.; van Rossum-Fikkert, S. E.; van Elk, R.; van Nierop, P.; Smit, A. B.; Sixma, T. K. Crystal structure of acetylcholine-binding protein from *Bulinus*

truncatus reveals the conserved structural scaffold and sites of variation in nicotinic acetylcholine receptors. *J. Biol. Chem.* **2005**, 280, 26457–26466.

Charnet, P.; Labarca, C.; Leonard, R. J.; Vogelaar, N. J.; Czyzyk, L.; Gouin, A.; Davidson, N.; Lester, H. A. An open-channel blocker interacts with adjacent turns of α-helices in the nicotinic acetylcholine receptor. *Neuron* **1990**, 2, 87–95.

Cole, L. M.; Casida, J. E. GABA-gated chloride channel: binding site for 4'-ethynyl-4-n-[2,3-$^{3}H_2$]propylbicycloorthobenzoate ([^{3}H]EBOB) in vertebrate brain and insect head. *Pestic. Biochem. Physiol.* **1992**, 44, 1–8.

Comitani, F.; Cohen, N.; Ashby, J.; Botten, D.; Lummis, S. C. R.; Molteni, C. Insights into the binding of GABA to the insect RDL receptor from atomistic simulations: a comparison of models. *J. Comput. Aided Mol. Des.* **2014**, 28, 35–48.

daCosta, C. J. B.; Baenziger, J. E. Gating of pentameric ligand-gated ion channels: structural insights and ambiguities. *Structure* **2013**, 21, 1271–1283.

Das, P.; Bell-Horner, C. L.; Machu, T. K.; Dillon, G. H. The $GABA_A$ receptor antagonist picrotoxin inhibits 5-hydroxytryptamine type 3A receptors. *Neuropharmacology* **2003**, 44, 431–438.

Dellisanti, C. D.; Yao, Y.; Stroud, J. C.; Wang, Z. Z.; Chen, L. Crystal structure of the extracellular domain of nAChR α1 bound to α-bungarotoxin at 1.94 Å resolution. *Nat. Neurosci.* **2007**, 10, 953–962.

Domingues, L. N.; Guerrero, F. D.; Becker, M. E.; Alison, M. W.; Foil, L. D. Discovery of the Rdl mutation in association with a cyclodiene resistant population of horn flies, *Haematobia irritans* (Diptera: Muscidae). *Vet. Parasitol.* **2013**, 198, 172–179.

Duittoz, A. H.; Martin, R. J. Antagonist properties of arylaminopyridazine GABA derivatives at the *Ascaris* muscle GABA receptor. *J. Exp. Biol.* **1991**, 159, 149–164.

Enna, S. J.; Möhler, H. In *The GABA Receptors*, Third edition; Humana Press: Totowa, NJ, USA, **2007**; pp 1–109.

Eguchi, Y.; Ihara, M.; Ochi, E.; Shibata, Y.; Matsuda, K.; Fushiki, S.; Sugama, H.; Hamasaki, Y.; Niwa, H.; Wada, M.; Ozoe, F.; Ozoe, Y. Functional characterization of *Musca* glutamate- and GABA-gated chloride channels expressed independently and coexpressed in *Xenopus* oocytes. *Insect Mol. Biol.* **2006**, 15, 773–783.

ffrench-Constant, R. H.; Mortlock, D. P.; Shaffer, C. D.; MacIntyre, R. J.; Roush, R. T. Molecular cloning and transformation of cyclodiene resistance in *Drosophila*: an invertebrate γ-aminobutyric acid subtype A receptor locus. *Proc. Natl. Acad. Sci. U.S.A.* **1991**, 88, 7209–7213.

ffrench-Constant, R. H.; Rocheleau, T. A. *Drosophila* γ-aminobutyric acid receptor gene *Rdl* shows extensive alterntive splicing. *J. Neurochem.* **1993**, 60, 2323–2326.

ffrench-Constant, R. H.; Rocheleau, T. A.; Steichen, J. C.; Chalmers, A. E. A point mutation in a *Drosophila* GABA receptor confers insecticide resistance. *Nature* **1993**, 363, 449–451.

Frey, M.; Jäger, V. Synthesis of *N*-substituted muscimol derivatives including *N*-glycylmuscimol. *Synthesis* **1985**, 12, 1100–1104.

Frølund, B.; Kristiansen, U.; Brehm, L.; Hansen, A. B.; Krogsgaard-Larsen, P.; Falch, E. Partial $GABA_A$ receptor agonists. Synthesis and in vitro pharmacology of a series of

nonannulated analogs of 4,5,6,7-tetrahydroisoxazolo[5,4-c]pyridin-3-ol, *J. Med. Chem.* **1995**, 38, 3287–3296.

Frølund, B.; Tagmose, L.; Liljefors, T.; Stensbøl, T. B.; Engblom, C.; Kristiansen, U.; Krogsgaard-Larsen, P. A novel class of potent 3-isoxazolol $GABA_A$ antagonists: design, synthesis, and pharmacology. *J. Med. Chem.* **2000**, 43, 4930–4933.

Frølund, B.; Jørgensen, A. T.; Tagmose, L.; Stensbøl, T. B.; Vestergaard, H. T.; Engblom, C.; Kristiansen, U.; Sanchez, C.; Krogsgaard-Larsen, P.; Liljefors, T. Novel class of potent 4-arylalkyl substituted 3-isoxazolol $GABA_A$ antagonists: synthesis, pharmacology, and molecular modeling. *J. Med. Chem.* **2002**, 45, 2454–2468.

Frølund, B.; Jensen, L. S.; Guandalini, L.; Canillo, C.; Vestergaard, H. T.; Kristiansen, U.; Nielsen, B.; Stensbøl, T. B.; Madsen, C.; Krogsgaard-Larszen, P.; Liljefors, T. Potent 4-aryl- or 4-arylalkyl-substituted 3-isoxazolol $GABA_A$ antagonists: synthesis, pharmacology, and molecular modeling. *J. Med. Chem.* **2005**, 48, 427–439.

Frølund, B., Jensen, L. S.; Storustovu, S. I.; Stensbøl, T. B.; Ebert, B.; Kehler, J.; Krogsgaard-Larsen, P.; Liljefors, T. 4-Aryl-5-(4-piperidyl)-3-isoxazolol $GABA_A$ antagonists: synthesis, pharmacology, and structure–activity relationships. *J. Med. Chem.* **2007**, 50, 1988–1992.

Gassel, M.; Wolf, C.; Noack, S.; Williams, H.; Ilg, T. The novel isoxazoline ectoparasiticide fluralaner: Selective inhibition of arthropod γ-aminobutyric acid- and L-glutamate-gated chloride channels and insecticidal/acaricidal activity. *Insect Biochem. Mol. Biol*. **2014**, 45, 111–124.

Gisselmann, G.; Plonka, J.; Pusch, H.; Hatt, H. *Drosophila melanogaster* GRD and LCCH3 subunits form heteromultimeric GABA-gated cation channels. *Br. J. Pharmacol.* **2004**, 142, 409–413.

Goldschen-Ohm, M. P.; Wagner, D. A.; Jones, M. V. Three arginines in the $GABA_A$ receptor binding pocket have distinct roles in the formation and stability of agonist- versus antagonist-bound complexes. *Mol. Pharmacol.* **2011**, 80, 647–656.

Goto, J.; Kataoka, R.; Muta, H.; Hirayama, N. ASEDock-docking based on alpha spheres and excluded volumes. *J. Chem. Inf. Model.* **2008**, 48, 583–590.

Hansen, S. B.; Sulzenbacher, G.; Huxford, T.; Marchot, P.; Taylor, P.; Bourne, Y. Structures of *Aplysia* AChBP complexes with nicotinic agonists and antagonists reveal distinctive binding interfaces and conformations. *EMBO J.* **2005**, 24, 3635–3646.

Harvey, R. J.; Schmitt, B.; Hermans-Borgmeyer, I.; Gundelfinger, E. D.; Betz, H.; Darlison, M. G. Sequence of a *Drosophila* ligand-gated ion-channel polypeptide with an unusual amino-terminal extracellular domain. *J. Neurochem.* **1994**, 62, 2480–2483.

Henderson, J. E.; Soderlund, D. M.; Knipple, D. C. Characterization of a putative γ-aminobutyric acid (GABA) receptor β subunit gene from *Drosophila melanogaster*. *Biochem. Biophys. Res. Commun.* **1993**, 193, 474–482.

Henderson, J. E.; Knipple, D. C.; Soderlund, D. M. PCR-based homology probing reveals a family of GABA receptor-like genes in *Drosophila melanogaster*. *Insect Biochem. Mol. Biol.* **1994**, 24, 363–371.

Hibbs, R. E.; Gouaux, E. Principles of activation and permeation in an anion-selective Cys-loop receptor. *Nature* **2011**, 474, 54–60.

Hilf, R. J.; Dutzler, R. X-ray structure of a prokaryotic pentameric ligand-gated ion channel. *Nature* **2008**, 452, 375–379.

Hilf, R. J.; Dutzler, R. Structure of a potentially open state of a proton-activated pentameric ligand-gated ion channel. *Nature* **2009**, 457, 115–118.

Hoestgaard-Jensen, K.; O'Connor, R. M.; Dalby, N. O.; Simonsen, C.; Finger, B. C.; Golubeva, A.; Hammer, H.; Bergmann, M. L.; Kristiansen, U.; Krogsgaard-Larsen, P.; Bräuner-Osborne, H.; Ebert, B.; Frølund, B.; Cryan, J. F.; Jensen, A. A. The orthosteric $GABA_A$ receptor ligand Thio-4-PIOL displays distinctly different functional properties at synaptic and extrasynaptic receptors. *Br. J. Pharmacol.* **2013**, 170, 919–932.

Hosie, A. M.; Sattelle, D. B. Agonist pharmacology of two *Drosophila* GABA receptor splice variants. *Br. J. Pharmacol.* **1996**, 119, 1577–1585.

Hosie, A. M.; Buckingham, S. D.; Presnail, J. K.; Sattelle, D. B. Alternative splicing of a *Drosophila* GABA receptor subunit gene identifies determinants of agonist potency. *Neuroscience* **2001**, 102, 709–714.

Johnston, G. A.; Chebib, M.; Hanrahan, J. R.; Mewett, K. N. Neurochemicals for the investigation of $GABA_C$ receptors. *Neurochem. Res.* **2010**, 35, 1970–1977.

Johnston, G. A. Advantages of an antagonist: bicuculline and other GABA antagonists. *Br. J. Pharmacol.* **2013**, 169, 328–336.

Jones, A. K.; Buckingham, S. D.; Papadaki, M.; Yokota, M.; Sattelle, B. M.; Matsuda, K.; Sattelle, D. B. Splice-variant- and stage-specific RNA editing of the *Drosophila* GABA receptor modulates agonist potency. *J. Neurosci.* **2009**, 29, 4287–4292.

Ju, X.-L.; Ozoe, Y. Bicyclophosphorothionate antagonists exhibiting selectivity for housefly GABA receptors. *Pestic. Sci.* **1999**, 55, 971–982.

Ju, X.-L.; Ozoe, Y. Noncompetitive antagonist-binding sites of rat and housefly γ-aminobutyric acid receptors display different enantiospecificities for *tert*-butyl(isopropyl)bicyclophosphorothionate. *Bioorg. Med. Chem.* **2000**, 8, 2337–2341.

Ju, X.-L.; Fusazaki, S.; Hishinuma, H.; Qiao, X.; Ikeda, I.; Ozoe, Y. Synthesis and structure-activity relationship analysis of bicyclophosphorothionate blockers with selectivity for housefly γ-aminobutyric acid receptor channels. *Pest Manag. Sci.* **2010**, 66, 1002–1010.

Kaji, M. D.; Kwaka, A; Callanan, M. K.; Nusrat, H.; Desaulniers, J. P.; Forrester, S. G. A molecular characterization of the agonist binding site of a nematode cys-loop GABA receptor. *Br. J. Pharmacol.* **2015**, 172, 3737–3747.

Kita, M.; Ozoe, F.; Ozoe, Y. Expression pattern and function of alternative splice variants of glutamate-gated chloride channel in the housefly *Musca domestica*. *Insect Biochem. Mol. Biol.* **2014**, 45, 1–10.

Krall, J.; Balle, T.; Krogsgaard-Larsen, N.; Sørensen, T. E.; Krogsgaard-Larsen, P.; Kristiansen, U.; Frølund, B. $GABA_A$ receptor partial agonists and antagonists: structure, binding mode, and pharmacology. *Adv. Pharmacol.* **2015**, 72, 201–227.

Krehan, D.; Storustovu, S.; Lijefors, T.; Ebert, B.; Nielsen, B.; Krogsgaard-Larsen, P.; Frølund, B. Potent 4-arylalkyl-substituted 3-isothiazolol $GABA_A$ competitive/non-

competitive antagonists: synthesis and pharmacology. *J. Med. Chem.* **2006**, 49, 1388–1396.

Lahm, G. P.; Cordova, D.; Barry, J. D.; Pahutski, T. F.; Smith, B. K.; Long, J. K.; Benner, E. A.; Holyoke, C. W.; Joraski, K.; Xu, M.; Schroeder, M. E.; Wagerle, T.; Mahaffey, M. J.; Smith R. M.; Tong. M.-H. 4-Azolylphenyl isoxazoline insecticides acting at the GABA gated chloride channel. *Bioorg. Med. Chem. Lett.* **2013**, 23, 3001–3006.

Lester, H. A.; Dibas, M. I.; Dahan, D. S.; Leite, J. F.; Dougherty, D. A. Cys-loop receptors: new twist and turns. *Trends Neurosci.* **2004**, 27, 329–336.

Liu, G.; Furuta, K.; Nakajima, H.; Ozoe, F.; Ozoe, Y. Competitive antagonism of insect GABA receptors by 4-substituted 5-(4-piperidyl)-3-isothiazolols. *Bioorg. Med. Chem.* **2014**, 22, 4637–4645.

Lummis, S. C. R.; McGonigle, I.; Ashby, J. A.; Dougherty, D. A. Two amino acid residues contribute to a cation-π binding interaction in the binding site of an insect GABA receptor. *J. Neurosci.* **2011**, 31, 12371–12376.

Lummis, S. C. R.; Harrison, N. J.; Wang, J.; Ashby, J. A.; Millen, K. S.; Beene, D. L.; Dougherty, D. A. Multiple tyrosine residues contribute to GABA binding in the $GABA_C$ receptor binding pocket. *ACS Chem. Neurosci.* **2012**, 3, 186–192.

McGonigle, I.; Lummis, S. C. R. Molecular characterization of agonists that bind to an insect GABA receptor. *Biochemistry* **2010**, 49, 2897–2902.

Martin, R. J.; Sitamze, J.-M.; Duittoz, A. H.; Wermuth, C. G. Novel arylaminopyridazine-GABA receptor antagonists examined electrophysiologically in *Ascaris suum*. *Eur. J. Pharmacol.* **1995**, 276, 9–19.

Millar, N. S.; Buckingham, S. D.; Sattelle, D. B. Stable expression of a functional homo-oligomeric *Drosophila* GABA receptor in a *Drosophila* cell line. *Proc. R. Soc. Lond. B Biol. Sci.* **1994**, 258, 307–314.

Miller, P. S.; Smart, T. G. Binding, activation and modulation of Cys-loop receptors. *Trends Pharmacol. Sci.* **2010**, 31, 161–174.

Miller, P. S.; Aricescu, A. R. Crystal structure of a human $GABA_A$ receptor. *Nature* **2014**, 512, 270–275.

Møller, H. A.; Sander, T.; Kristensen, J. L.; Nielsen, B.; Krall, J.; Bergmann, M. L.; Christiansen, B.; Balle, T.; Jensen, A. A.; Frølund, B. Novel 4-(piperidin-4-yl)-1-hydroxypyrazoles as γ-aminobutyric $acid_A$ receptor ligands: synthesis, pharmacology, and structure–activity relationships. *J. Med. Chem.* **2010**, 53, 3417–3421.

Mortensen, M.; Frølund, B.; Jørgensen, A. T.; Liljefors, T.; Krogsgaard-Larsen, P.; Ebert, B. Activity of novel 4-PIOL analogues at human α1β2γ2S $GABA_A$ receptors–correlation with hydrophobicity. *Eur. J. Pharmacol.* **2002**, 451, 125–132.

Nakao, T.; Naoi, A.; Kawahara, N.; Hirase, K. Mutation of the GABA receptor associated with fipronil resistance in the whitebacked planthopper, *Sogatella furcifera*. *Pestic. Biochem. Physiol.* **2010**, 97, 262–266.

Nakao, T.; Kawase, A.; Kinoshita, A.; Abe, R.; Hama, M.; Kawahara, N.; Hirase, K. The A2'N mutation of the RDL γ-aminobutyric acid receptor conferring fipronil resistance in *Laodelphax striatellus* (Hemiptera: delphacidae). *J. Econ. Entomol.* **2011**, 104, 646–652.

Nakao, T.; Hama, M.; Kawahara, N.; Hirase, K. Fipronil resistance in *Sogatella furcifera*: molecular cloning and functional expression of wild-type and mutant RDL GABA receptor subunits. *J. Pestic. Sci.* **2012**, 37, 37–44.

Nakao, T.; Banba, S.; Nomura, M.; Hirase, K. Meta-diamide insecticides acting on distinct sites of RDL GABA receptor from those for conventional noncompetitive antagonists. *Insect Biochem. Mol. Biol.* **2013**, 43, 366–375.

Nakao, T.; Banba, S. Broflanilide: a meta-diamide insecticide with a novel mode of action. *Bioorg. Med. Chem.* **2016**, 24, 372–377.

Narusuye, K.; Nakao, T.; Abe, R.; Nagatomi, Y.; Hirase, K.; Ozoe, Y. Molecular cloning of a GABA receptor subunit from *Laodelphax striatella* (Fallén) and patch clamp analysis of the homo-oligomeric receptors expressed in a *Drosophila* cell line. *Insect Mol. Biol.* **2007**, 16, 723–733.

Nys, M.; Kesters, D.; Ulens, C. Structural insights into Cys-loop receptor function and ligand recognition. *Biochem. Pharmacol.* **2013**, 86, 1042–1053.

Olsen, R. W. γ-Aminobutyric acid receptor binding antagonism by the amidine steroid RU5135. *Eur. J. Pharmacol.* **1984**, 103, 333–337.

Olsen, R. W.; Sieghart, W. International Union of Pharmacology. LXX. Subtypes of γ-aminobutyric $acid_A$ receptors: classification on the basis of subunit composition, pharmacology, and function. Update. *Pharmacol. Rev.* **2008**, 60, 243–260.

Olsen R. W.; Sieghart, W. $GABA_A$ receptors: Subtypes provide diversity of function and pharmacology. *Neuropharmacology* **2009**, 56,141–148

Othman, N. A.; Gallacher, M.; Deeb, T. Z.; Baptista-Hon, D. T.; Perry, D. C.; Hales, T. G. Influences on blockade by *t*-butylbicyclo-phosphoro-thionate of $GABA_A$ receptor spontaneous gating, agonist activation and desensitization. *J. Physiol.* **2012**, 590, 163–178.

Ozoe, Y.; Takeda, M.; Matsuda, K. γ-Aminobutyric acid receptors: a rationale for developing selective insect pest control chemicals. In *Biorational Control of Arthropod Pests*; Ishaaya, I., Horowitz, A. R., Eds.; Springer: Heidelberg, DE, **2009**; pp 131–162.

Ozoe, Y.; Asahi, M.; Ozoe, F.; Nakahira, K.; Mita, T. The antiparasitic isoxazoline A1443 is a potent blocker of insect ligand-gated chloride channels. *Biochem. Biophys. Res. Commun.* **2010**, 391, 744–749.

Ozoe, Y. γ-Aminobutyrate- and glutamate-gated chloride channels as targets of insecticides. In *Advances in Insect Physiology*; Ephraim, C., Ed.; Academic Press: Burlington, MA, **2013**; Vol. 44, pp 211–286.

Ozoe, Y.; Kita, T.; Ozoe, F.; Nakao, T.; Sato, K.; Hirase, K. Insecticidal 3-benzamido-*N*-phenylbenzamides specifically bind with high affinity to a novel allosteric site in housefly GABA receptors. *Pestic. Biochem. Physiol.* **2013**, 107, 285–292.

Rahman, M. M.; Akiyoshi, Y.; Furutani, S.; Matsuda, K.; Furuta, K.; Ikeda, I.; Ozoe, Y. Competitive antagonism of insect GABA receptors by iminopyridazine derivatives of GABA. *Bioorg. Med. Chem.* **2012**, 20, 5957–5964.

Rahman, M. M.; Liu, G.; Furuta, K.; Ozoe, F.; Ozoe, Y. Synthesis of 1,3-di- and 1,3,4-trisubstituted 1,6-dihydro-6-iminopyridazines as competitive antagonists of insect GABA receptors. *J. Pestic. Sci.* **2014**, 39, 133–143.

Riess, R.; Schön, M.; Laschat, S.; Jäger, V. Evaluation of protecting groups for 3-hydroxyisoxazoles – short access to 3-alkoxyisoxazole-5-carbaldehydes and 3-hydroxyisoxazole-5-carbaldehyde, the putative toxic metabolite of muscimol. *Eur. J. Org. Chem.* **1998**, 3, 473–479.

Roberts, E.; Frankel, S. γ-Aminobutyric acid in brain: its formation from glutamic acid. *J. Biol. Chem.* **1950**, 187, 55–63.

Rudolph, U.; Möhler, H. GABA-based therapeutic approaches: $GABA_A$ receptor subtype functions. *Curr. Opin. Pharmacol.* **2006**, 6, 18–23

Sander, T.; Frølund, B.; Bruun, A. T.; Ivanov, I.; McCammon, J. A.; Balle, T. New insights into the $GABA_A$ receptor structure and orthosteric ligand binding: receptor modeling guided by experimental data. *Proteins* **2011**, 79, 1458–1477.

Schofield, P. R.; Darlison, M. G.; Fujita, N.; Burt, D. R.; Stephenson, F. A.; Rodriguez, H.; Rhee, L. M.; Ramachandran, J.; Reale, V.; Glencorse, T. A.; Seeburg, P. H.; Barnard, E. A. Sequence and functional expression of the $GABA_A$ receptor shows a ligand-gated receptor super-family. *Nature* **1987**, 328, 221–227.

Sieghart, W.; Sperk, G. Subunit composition, distribution and function of $GABA_A$ receptor subtypes. *Curr. Top. Med. Chem.* **2002**, 2, 795–816.

Sine, S. M.; Engel, A. G. Recent advances in Cys-loop receptor structure and function. *Nature* **2006**, 440, 488–455.

Taylor-Wells, J.; Brooke, B. D.; Bermudez, I.; Jones, A. K. The neonicotinoid imidacloprid, and the pyrethroid deltamethrin, are antagonists of the insect Rdl GABA receptor. *J. Neurochem.* **2015**, 135, 705–713.

Unwin, N. Refined structure of the nicotinic acetylcholine receptor at 4Å resolution. *J. Mol. Biol.* **2005**, 346, 967–989.

Wang, D. S.; Mangin, J. M.; Moonen, G.; Rigo, J. M.; Legendre, P. Mechanisms for picrotoxin block of α_2 homomeric glycine receptors. *J. Biol. Chem.* **2006**, 281, 3841–3855.

Wang, X. C.; Hu, Y.; Bonacorsi, S.; Hong, Y.; Burrell, R.; Yu, J. Q. Pd(II)-catalyzed C–H iodination using molecular I_2 as the sole oxidant. *J. Am. Chem. Soc.* **2013**, 135, 10326–10329.

Xu, Y.; Furutani, S.; Ihara, M.; Ling, Y.; Yang, X.; Kai, K.; Hayashi, H.; Matsuda, K. Meroterpenoid chrodrimanins are selective and potent blockers of insect GABA-gated chloride channels. *PLoS ONE*, **2015**, 10: e0122629, doi: 10.1371/journal.pone.0122629.

Zhang, D.; Pan, Z.-H.; Awobuluyi, M.; Lipton, S. A. Structure and function of $GABA_C$ receptors: a comparison of native versus recombinant receptors. *Trends Phamacol. Sci.* **2001**, 22, 121–132.

Zhang, J.; Polishchuk, E. A.; Chen, J.; Ciufolini, M. A. Development of an oxazole conjunctive reagent and application to the total synthesis of siphonazoles. *J. Org. Chem.* **2009**, 74, 9140–9151.

Zhang, J.; Xue, F.; Chang, Y. Structural determinants for antagonist pharmacology that distinguish the ρ1 $GABA_C$ receptor from $GABA_A$ receptors. *Mol. Pharmacol.* **2008**, 74, 941–951.

Zhao, X.; Yeh, J. Z.; Salgado, V. L.; Narahashi, T. Fipronil is a potent open channel blocker of glutamate-activated chloride channels in cockroach neurons. *J. Pharmacol. Exp. Ther.* **2004**, 310, 192–201.

Acknowledgments

I would like to express sincere gratitude to my respected advisor, Dr. Yoshihisa Ozoe, Professor, Department of Life Science and Biotechnology, Faculty of Life and Environmental Science, Shimane University, for his invaluable guidance throughout my graduate research, for his warm encouragement and kind consideration, and for his personal support to my study and life. Without his guidance, I could not complete this dissertation and related publications. His enthusiasm for research and rigorous scholarship will deeply influence and inspire me in my future research and life.

I am greatly indebted to my co-advisors Dr. Hiromitsu Nakajima, Professor of Tottori University, and Dr. Kenjiro Furuta, Assistant Professor of Shimane University, for their helpful discussion and suggestions for my research. I especially thank Ms. Fumiyo Ozoe, Senior researcher of Shimane University, for her valuable guidance and kind assistance in my experiments. I would also like to thank Dr. Izumi Ikeda, Associate professor of Shimane University, for his assistance in many aspects of laboratory experiments.

I would like to appreciate all those people who have assisted in the completion of my work. Special thanks go to my lab mates, Dr. Kita, Mr. Fuse, Mr. Nomura, Dr. Rahman, Ms. Takashima, Mr. Nakata, and Mr. Takatsu for their friendly collaboration and assistance for my study as well as life. To all the past and present lab members, thank you for creating an ideal research environment.

I am grateful to Dr. Toshifumi Nakao, Mitsui Chemicals Agro, Inc., Japan, for performing the FMP assays and sharing the *LsRdl* plasmid.

I would like to thank Dr. Bente Frølund, Associate Professor, Faculty of Health and Medical Sciences, University of Copenhagen, for sharing their precious compounds.

I wish to convey my thanks to the Ministry of Education, Culture, Sports, Science and Technology (Monbukagakusho: MEXT), Japan Government, for offering me the scholarship during my graduate study.

I must thank all the staffs of the United Graduate School of Agricultural Sciences of Tottori University & Shimane University for their warmhearted cooperation.

Finally and most importantly, I am forever grateful to my families. To my loving parents, thank you for your constant encouragement and love, without which the pursuit of this degree would not have been possible. To my beautiful wife, thank you for your endless support and for the many sacrifices you have made. I would like to dedicate this thesis to you.

List of publications

1. **Genyan Liu**, Kenjiro Furuta, Hiromitsu Nakajima, Fumiyo Ozoe, Yoshihisa Ozoe. Competitive antagonism of insect GABA receptors by 4-substituted 5-(4-piperidyl)-3-isothiazolols. *Bioorg. Med. Chem.*, **2014**, 22, 4637–4645 (**Chapter 2**).
2. **Genyan Liu**, Fumiyo Ozoe, Kenjiro Furuta, Yoshihisa Ozoe. 4,5-Substituted 3-isoxazolols with insecticidal activity act as competitive antagonists of housefly GABA receptors. *J. Agri. Food Chem.*, **2015**, 63, 6304−6312 (**Chapter 3**).
3. **Genyan Liu**, Bente Frølund, Fumiyo Ozoe, Yoshihisa Ozoe. Differential interactions of 5-(4-piperidyl)-3-isoxazolol analogues with insect γ-aminobutyric acid receptors leading to functional selectivity. *Insect Biochem. Mol. Biol*., **2015**, 66, 64−71 (**Chapter 4**).

List of sub-publications

1. Mohammad Mostafizur Rahman, **Genyan Liu**, Kenjiro Furuta, Fumiyo Ozoe, Yoshihisa Ozoe. Synthesis of 1,3-di- and 1,3,4-trisubstituted 1,6-dihydro-6-iminopyridazines as competitive antagonists of insect GABA receptors. *J. Pestic. Sci.* **2014**, 39, 133–143.
2. Yoshihisa Ozoe, Fumiyo Ozoe, Tomo Kita, Mohammad Mostafizur Rahman, **Genyan Liu**, Kazutoshi Hisano, Madoka Takashima, Yunosuke Nakata. Multiple sites of insecticidal action in ionotropic GABA receptors, *ACS Symposium Series* titled "Discovery and Synthesis of Crop Protection Products", **2015**, Vol. 1024, Chapter 30, pp 431–446.

Summary

γ-Aminobutyric acid (GABA) is the primary inhibitory neurotransmitter in the nervous system of animals. Insect ionotropic GABA receptors (GABARs) are important targets for insecticides and parasiticides. Noncompetitive antagonists (NCAs) of GABARs such as fipronil have been exploited as commercial insecticides. However, no potent competitive antagonist (CA) of insect GABARs is available at present. CAs might be utilized to develop novel insecticides as they inhibit GABAR activation by acting at the orthosteric site, which differs from the allosteric sites of NCA insecticides. The objective of this study is to identify effective CAs of insect GABARs. Three classes of five-membered heterocyclic compounds, including 4-substituted 5-(4-piperidyl)-3-isothiazolols (thio-4-PIOL), 4,5-disubstituted 3-isoxazolols, and 4-substituted 5-(4-piperidyl)-3-isoxazolols (4-PIOL) were synthesized and examined for their antagonism of insect GABARs.

Eleven 4-substituted thio-4-PIOL analogues were first synthesized in eight steps. The antagonism of common cutworm (CC), small brown planthopper (SBP), and housefly (HF) GABARs by the thio-4-PIOLs were examined by a fluorometric imaging plate reader membrane potential assay or a two-electrode voltage clamp (TEVC) method. Thio-4-PIOL showed weak antagonism of three insect GABA receptors. The antagonistic activity of thio-4-PIOL was enhanced by introducing bicyclic aromatic substituents into the 4-position of the isothiazole ring. The 2-naphthyl and the 3-biphenylyl analogues displayed antagonist potencies with half maximal inhibitory concentrations (IC_{50}s) in the low micromolar range. The 2-naphthyl analogue induced a parallel rightward shift of the GABA concentration–

response curve, suggesting competitive antagonism by these analogues. Both compounds exhibited weak insecticidal activities against HFs. Thus, the orthosteric site of insect GABA receptors might be a potential target site of insecticides. Ligand docking studies using a HF GABAR homology model predicted that the orthosteric site contains two cavities large enough to accommodate bicyclic aromatic 4-substituents of thio-4-PIOL analogues.

A series of 4,5-disubstituted 3-isoxazolols, including muscimol analogues, were next synthesized and examined for their activities against four splice variants (ac, ad, bc, and bd) of HF GABARs expressed in *Xenopus* oocytes using the TEVC assay. Muscimol was a more potent agonist than GABA in all four splice variants, whereas synthesized analogues did not exhibit agonism but rather antagonism in HF GABARs. The introduction of bicyclic aromatic groups at the 4-position of muscimol and the simultaneous replacement of the aminomethyl group with a carbamoyl group at the 5-position to afford six 4-aryl-5-carbamoyl-3-isoxazolols resulted in compounds that exhibited significantly enhanced antagonism with IC_{50} values in the low micromolar range in the ac variant. The inhibition of GABA-induced currents by 100 μM analogues was approximately 1.5- to 4-fold greater in the ac and bc variants than in the ad and bd variants. 4-(3-Biphenylyl)-5-carbamoyl-3-isoxazolol displayed competitive antagonism, with IC_{50} values of 30, 34, 107, and 96 μM in the ac, bc, ad, and bd variants, respectively, and exhibited moderate insecticidal activity against HFs, with a median lethal dose of 5.6 nmol/HF. These findings suggest that these 3-isoxazolol analogues are novel lead compounds for the development of insecticides that act at the orthosteric site of HF GABARs. Docking studies indicated that a cation-π interaction between the 3-biphenylyl

group and an Arg residue in loop C of the orthosteric site might be beneficial for the antagonism of HF GABARs.

To better understand the molecular interactions of ligands with the orthosteric sites of GABARs, three 4-aryl/arylalkyl-4-PIOL and a 5-(3-biphenylyl)-4-(4-piperidyl)-1-hydroxy-pyrazole were examined for their antagonism with regard to the three insect GABARs. The 3-isoxazolol was preferable to the 3-isothiazolol and 1-hydroxypyrazole in antagonism to CC and HF GABARs. Of the tested analogues, 4-(3-biphenylyl)-4-PIOL displayed the greatest antagonism for CC and HF GABARs, with IC_{50} values of 3.4 and 10.2 μM, respectively. In contrast to the antagonism of the two GABARs, 4-(3-biphenylyl)-4-PIOL showed partial agonism for the case of SBP GABARs, with a half maximal effective concentration of 31.3 μM. Homology models and docking simulations revealed that a cation-π interaction between an analogue and an Arg residue in loop C or E of the orthosteric site is a key component of antagonism. This specific phenomenon was lacking in the interactions between 4-(3-biphenylyl)-4-PIOL and the orthosteric site of SBP GABARs. To our knowledge, 4-(3-biphenylyl)-4-PIOL is the most potent CA of insect GABARs reported to date. These findings in the studies for this dissertation provide important insights into designing and developing novel insecticides that target the orthosteric site of insect GABARs.

要 旨

γ-アミノ酪酸（GABA）は、動物の神経系における主要な抑制性神経伝達物質である。昆虫のイオンチャネル型 GABA 受容体（GABAR）は殺虫剤や外部寄生虫薬の主要な標的であり、フィプロニルのような GABAR の非競合アンタゴニスト（NCA）が殺虫剤として実用されている。昆虫の GABAR の競合アンタゴニスト（CA）も殺虫剤として利用可能と思われるが、そのような CA は現在存在しない。本研究では、オルソステリック結合部位に作用して GABAR の活性化を阻害する殺虫剤を開発するため、昆虫 GABAR に対する効果的な競合アンタゴニストを同定することを目的としている。3 種の 5 員環構造を含む化合物、4-置換 5-(4-piperidyl)-3-isothiazolol（thio-4-PIOL）類、4,5-二置換 3-isoxazolol 類および 4-置換 5-(4-piperidyl)-3-isoxazolol（4-PIOL）類を合成し、昆虫 GABAR に対するアンタゴニスト活性を調べた。

最初に、11 種の 4-置換 thio-4-PIOL 類縁体を 8 段階の反応を経て合成し、蛍光イメージングプレートリーダーを用いた膜電位試験法や二電極膜電位固定法（TEVC）により、ハスモンヨトウ、ヒメトビウンカおよびイエバエの GABAR に対するアンタゴニスト活性を測定した。Thio-4-PIOL 類縁体は 3 種の昆虫 GABAR に対して弱いアンタゴニスト活性を示し、isothiazole 環の 4 位に二環式芳香族基を導入することによりアンタゴニスト活性が増強された。2-ナフチル類縁体と 3-ビフェニリル類縁体の半数阻害濃度（IC_{50}）は μM オーダーであった。2-ナフチル類縁体は、GABA の濃度応答曲線を右シフトさせたことから、これらの類縁体は、GABA と競合して GABAR 阻害をすることが示唆された。両化合物は、イエバエを用いた殺虫活性試験において弱い殺虫活性を示した。このことは、昆虫 GABAR のオルソステリック部位が殺虫剤

の標的となることを示唆している。イエバエ GABAR のホモロジーモデルを用いたドッキングシミュレーションにより、オルソステリック部位には、thio-4-PIOL 類の二環式芳香族基が相互作用をするのに十分な大きさの 2 つのポケットが存在することが推測された。

次に、ムシモールの類縁体を含む一連の 4,5-二置換 3-isoxazolol 類を合成し、アフリカツメガエル卵母細胞に発現させたイエバエ GABAR の 4 種のスプライスバリアント (ac、ad、bc、bd) に対する化合物の活性を TEVC 法により調べた。ムシモールは、イエバエ GABAR の 4 種のバリアント全てに対して強力なアゴニストとして作用したが、合成した類縁体はアゴニスト活性を示さず、アンタゴニストとして作用した。ムシモールの 4 位への二環式芳香族基の導入と 5 位アミノメチル基のカルバミル基への置換により、ac バリアントにおいて IC_{50} 値が μM オーダーとなり、アンタゴニスト活性が大きく増強された。また、100 μM で試験したとき、ad と bd バリアントより ac と bc バリアントが 1.5～4 倍効果的に GABA 誘起電流を阻害した。4-(3-Biphenylyl)-5-carbamoyl-3-isoxazolol は、ac、bc、ad および bd の 4 種のバリアントに対して競合的にアンタゴニスト活性を示し、各バリアントに対する IC_{50} 値はそれぞれ 30、34、107 および 96 μM であった。また、イエバエを用いた殺虫活性試験における半数致死濃度（LD_{50}）は 5.6 nmol/匹であり、高い殺虫活性を示した。これらの結果から、3-isoxazolol 類は、イエバエ GABAR のオルソステリック部位に作用する殺虫剤を開発するための有効なリード化合物であることが示唆された。ドッキングシミュレーションでは、オルソステリック部位ループ C に位置するアルギニン残基と 3-ビフェニリル基との間のカチオン-π 相互作用によりイエバエ GABAR においてアンタゴニスト活性を示すということが推測された。

最後に、リガンドと GABAR のオルソステリック部位の分子間相互作用をより深く理解するため、3 種の昆虫 GABAR に対する 3 種の 4-aryl/arylalkyl-4-PIOL と 5-(3-biphenylyl)-4-(4-piperidyl)-1-hydroxypyrazole のアンタゴニスト活性について調べた。3-isoxazolol は、ハスモンヨトウとイエバエの GABAR に対して、3-isothiazolol や 1-hydroxypyrazole より高いアンタゴニスト活性を示した。4-(3-Biphenylyl)-4-PIOL は、ハスモンヨトウとイエバエの GABAR に対する IC_{50} 値がそれぞれ 3.4 μM と 10.2 μM であり、高いアンタゴニスト活性を示した。4-(3-Biphenylyl)-4-PIOL は、ハスモンヨトウとイエバエの GABAR に対してアンタゴニスト活性を示すのと対照的に、ヒメトビウンカの GABAR に対してはアゴニスト活性を示した（EC_{50} = 31.3 μM）。ホモロジーモデリングを用いたドッキングシミュレーションから、化合物とオルソステリック部位のループ C/E の間におけるカチオン-π 相互作用がアンタゴニスト活性に重要な要素であることが推測された。4-(3-Biphenylyl)-4-PIOL とヒメトビウンカの GABAR オルソステリック部位の間の相互作用ではこの特異的な現象が欠けていた。本研究において試験した化合物うち、4-(3-biphenylyl)-4-PIOL は昆虫 GABAR に対する最も強力な CA であるということが分かった。本研究で得られたこれらの知見は、昆虫 GABAR のオルソステリック部位を標的とした新規殺虫剤のデザインと開発に重要な情報を提供すると考えられる。